

**Three-Dimensional Conceptual Model
for the Hanford Site Unconfined
Aquifer System:
FY 1994 Status Report**

P. D. Thorne S. E. Schubert
M. A. Chamness V. R. Vermeul
Q. C. Macdonald

November 1994

Prepared for
the U.S. Department of Energy
under Contract DE-AC06-76RLO 1830

Pacific Northwest Laboratory
Richland, Washington 99352

MASTER

DISTRIBUTION OF THIS DOCUMENT IS UNLIMITED

for

DISCLAIMER

This report was prepared as an account of work sponsored by an agency of the United States Government. Neither the United States Government nor any agency thereof, nor any of their employees, make any warranty, express or implied, or assumes any legal liability or responsibility for the accuracy, completeness, or usefulness of any information, apparatus, product, or process disclosed, or represents that its use would not infringe privately owned rights. Reference herein to any specific commercial product, process, or service by trade name, trademark, manufacturer, or otherwise does not necessarily constitute or imply its endorsement, recommendation, or favoring by the United States Government or any agency thereof. The views and opinions of authors expressed herein do not necessarily state or reflect those of the United States Government or any agency thereof.

DISCLAIMER

Portions of this document may be illegible in electronic image products. Images are produced from the best available original document.

Summary

This report provides an update on the development of a three-dimensional conceptual model of ground-water flow in the unconfined aquifer system for the Hanford Site. The conceptual model will provide a basis for three-dimensional numerical modeling and will enable better understanding and more accurate predictions of contaminant transport under changing site conditions.

The area included in the conceptual model has been extended to include the entire Hanford Site south and west of the Columbia River, and the area south of the Hanford Site to the confluence of the Yakima and Columbia rivers. The conceptual model within the earlier study area, south of Gable Mountain to the 300 Area, was also refined and updated.

Geologic descriptions of samples from selected wells were interpreted to determine the extent and thickness of hydrogeologic units within the unconfined aquifer system. Nine hydrologically significant units were previously defined above the underlying basalt. These units have been extended into the expanded model area and refined within the previously defined area. Definition of the units is based on textural differences that are expected to reflect differences in hydraulic properties. The geologic data have been entered into a geographical information system. Maps showing the extent of each unit are presented.

Additional hydraulic property data were obtained by conducting aquifer tests at six wells. These and other available data were used to develop a new transmissivity distribution for the model area that is being applied in inverse calibration of the existing two-dimensional numerical flow model. A single value of hydraulic conductivity was assigned for mud-dominated units within the flow system. This was based on a few test results for the Hanford Site and representative values presented in the literature.

Additional geologic and water-level information was collected to help define the flow system boundary corresponding to the Yakima River. The lower reach of the river appears to have poor hydraulic communication with the unconfined aquifer. The range of possible recharge from Cold Creek and Dry Creek valleys also needs to be better defined. An aquifer test was conducted at well 699-43-104 and provides an estimate of hydraulic conductivity for the mouth of the Cold Creek Valley. However, the gradient in this area is uncertain. Possible methods of determining interflow between the unconfined and confined aquifer systems are being evaluated. Analysis for tritium and iodine-129 at the reconfigured "Golder" well 699-18-21 is presented.

Contents

Summary	iii
1.0 Introduction	1.1
1.1 Three-Dimensional Modeling Objectives	1.1
1.2 Scope of the Conceptual Model	1.1
2.0 Hydrogeologic Setting	2.1
3.0 Data Sources	3.1
4.0 Hydrogeologic Structure	4.1
5.0 Hydraulic Properties	5.1
5.1 Conceptual and Numerical Modeling Relationship	5.1
5.2 Updated Transmissivity Distribution	5.1
5.3 Results of Aquifer Tests Conducted to Support the Conceptual Model	5.2
5.4 Hydraulic Conductivity of Hydrogeologic Units	5.2
6.0 Boundary Conditions	6.1
6.1 Columbia River Boundary	6.1
6.2 Yakima River Boundary	6.1
6.3 Cold Creek Valley	6.4
6.4 Interflow with Confined Basalt Aquifer System	6.4
6.5 Natural Areal Recharge	6.5
6.6 Artificial Recharge	6.5
7.0 Hydraulic Heads	7.1
8.0 Contaminant Distributions	8.1
9.0 References	9.1
Appendix A - Analysis of Constant-Rate Discharge Tests Conducted to Support the Three-Dimensional Conceptual Model	A.1
Appendix B - Temperature Logging as a Means for Quantifying Aquifer Intercommunication	B.1

Figures

1.1	Location of the Hanford Site	1.2
3.1	Locations of Wells Used for Defining Hydrogeologic Structure	3.3
4.1	Stratigraphic Correlation to Various Authors	4.2
4.2	Structural Contours for the Top of Basalt	4.3
4.3	Map of Boundary of Unit 9	4.4
4.4	Map of Boundary of Unit 8	4.6
4.5	Map of Boundary of Unit 7	4.7
4.6	Map of Boundary of Unit 6	4.8
4.7	Map of Boundary of Unit 5	4.9
4.8	Map of Boundary of Unit 4	4.10
4.9	Map of Boundary of Unit 3	4.11
4.10	Map of Boundary of Unit 2	4.13
4.11	Map of Boundary of Unit 1	4.14
5.1	Transmissivity Distribution Determined from the Inverse Calibration Model of Jacobsen and Freshley (1990)	5.3
5.2	Updated Transmissivity Distribution for Two-Dimensional Model Calibration	5.5
5.3	Locations of Constant-Rate Tests Conducted to Support the Three-Dimensional Conceptual Model	5.7
6.1	Major-Ion Composition of Water from the Ringold Formation, the Saddle Mountain Basalt, and the Yakima River at Kiona	6.3
8.1	Corrected As-Built Diagram for the Reconfigured Well 699-18-21 (Golder S-12)	8.2
8.2	Tritium Concentration Trend During Development Pumping of the Reconfigured Golder Well 699-18-21	8.3

Tables

5.1 Results of Constant-Rate Discharge Tests Conducted During 1994	5.8
5.2 Hydraulic Test Results for Mud-Dominated Units	5.9

1.0 Introduction

This report documents work conducted during the fiscal year 1994 (FY 94) to develop an improved three-dimensional conceptual model of ground-water flow in the unconfined aquifer system across the entire Hanford Site (Figure 1.1). Development of an improved conceptual model is supported by the Hanford Site Ground-Water Surveillance Project, which is managed by Pacific Northwest Laboratory (PNL).^(a) This project is responsible for monitoring the movement of contaminants in ground water beneath the Hanford Site to ensure that public health and the environment are protected. Separate annual reports document the observed movement of chemical and radiological contaminant plumes in Hanford Site ground water and the measured elevations of the water table across the site (for example, see Dresel et al. 1994). Earlier status reports on development of the three-dimensional conceptual model are presented in Thorne and Chamness (1992) and Thorne et al. (1993).

1.1 Three-Dimensional Modeling Objectives

The main objective of the ongoing effort to develop an improved conceptual model of ground-water flow is to provide the basis for improved numerical transport models that will be capable of accurately predicting the movement of radioactive and chemical contaminant plumes in the aquifer beneath Hanford. More accurate ground-water flow models will also be useful in assessing the impacts of changes in facilities and operations. For example, decreasing volumes of operational waste-water discharge are resulting in a declining water table in parts of the unconfined aquifer. In addition to supporting numerical modeling, the conceptual model also provides a qualitative understanding of the movement of ground water and contaminants in the aquifer. This understanding is critical in determining optimum locations and depths for monitoring wells.

Past numerical models used for simulating ground-water flow and contaminant transport at the Hanford Site (Cearlock et al. 1975; Evans et al. 1988; Jacobson and Freshley 1990) have been two-dimensional, assuming that hydraulic properties, hydraulic head, and contaminant concentrations do not vary vertically through the aquifer thickness. This two-dimensional approach does not realistically represent ground-water flow in the aquifer. And, because contaminants are not evenly distributed through the thickness of the aquifer, two-dimensional transport models have not been successful at determining the flux of contaminants through the unconfined aquifer system. A three-dimensional flow model can provide more accurate predictions of contaminant transport. However, before such a numerical model can be built and used to simulate ground-water flow and contaminant transport, a conceptual model describing the flow system is needed.

1.2 Scope of the Conceptual Model

The area of interest is encompassed by the Columbia River on the east and north, and by basalt outcrops and the Yakima River on the west and south. A three-dimensional conceptual model for this

(a) PNL is operated for the U.S. Department of Energy by Battelle Memorial Institute.

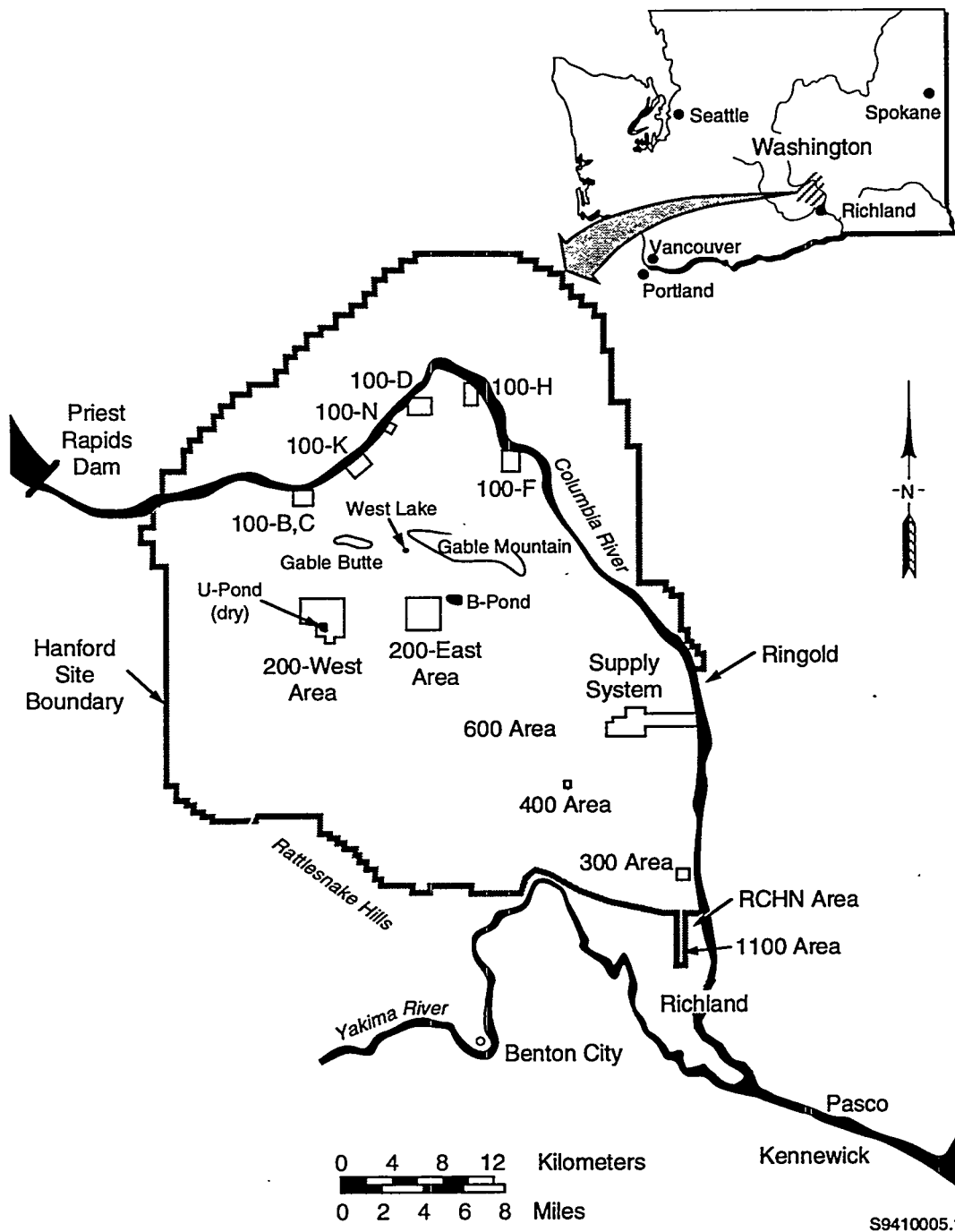


Figure 1.1. Location of the Hanford Site

area is being developed over a period of several years. Work conducted during the 1992 fiscal year (Thorne and Chamness 1992) focused on defining the hydrogeologic structure of the unconfined aquifer in the area extending eastward from the 200-East Area to the Columbia River. During the 1993 fiscal year, the conceptual model area included the Hanford Site south of the Gable Mountain - Gable Butte structure.

In FY 94, the conceptual model area has been extended to the Yakima and Columbia river confluence on the south and the Columbia River boundary on the north. Hydrogeologic layers have been refined and extended to cover most of the southern portion of the Hanford Site. Because the Columbia River forms a boundary to the unconfined aquifer, modelling will not extend north or east of the Columbia River. Additional information has been collected on geology and head relationships in the vicinity of the Yakima River to better define this boundary on the southwest edge of the site. Well hydraulic tests have been conducted and analyzed and additional existing hydraulic property data have been compiled to develop a new transmissivity distribution for the model area. The outcrop of basalt above the water-table has been revised. Possible methods of assessing interflow between the confined and unconfined aquifer systems have been evaluated. Water samples have been obtained from an intermediate depth in the aquifer system and contaminant concentrations found in these samples have been compared to the uppermost portion of the aquifer.

2.0 Hydrogeologic Setting

Hanford Site geology and hydrology have been studied extensively over the years. Detailed descriptions are provided in DOE (1988), Lindsey et al. (1992), and Cushing (1994). Consequently, information on the geology and hydrology of the site is only briefly summarized in this report.

The Hanford Site lies within the Pasco Basin, a structural depression that has accumulated a relatively thick sequence of fluvial, lacustrine, and glaciofluvial sediments. This structural depression and nearby anticlines and synclines are formed in the underlying Columbia River Basalt Group, a sequence of flood basalts. The most recent basalt flow underlying much of the Hanford Site is the Elephant Mountain Member of the Saddle Mountains Basalt.

Overlying the basalt are the fluvial and lacustrine sediments of the Ringold Formation. These consist of coarser-grained deposits of migrating channels and the finer-grained overbank deposits of the ancestral Columbia and/or Salmon-Clearwater river systems. The uppermost sedimentary unit covering a large part of the Hanford Site is the informally named Hanford formation, a complex series of coarse- and fine-grained layers deposited by cataclysmic floods during the last ice age. For the most part, the fine-grained sediments are found near the margins of the basin and in areas protected from the main flood currents that deposited the coarse-grained sediments. Where they are below the water table, the coarse-grained Hanford formation deposits make up the most permeable zones of the unconfined aquifer system.

An uppermost unconfined aquifer and a sequence of confined aquifers lie beneath most of the Hanford Site. The unconfined aquifer is generally located in unconsolidated to semiconsolidated sediments overlying the basalt bedrock. The confined aquifers are generally formed by brecciated tops of basalt flows and sedimentary interbeds located within the basalts. In some areas, deeper parts of the suprabasalt sediments are locally confined by overlying mud units. However, because the entire supra-basalt aquifer system is interconnected on a sitewide scale, it has commonly been referred to as the "Hanford unconfined aquifer." This nomenclature is used in this report. Aquifers located within the Columbia River Basalt are referred to as the basalt confined aquifer system.

Ground water in both the confined and unconfined aquifer systems generally flows toward the Columbia River, which acts as a drain for the ground-water flow system. However, in some places, ground water within the confined system flows under the river, apparently toward areas of higher vertical communication between the confined and unconfined aquifers (Bauer et al. 1985; Spane 1993). Ground water in the confined aquifers comes mainly from infiltration of precipitation and streamflow within recharge areas along the periphery of the Pasco Basin (DOE 1988). With regard to development of a conceptual model for the unconfined aquifer, the confined aquifer system is important because there is a potential for significant ground-water leakage between the two systems, particularly in areas of increased vertical permeability such as the area northeast of the 200-East Area (Graham et al. 1984).

The unconfined aquifer at Hanford lies mainly within the Ringold and Hanford formations. Because the sand and gravel facies of the Ringold Formation are generally more consolidated, contain more silt, and are less well sorted, they are about 10 to 100 times less permeable than the sediments of the overlying Hanford formation (DOE 1988). Prior to waste-water disposal operations at the Hanford

Site, the uppermost aquifer was almost entirely within the Ringold Formation and the water table extended into the Hanford formation at only a few locations near the Columbia River (Newcomb et al. 1972). However, waste-water discharges have increased the water-table elevation causing it to rise into the Hanford formation in the vicinity of the 200 East Area and in a wider area near the Columbia River.

Ground water in the unconfined aquifer at Hanford generally flows from recharge areas in the elevated region near the western boundary of the Hanford Site toward the Columbia River on the eastern and northern boundaries. The Yakima River borders the Hanford Site on the southwest and is generally regarded as a source of recharge. The Columbia River is the primary discharge area for the unconfined aquifer. Natural areal recharge from precipitation at the Hanford Site is low: less than 1.25 cm/yr (0.5 in./yr) over most of the site, although a few nonvegetated areas with coarse soils may reach 5 cm/yr (2 in./yr) of infiltration (Gee and Heller 1985; Bauer and Vaccaro 1990). Since 1944, the artificial recharge from Hanford waste-water disposal operations has been greater than the natural recharge. As of 1989, an estimated 444 billion gallons (1,681,000,000 m³) of liquid were discharged to the ground through disposal ponds, trenches, and cribs (Freshley and Thorne 1992).

3.0 Data Sources

The conceptual model describes the geometry of the flow system, defines hydraulic properties throughout the model region, describes boundary conditions, and establishes initial conditions for variables such as hydraulic head and contaminant concentrations. For the three-dimensional conceptual model, describing flow system geometry involves defining the orientation and extent of hydrogeologic units that make up the unconfined aquifer system. Hydraulic properties including both horizontal and vertical hydraulic conductivities, aquifer storativity, and specific yield must be defined for each hydrogeologic unit.

Data needed for developing a three-dimensional conceptual model were derived from a variety of previous studies and ongoing Hanford Site investigations, as well as from work conducted specifically to support the sitewide model. Hydraulic property data were obtained from the results of hydraulic tests documented in Bierschenk (1959), Kipp and Mud (1973), Deju (1974), Lindberg and Bond (1979), Graham et al. (1981), DOE (1988), Liikala and Aaberg (1988), Thorne and Newcomer (1992), Peterson (1992), Connelly et al. (1992a), Connelly et al. (1992b), Swanson (1992), Thorne et al. (1993), Connelly (1994), and Swanson (1994). Information was also obtained from new tests and tests that were previously undocumented. During FY94, constant-rate discharge tests were conducted at six wells to provide additional hydraulic property data for the conceptual model. These new data were combined with existing data and results from other investigations to update the Hanford Site transmissivity distribution.

Information on the subsurface geologic framework came primarily from interpreting geologic descriptions of samples acquired during well drilling. These interpretations were based on work by Lindsey (1992), Lindsey et al. (1991; 1992), Lindsey and Jaeger (1993), Lindberg (1993a; 1993b), Hartman and Lindsey (1993), and Swanson (1992) in the 100, 200, and 300 Areas of the Hanford Site, which use the lithofacies units outlined in Lindsey (1991). Many of the wells used to define the geologic framework were drilled to basalt as part of a study for a proposed nuclear power plant (PSPL 1982). Other information used in defining the top of basalt came from wells drilled for the Basalt Waste Isolation Project (DOE 1988), which studied the basalts underlying Hanford for disposal of high-level nuclear waste. Figure 3.1 shows the distribution of the approximately 550 wells that have been used to define the three-dimensional hydrogeologic structure of the unconfined aquifer system. Many of these wells were used to determine the elevation of the top of basalt, and not all have been interpreted over their entire depth. Information on the southern part of the Hanford Site and the Richland area came from studies conducted by the U.S. Geological Survey, from Liikala (1993), and from private well logs filed with the Washington State Department of Ecology. Information on the construction of Hanford Site wells was obtained from Chamness and Merz (1993) and from the Hanford Environmental Information System (HEIS) database.

4.0 Hydrogeologic Structure

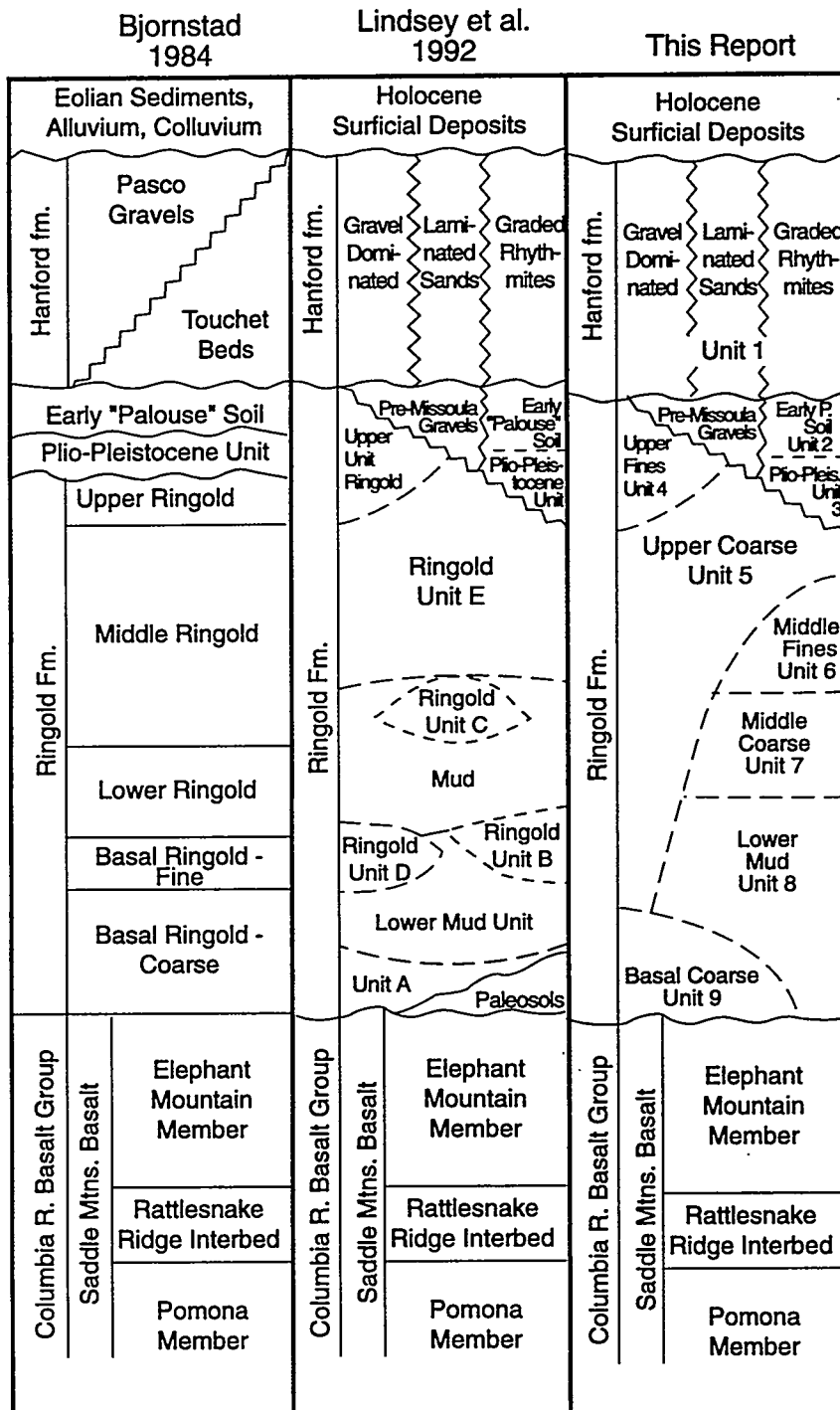
The unconfined aquifer system underlying the Hanford Site is composed of a sequence of mostly discontinuous sedimentary deposits with differing hydraulic properties that are related to the texture, degree of sorting, and cementation of the sediments. The first step in developing a conceptual model is to describe the three-dimensional geologic structure of the aquifer in enough detail to reflect major changes in hydraulic characteristics. The status of the nearly completed three-dimensional conceptual model is described in this section.

The hydrogeologic framework of the three-dimensional model needs to be accurate, but relatively simplistic, for two reasons. First, lateral and vertical variation are quite high in the primarily fluvial depositional environment of the Hanford Site and cannot be completely described with the distribution of boreholes and wells available for subsurface data. Second, the computer simulations would be very complex and difficult to run with a multitude of discrete sedimentary lenses. Therefore, the unconfined aquifer system has been divided into generalized, relatively extensive lithofacies units. Areal limited lenses within a unit are not recognized as separate layers in the hydrogeologic conceptual model.

Structure contour maps of the top of each hydrogeologic unit are being prepared and will be used to create the layered system for the numerical model. These maps are presently being modified through an iterative process to check interpretations and remove errors; consequently, these maps are not available for inclusion in this report. The boundaries that will be used for each of the layers is shown in figures at the end of this section. In the numerical model, the Columbia River is treated as a no-flow boundary, and the Yakima River is treated as a prescribed flow boundary. The boundary or areal extent of each unit (see Figures 4.3 through 4.11) was drawn to extend some distance beyond the rivers edges to provide a reasonable and continuous hydrogeologic system at the model's boundary, i.e., beneath the river. Some units probably extend beyond the boundaries shown in the figures and into areas outside the area to be modelled.

Classification of the sediments into lithofacies units is based on work by previous workers (see Section 3.0) and the available geologist's and driller's logs. In some areas, geophysical logs were also used to assist in correlation. The textural facies were often grouped into larger units based on assumed similarity in hydraulic parameters. Consequently, sands were generally grouped with sandy gravels, and silt was grouped with clay. This has resulted in the generation of 9 layers overlying the basalt, which generally forms the base of the unconfined aquifer system. Figure 4.1 provides a stratigraphic column of these layers. Because these layers are not correlated in all cases to Lindsey et al.'s (1992) revised stratigraphic column, they are numbered sequentially from top to bottom as Unit 1, 2, etc., in this report.

The uppermost basalt unit, generally either the Elephant Mountain or Ice Harbor member, forms the base of the layered system to be modelled (Figure 4.2). In the deepest parts of the Wahluke and Cold Creek synclines and the Wye Barricade depression is a sand and/or gravel unit, Unit 9, (Figure 4.3) that correlates to Lindsey's Ringold Unit A. Unit 9 tends to be basalt-poor in comparison to later Ringold gravels, except immediately above the basalt, where a rubble of extremely weathered



S9409051.1

Figure 4.1. Stratigraphic Correlation to Various Authors

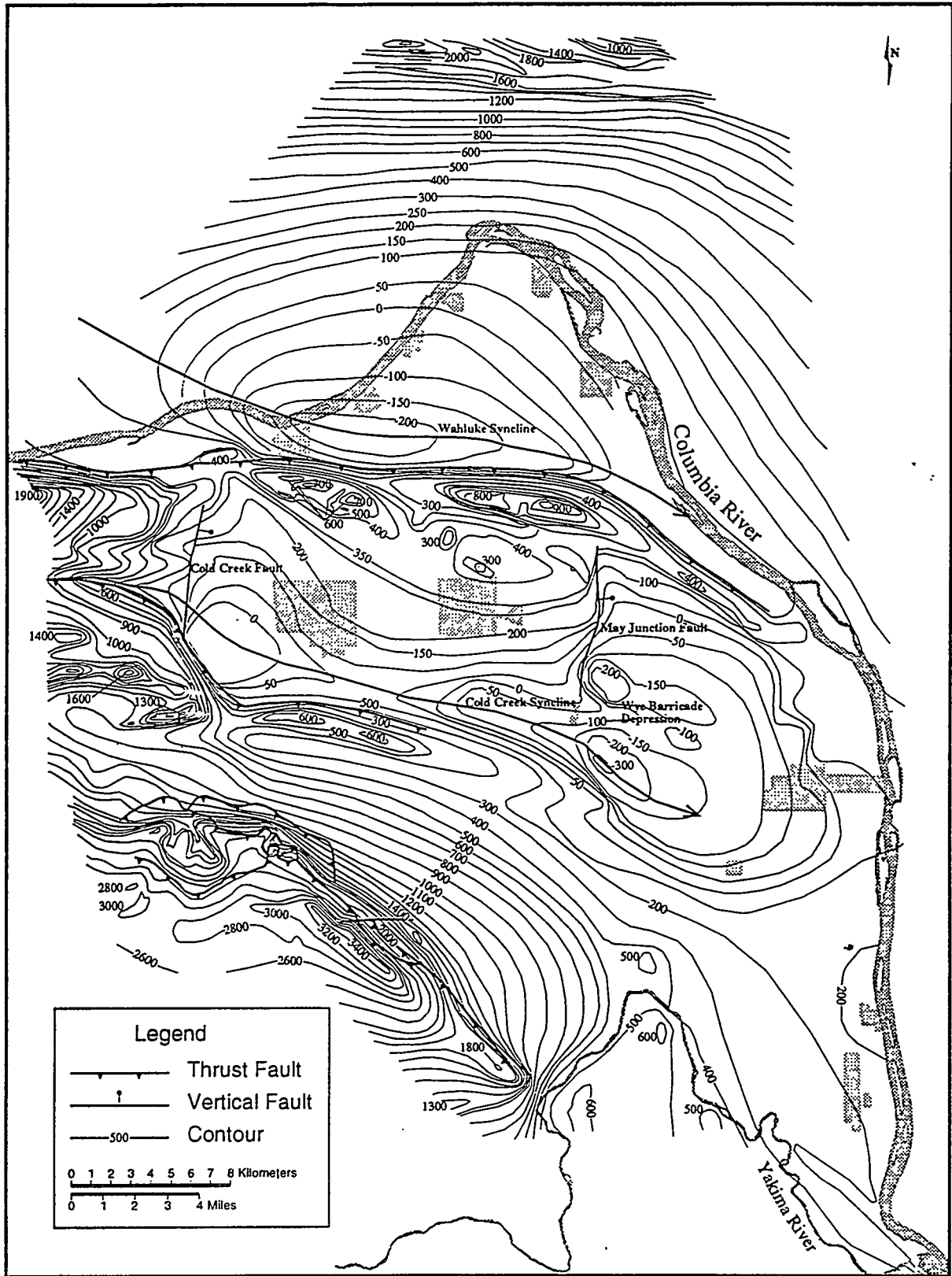


Figure 4.2. Structural Contours for the Top of Basalt

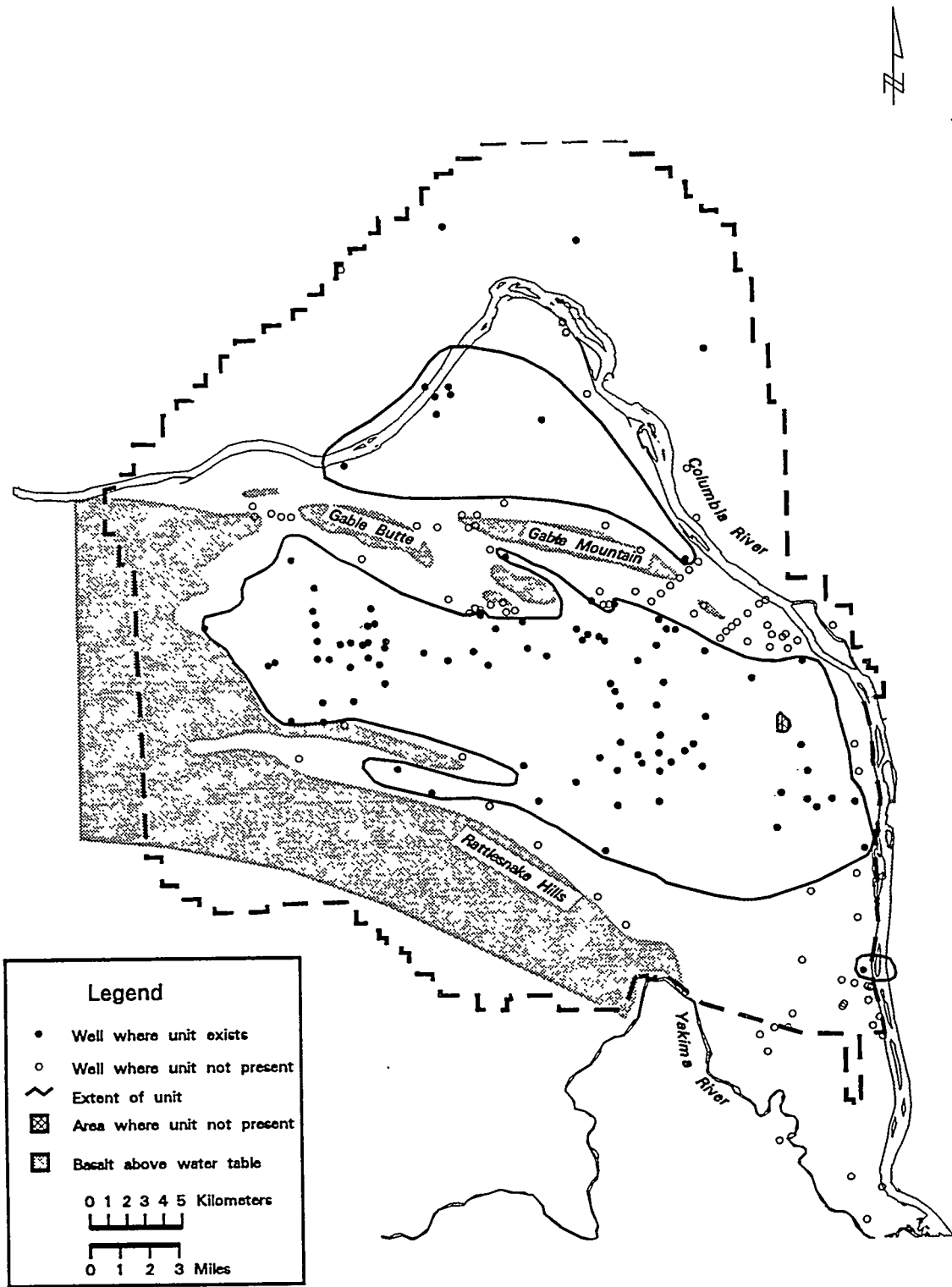


Figure 4.3. Map of Boundary of Unit 9

basalt clasts and clay is often found. Toward the edges of the synclines and depressions, Unit 9 pinches out and the clay or mud to sandy mud of overlying Unit 8 lies in contact with the basalt (Figure 4.4). Unit 8 corresponds to the finer-grained portion of Lindsey's Lower Mud Sequence. This unit may contain a layer of white volcanic ash and one or more paleosols. In some areas, calcium carbonate content increases and color changes due to paleosol development. Lower portions of Unit 8 often have a blue-green color, while the upper part may be yellow, tan, or blue-green. Unit 8 pinches out on the flanks of the anticlinal ridges; where it directly lies on top of the basalt, it includes basalt fragments and basalt altered to clay.

Unit 7 is a coarse-grained unit that consists of sand to muddy, sandy, basalt-poor gravel occurring primarily in the central and eastern portions of the basin (Figure 4.5). Some of the sandy portions of this unit correlate to parts of Lindsey's Lower Mud Sequence, which includes sands (Lindsey et al. 1992). The sands have been grouped with the gravelly portions of Unit 7 because their hydraulic properties are probably more similar to the coarse-grained sediments in Unit 7 than the mud and clay of Unit 8. In some areas near anticlinal ridges, Unit 7 lies directly on top of the basalt. This unit is distinguished from over- or underlying coarse-grained units primarily by the presence of intervening fine-grained unit(s). If the underlying Unit 8 muds are missing, Unit 9 sediments are grouped with those of Unit 7, since the hydraulic parameters are assumed to be similar.

Overlying Unit 7 through much of the central and eastern portion of the basin (Figure 4.6) is a sequence of mud and clay layers with intercalated sand and/or gravel layers called Unit 6. This unit corresponds to several unnamed mud layers identified between gravel units B, C, and D in Reidel et al. (1992) and which extend laterally a few kilometers. North of Gable Mountain, Unit 6 appears to become much thicker than it is to the south. This is caused by the lateral facies change from the coarse-grained, mainstream sediments of Unit 5 in the western part of this area to the fine-grained, overbank sediments of Unit 6 in the eastern part. Although the fine-grained sediments were deposited at the same time as the coarse-grained deposits, their hydraulic properties are very different. Consequently, the fine-grained deposits have been grouped with Unit 6.

The sand to muddy, sandy gravel of Unit 5 overlies Unit 6 and generally correlates to Lindsey's Unit E. This unit is widespread across the basin (Figure 4.7) and contains a relatively low percentage of basaltic gravels. Unit 5 cannot be distinguished readily from Unit 7, and where Unit 6 is not present, they have been grouped together as Unit 5 because their hydraulic parameters are assumed to be similar. This causes Unit 5 to appear to thicken toward the west where Unit 6 is not present.

In many areas, Unit 5 is the uppermost Ringold unit, except in those areas where it is overlain by Unit 4 (Figure 4.8). Unit 4 corresponds to the fine-grained portion of Lindsey's Upper Ringold Unit. In this report, Unit 4 is restricted to the silt and clay deposits, while the sand deposits included by Lindsey et al. (1992) are grouped with the coarser underlying or overlying units, as appropriate. Unit 4 forms the White Bluffs on the east side of the Columbia River. Unit 4 also occurs in the western and east-central portions of the Site in a complicated pattern caused by erosion (Figure 4.8).

Erosion of Unit 4 probably occurred during the hiatus during which the Plio-Pleistocene and early "Palouse" soil units were deposited. The Plio-Pleistocene unit (Unit 3) is a localized basaltic side-stream gravel deposit which grades laterally and vertically into a moderately well-developed caliche horizon. Unit 3 has only been defined in the western portion of the Hanford Site (Figure 4.9). The Plio-Pleistocene unit was deposited and/or developed on the eroded surface of Unit 4 or Unit 5.

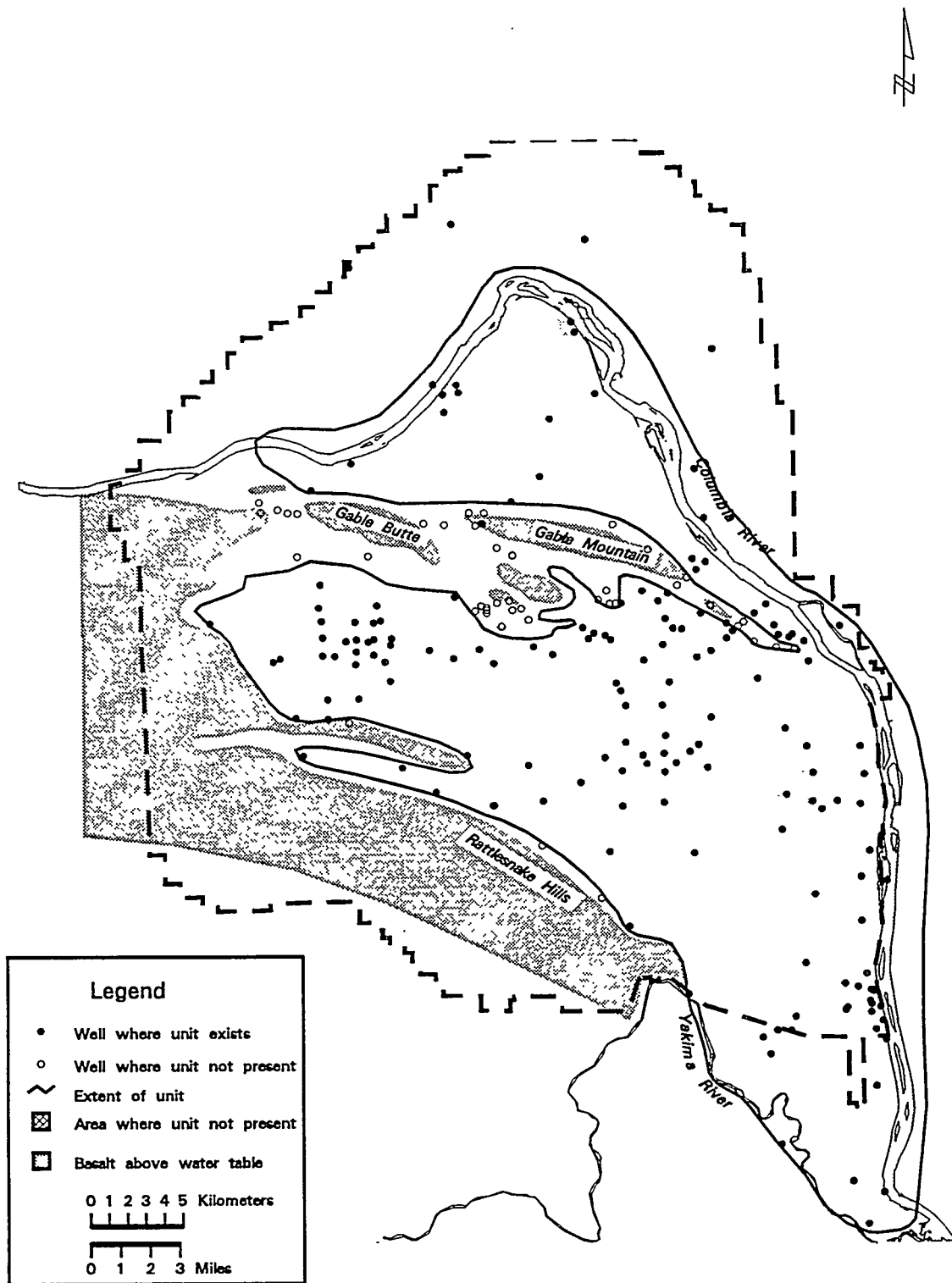


Figure 4.4. Map of Boundary Unit 8

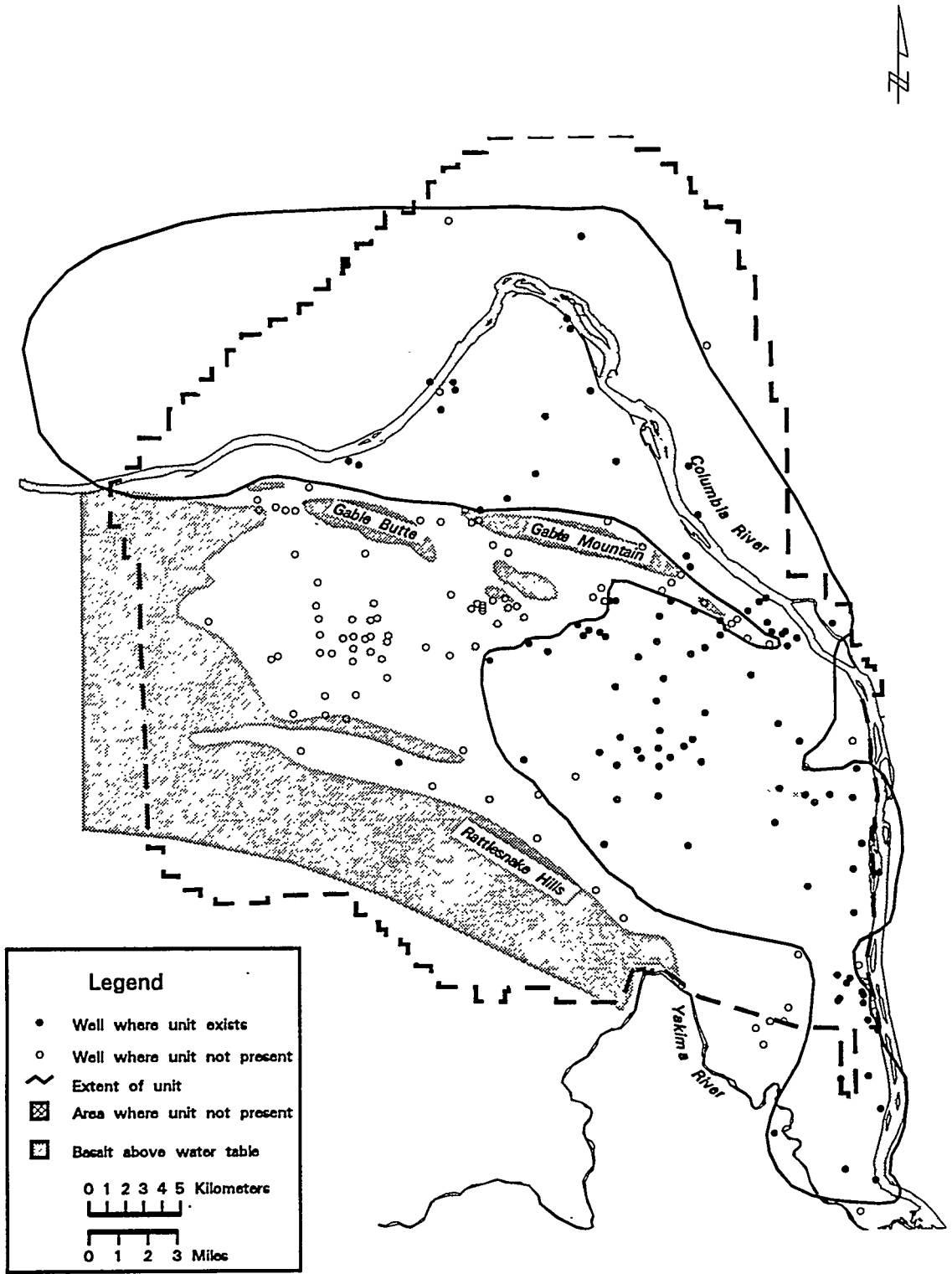


Figure 4.5. Map of Boundary of Unit 7

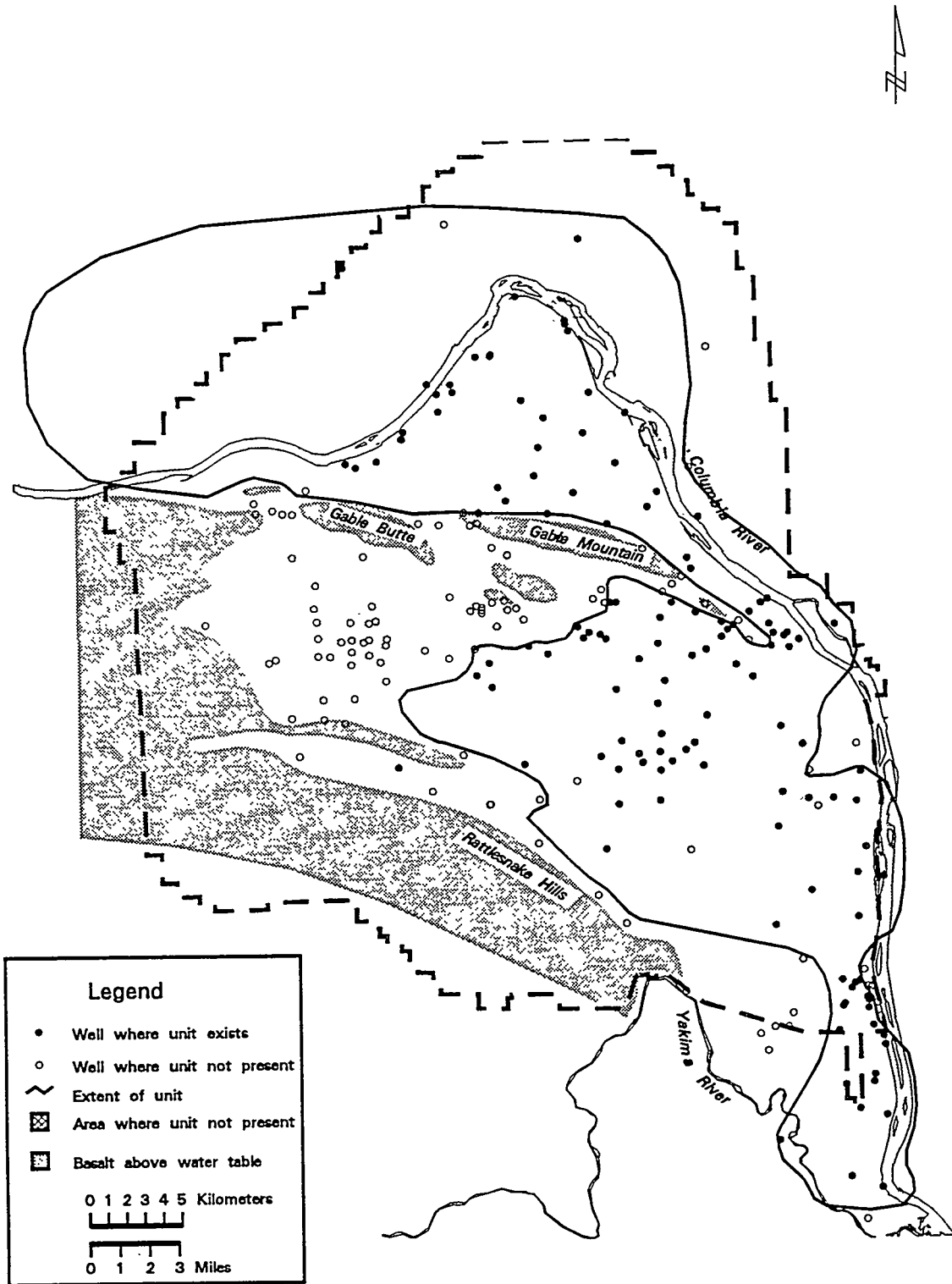


Figure 4.6. Map of Boundary of Unit 6

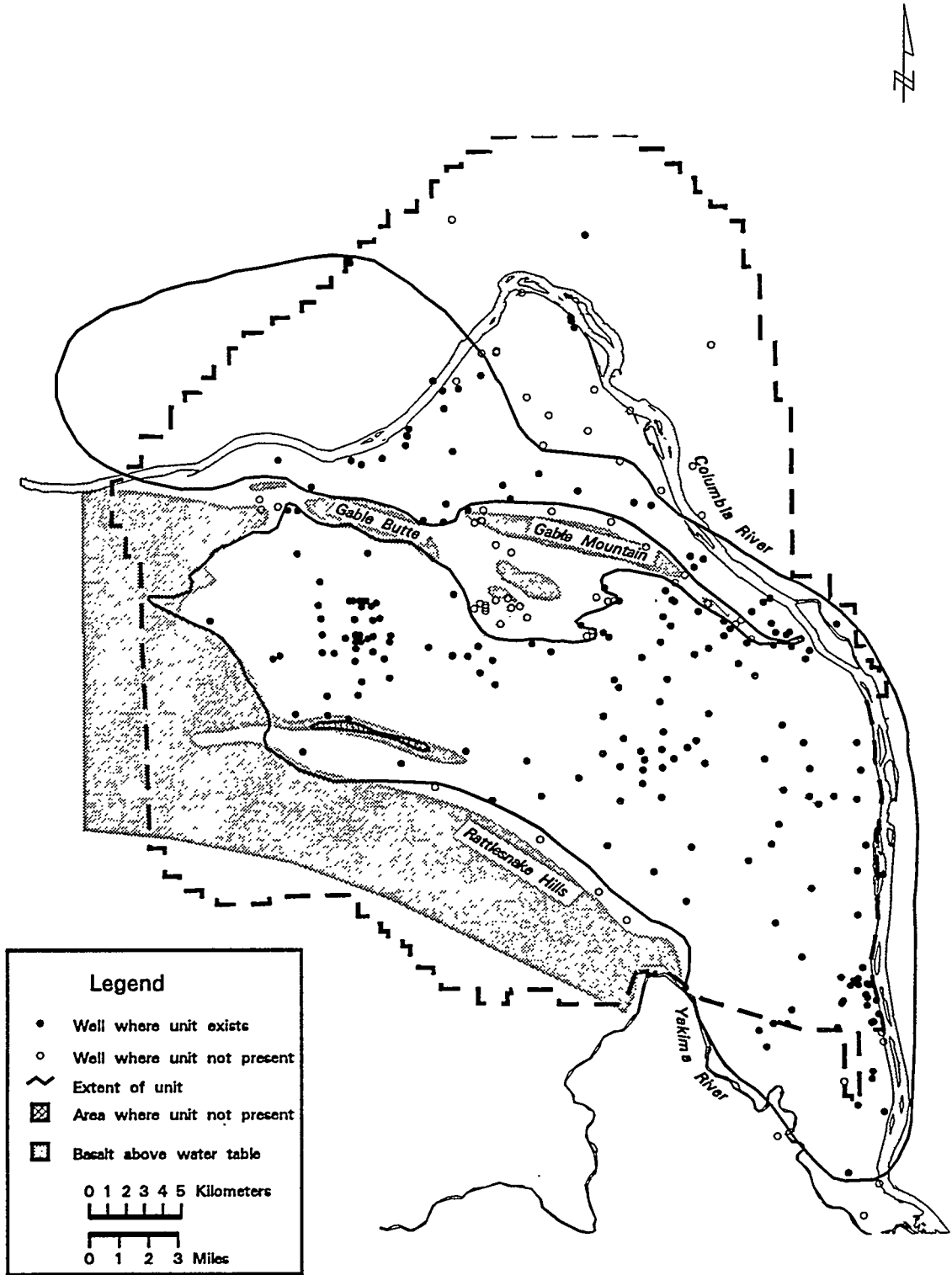


Figure 4.7. Map of Boundary of Unit 5

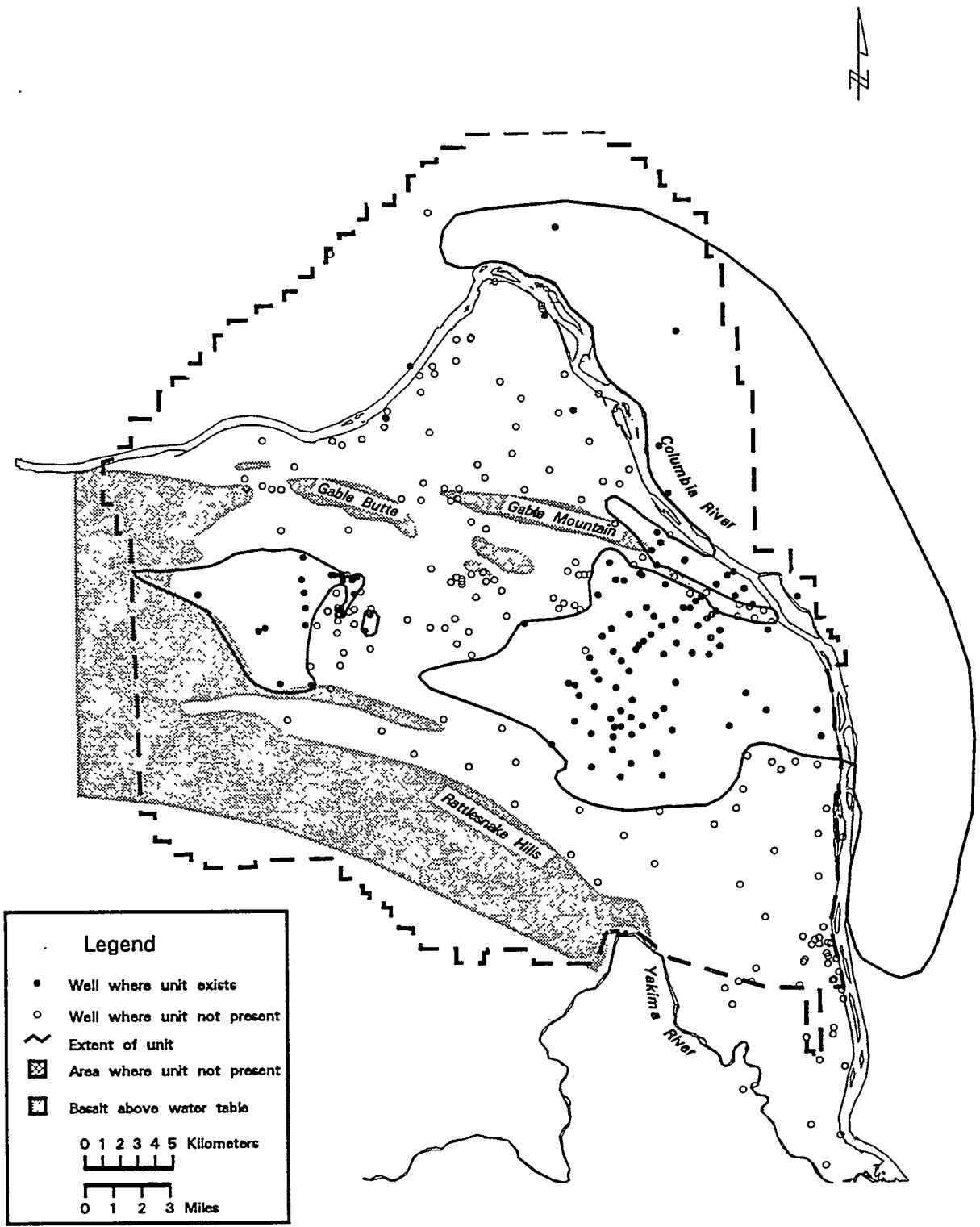


Figure 4.8. Map of Boundary of Unit 4

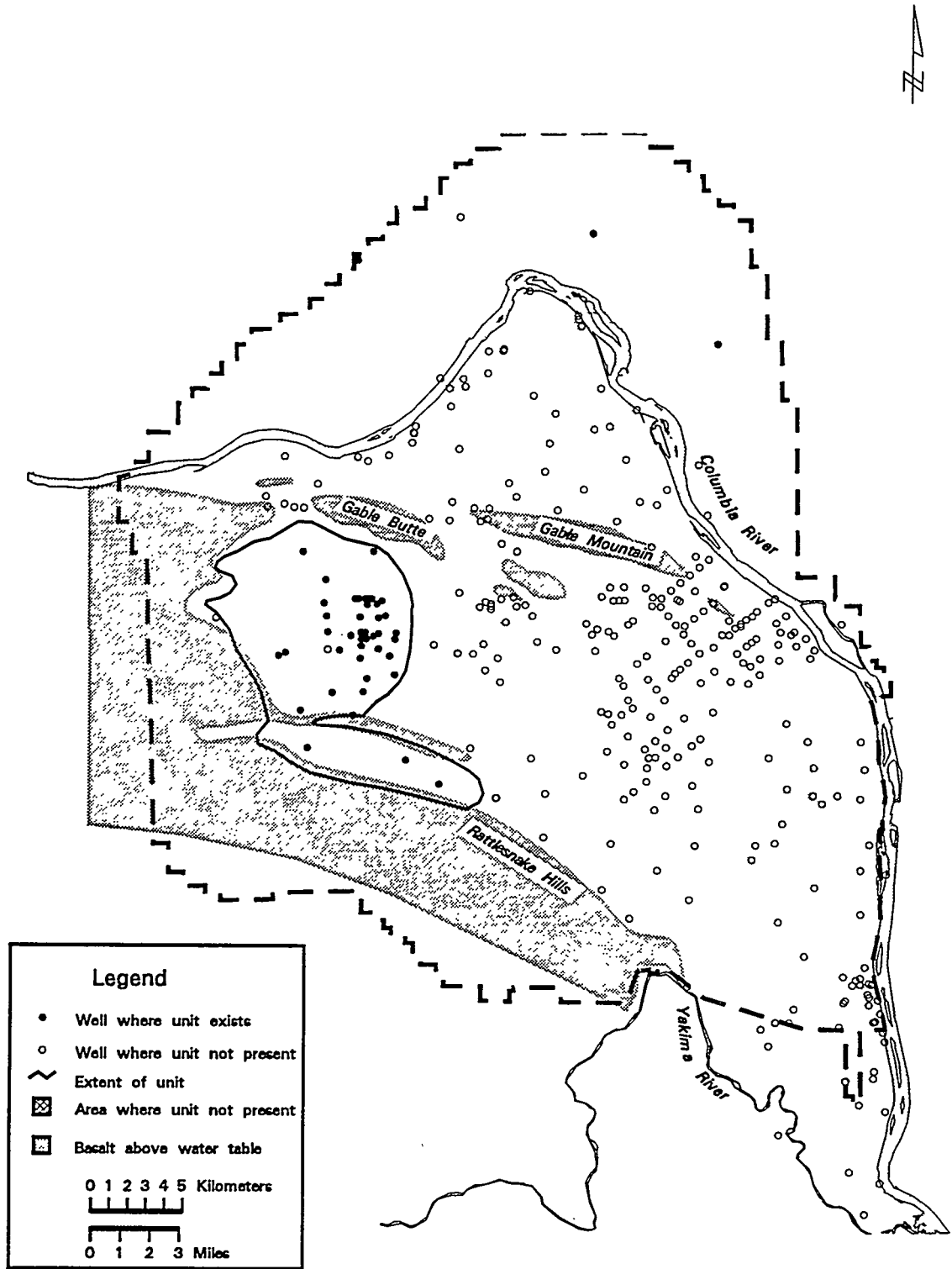


Figure 4.9. Map of Boundary of Unit 3

Although Unit 3 undoubtedly occurs elsewhere in the Pasco Basin, it cannot be correlated with other caliche horizons. Just south of the 200 West Area, the water table is located in the basaltic side-stream facies of Unit 3, which has a higher permeability than either underlying or overlying units.

The extent and thickness of Unit 2, the wind-deposited sand and silt of the early "Palouse" soil, is presently under evaluation. An effort has been made to incorporate this re-evaluation into the data set, but there will undoubtedly be more modifications of this unit in the future. Figure 4.10 shows the presently-defined boundaries of Unit 2. Since this unit is not known to contain the water table, it is of little importance for the saturated zone modelling.

Overlying all of the previous units on the Hanford Site, and in a few places resting on top of basalt, is Unit 1, the glaciofluvial, generally basalt-rich Hanford formation. This unit consists of three primary facies, a "gravel-dominated" facies known as the Pasco Gravels, a "sand-dominated" facies, and a "mud-dominated" facies known as the Touchet Beds. For the purposes of this report and the modelling effort to date, the Hanford formation has not been divided into these individual facies. With the exception of areas near the Columbia River and the 200 East Area, the water table is below the Hanford formation. However, because of its relatively high permeability, the Hanford formation plays an important role in ground-water flow in those areas where it makes up the upper part of the aquifer.

Lying beneath gravels of the Hanford formation in the central portion of the Hanford Site are the sand and gravel deposits commonly called the "pre-Missoula gravels" (PSPL 1982). These sediments have been grouped with the Hanford formation for the following reasons: 1) the pre-Missoula gravels cannot be readily distinguished from the Hanford formation in most driller's or geologist's logs, 2) there are no known hydraulic property data for the pre-Missoula gravels, although its properties probably lie between the younger Hanford gravel-dominated facies and older sandy gravel of Unit 5, and 3) the pre-Missoula gravels are above the water table except in some areas near the Hanford Townsite and near the solid waste landfill in the center of the Hanford Site. Therefore, they do not present a primary pathway for ground-water movement. The surficial eolian sediments have an insignificant effect on ground-water movement and have also been grouped with the Hanford formation. Figure 4.11 shows the extent of Unit 1 that will be used in the modelling.

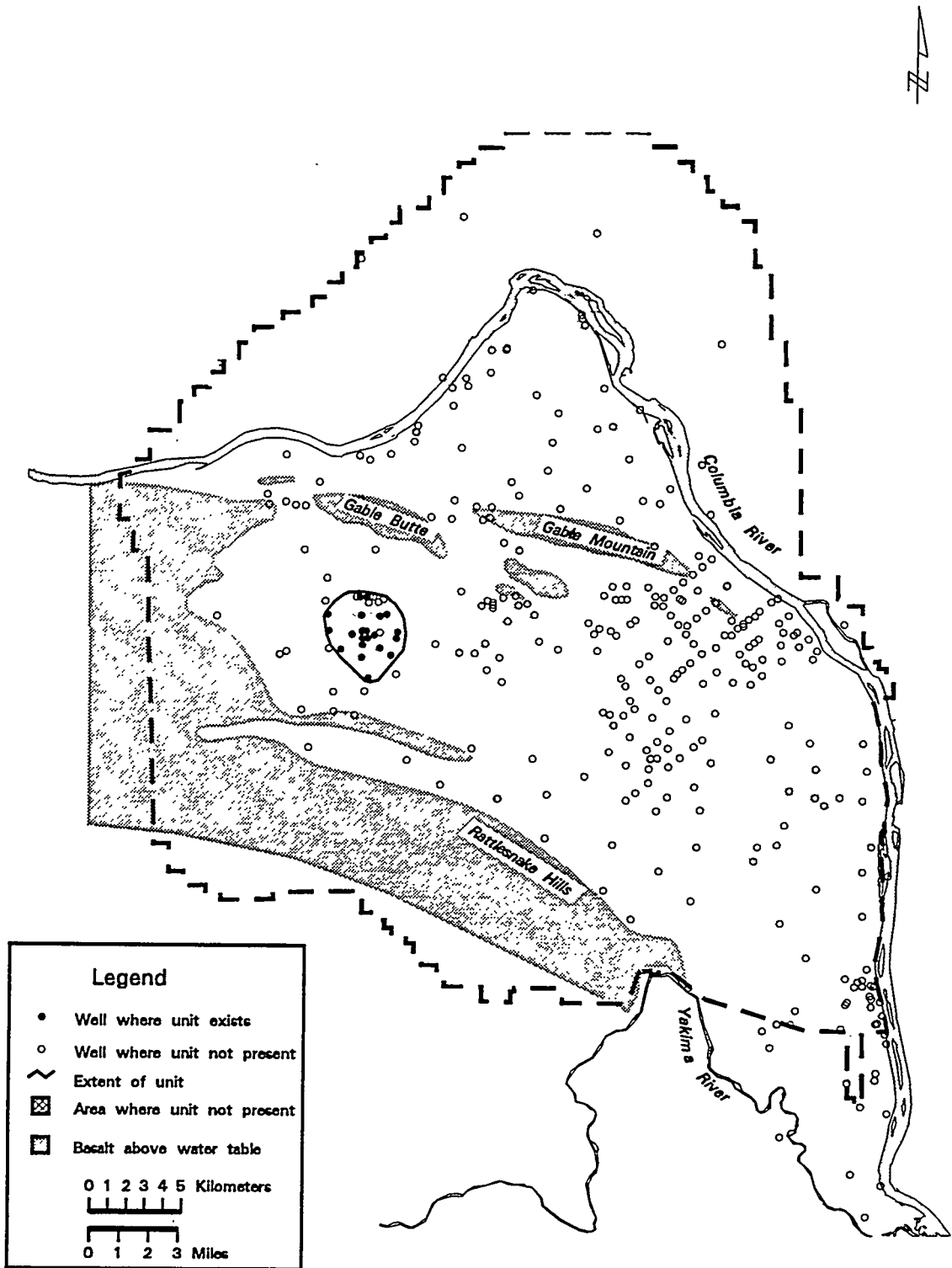


Figure 4.10. Map of Boundary of Unit 2

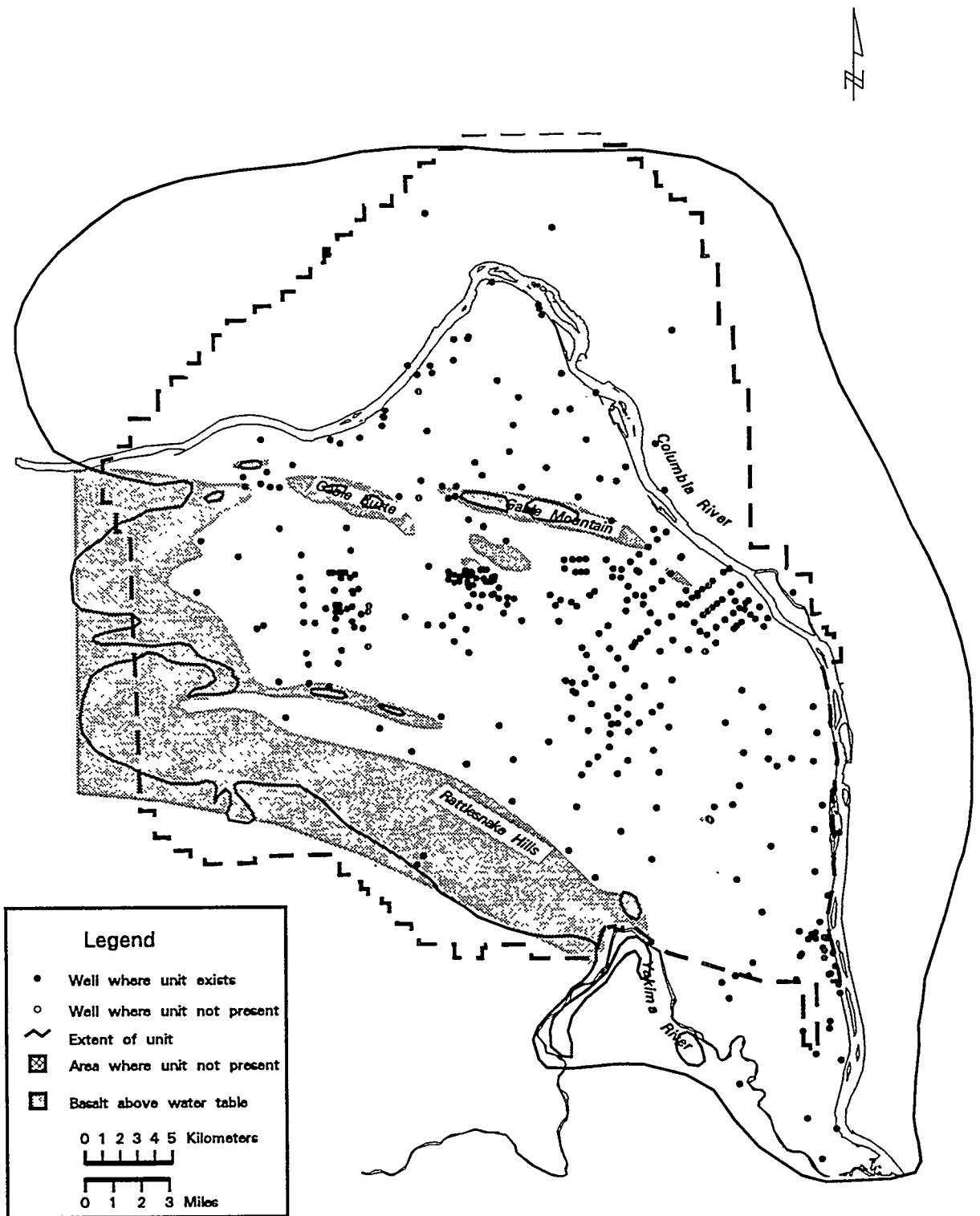


Figure 4.11. Map of Boundary of Unit 1

5.0 Hydraulic Properties

Hydraulic properties including both horizontal and vertical hydraulic conductivity (K_h and K_v), storativity (S), and specific yield (S_y) are key components of both the conceptual and numerical flow models. To support three-dimensional numerical modeling, the distribution of each of these parameters must be specified for each hydrogeologic unit. Hydraulic conductivity controls the rate of water flow through a unit thickness of the aquifer at a given hydraulic gradient. Storativity and specific yield determine the change in water-table elevation that will occur in response to a change in the volume of water stored in the aquifer. Additional parameters, such as dispersion coefficients and contaminant retardation factors, may also be required to support transport modeling.

Hydraulic conductivity data for various units has been derived mainly from aquifer tests and, in a few cases, from laboratory permeameter tests. A few estimates of storativity and specific yield are also available from multiple-well aquifer tests. However, storativity and specific yield data are limited and some of the data that do exist are highly uncertain because the effects of nonideal test conditions, such as partially penetrating wells and aquifer heterogeneity. Storativity and specific yield assigned to various units are, therefore, based mainly on values from the literature.

5.1 Conceptual and Numerical Modeling Relationship

The conceptual model provides initial hydraulic property data for numerical modeling. On the other hand, the conceptual model may be modified based on the results of subsequent numerical model calibration, especially in areas where hydraulic property data is lacking or uncertain.

Hydraulic property estimates based on aquifer testing and geologic information are used to develop initial hydraulic property distributions. These initial distributions are input to the numerical model along with boundary conditions and other information from the conceptual model. Calibration of the numerical model is then performed, either by trial and error or through an automated inverse-modeling process. Calibration involves adjusting both the distribution of hydraulic properties and the boundary conditions until model predicted hydraulic heads match the observed hydraulic heads within an acceptable tolerance. Model calibration usually results in modifications to the hydraulic property distributions, especially the distributions of hydraulic conductivities (K_h and K_v), and may also result in changes to boundary conditions. If these changes are reasonable, they are incorporated into a revised conceptual model. Numerical model calibration thus provides estimates of hydraulic properties in areas where test data is not available.

5.2 Updated Transmissivity Distribution

Before a three-dimensional numerical flow model is constructed for the Hanford Site, the existing two-dimensional model will be updated by adding additional hydraulic property information from aquifer tests and geologic studies. This effort, which is now underway, will culminate in a revised calibration of the two-dimensional model. An earlier two-dimensional calibration is described in Jacobson and Freshley (1990). The new calibration of the model will provide a revised transmissivity

(T) distribution that will form the basis for hydraulic properties in the three-dimensional model. Transmissivity is the product of aquifer thickness and horizontal hydraulic conductivity. To determine the hydraulic conductivity distribution for the three-dimensional model, transmissivity at each model node will be apportioned between the hydrogeologic units present at that location based on the thickness and relative hydraulic properties of the units present.

The transmissivity distribution resulting from Jacobson and Freshley's (1990) model calibration is shown in Figure 5.1. This distribution was updated based on the results of new aquifer tests conducted at selected wells, and reanalysis of previous tests using improved diagnostic techniques (Spane 1993; Thorne and Newcomer 1992). The updated transmissivity distribution for input into the calibration process is shown in Figure 5.2.

5.3 Results of Aquifer Tests Conducted to Support the Conceptual Model

Hydraulic tests were conducted at six wells during the past year to support continued development of the three-dimensional conceptual model. Constant-rate discharge tests were conducted at wells 699-S19-11, 699-S14-20, 699-4E-6, 699-18-21, 699-31-11, and 699-43-104. Test well locations are shown in Figure 5.3 and results are summarized in Table 5.1. The tested wells were selected based on their location and the lack of previous reliable hydraulic tests in that area. Two of the wells, 699-18-21 and 699-31-11, are "Golder" wells that were reconfigured during 1993 as reported in Thorne et al. (1993). Details concerning the testing procedures and analysis of each of the constant-rate tests are provided in Appendix A.

5.4 Hydraulic Conductivity of Hydrogeologic Units

As discussed in earlier status reports (Thorne and Chamness 1992; Thorne et al. 1993), the current approach for the three-dimensional conceptual model is to assign an areal distribution of K_h to permeable units that form the upper part of the unconfined aquifer system. Most ground-water flow and contaminant transport takes place in this part of the aquifer system. Single values of K_h will be assigned to mud-dominated units and to deeper permeable units.

The uppermost permeable unit for most of the model region is either Unit 1 or Unit 5. Units 7 and 9 represent deeper permeable units. The hydraulic conductivity of Unit 1 is generally much higher than any of the other units that compose the unconfined aquifer system. Therefore, where it is present below the water table, this unit usually provides the dominant flow path within the aquifer. Unit 1 consists of sand and gravel of the Hanford formation and the pre-Missoula gravel deposits. The fine-grained Touchet beds, which are also within the Hanford formation, are not found below the water table within the model region. In the vicinity of B Pond, the saturated portion of the Hanford formation is composed of muddy sandy gravels that probably represent the lower limit of hydraulic conductivity for Unit 1. Aquifer tests (Thorne et al. 1993) indicate that the minimum K_h is about 1 m/d and the minimum K_v is about 0.02 m/d for Unit 1. The maximum K_h for Unit 1, which has been measured in coarse gravel flood deposits, is about 9,000 m/d (Thorne and Newcomer 1992; DOE 1988). Maximum K_v is unknown, but may approach the value for K_h in relatively clean gravel zones where layers

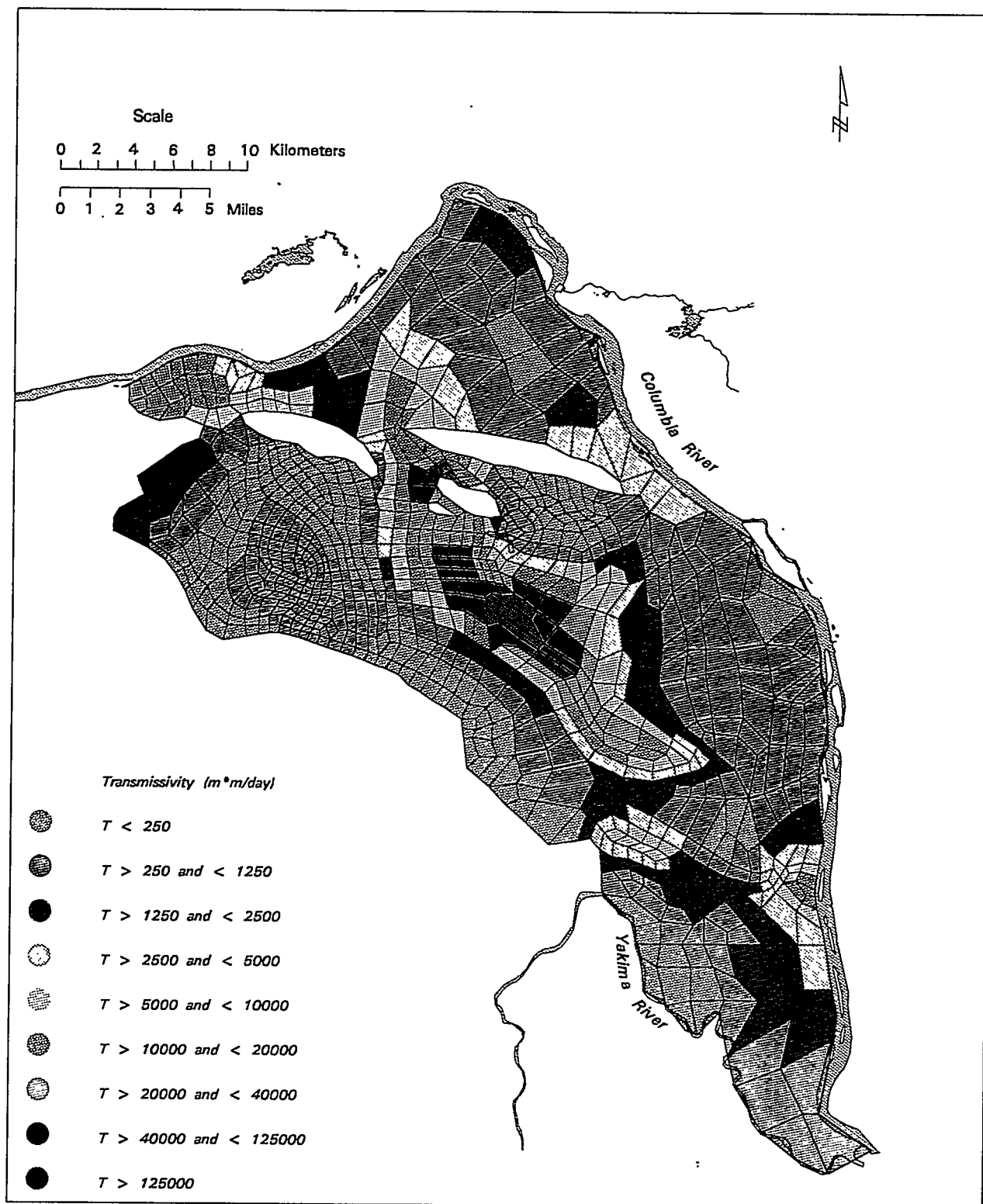


Figure 5.1. Transmissivity Distribution Determined from the Inverse Calibration Model of Jacobsen and Freshley (1990)

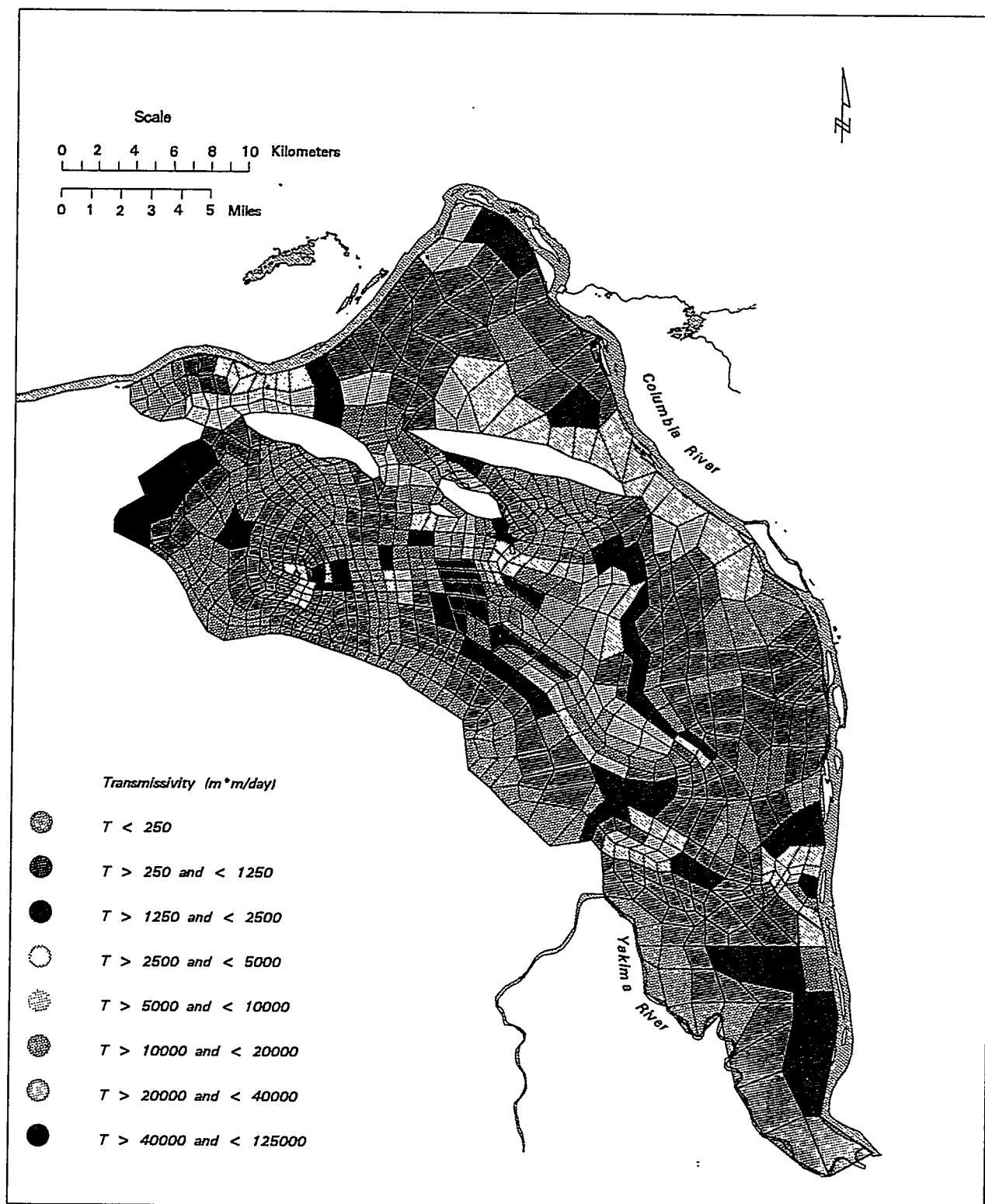
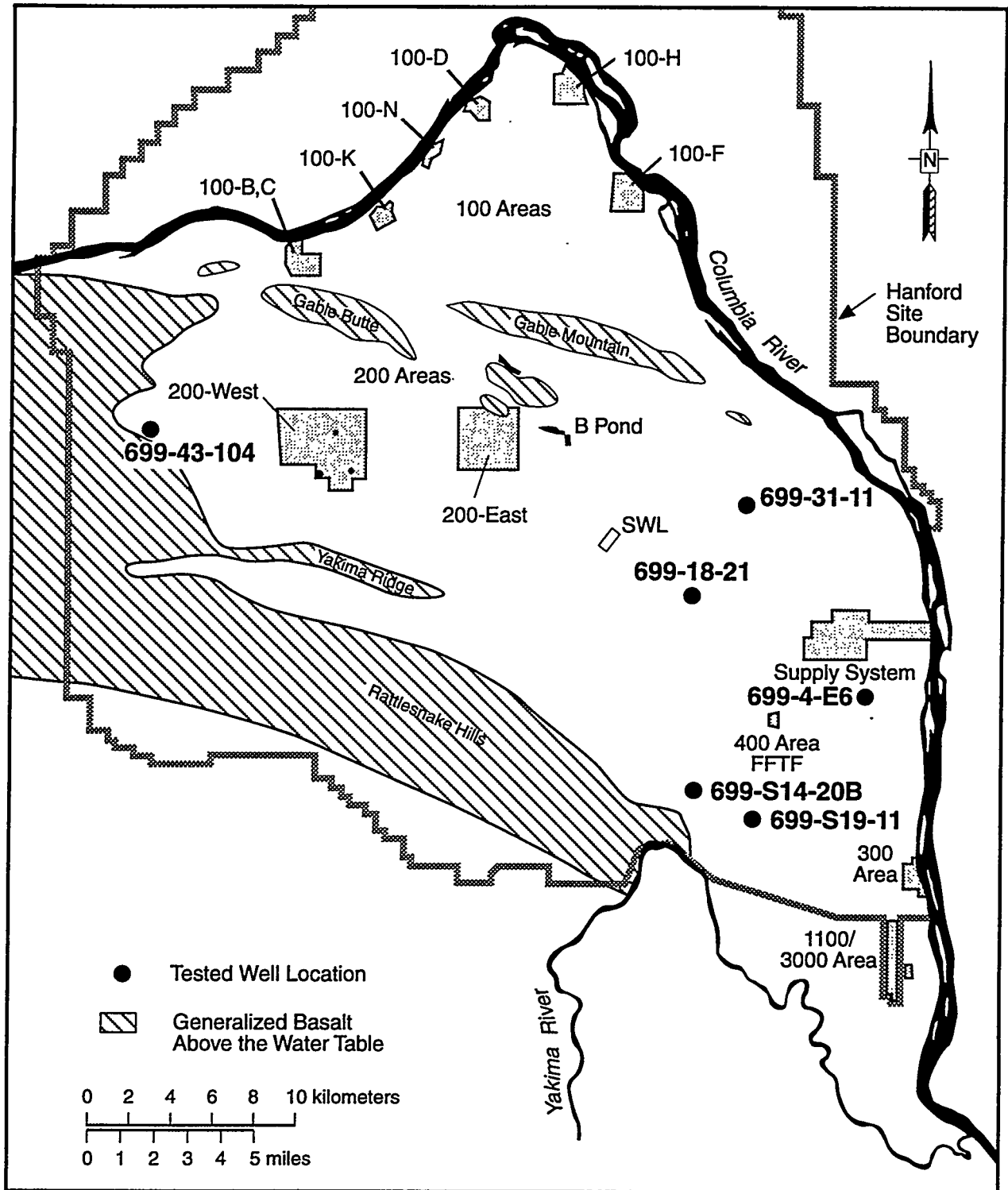


Figure 5.2. Updated Transmissivity Distribution for Two-Dimensional Model Calibration



S9410005.2

Figure 5.3. Locations of Constant-Rate Tests Conducted to Support the Three-Dimensional Conceptual Model

Table 5.1. Results of Constant-Rate Discharge Tests Conducted During 1994

Well number	Test Interval (m)	T (m ² /d)	K _h (m/d)	Hydrogeologic unit
699-S19-11	27.6 - 35.0	600	40	5
699-S14-20B	27.5 - 48.8	450	21	5
699-4-E6	20.8 - 26.4	> 10,000	> 890	1
699-18-21	58.5 - 70.7	300-3100	10-100	1
699-31-11	56.7 - 72.0	100-320	7-21	5
699-43-104	84.7 - 104.2	25	1.2	5

of finer grained material are not present. Specific yield for Unit 1 is estimated to range from about 0.1 to 0.3 and is expected to be higher for coarse, well-sorted gravel than for poorly sorted mixtures of sand and gravel. Storativity is estimated to range from 0.0001 to 0.0005.

Units 5, 7 and 9 are all within the Ringold Formation and consist of sand to muddy sandy gravel with varying degrees of cementation. Unit 5 is the most widespread unit within the unconfined aquifer and is found below the water table across most of the model region (see Figure 4.7). Hydraulic conductivities of Units 5, 7 and 9 vary within the range of about 0.1 to 200 m/d (Thorne and Chamness 1992; Thorne and Newcomer 1992; DOE 1988). Because these units are hydrologically similar, they were grouped together in areas where the intervening mud units do not exist. A few aquifer tests suggest vertical anisotropy is in the range of 0.01 to 0.1. Therefore, the range of K_v is estimated at about 0.001 to 20 m/d. Specific yield is estimated to range from 0.05 to 0.15 for the generally poorly sorted sediments of Units 5, 7 and 9. Storativity is estimated to range from 0.0001 to 0.001 for these units.

Mud-dominated units within the unconfined aquifer system include Unit 4, also known as the upper Ringold fines, Unit 6, which is a composite of intercalated mud and sand and gravel layers, and Unit 8, which is an extensive lower Ringold mud unit. Hydraulic conductivity of these units is generally about 2 to 5 orders of magnitude less than that of the permeable sand and gravel units. Therefore, the mud units are essentially aquitards and are not expected to transmit significant quantities of water or contaminants in the horizontal direction. They are significant in slowing the vertical migration of contaminants and influencing vertical head distributions. Therefore, the values of K_v assigned to mud units are probably more important than the ones assigned values of K_h.

Hydraulic test results for mud-dominated units are listed in Table 5.2. These few tests yielded K values of 0.0003 to 0.09 m/d. Some of the results are from well tests and some are from laboratory tests. Because of a tendency to complete wells only in zones that are likely to produce some water, these values may represent the higher range of K_h for the mud units. Test results for Unit 6 indicate that this unit has higher K_h than Unit 4. This is expected because of the sand and gravel layers included in Unit 6. Unit 8 is expected to have hydraulic conductivity similar to Unit 4. Freeze and

Table 5.2. Hydraulic Test Results for Mud-Dominated Units

Hanford well number	Hydraulic conductivity (m/d)	Hydrogeologic unit
299-W26-11	0.002	Unit 6
299-W7-9	0.09	Unit 4 (vadose)
699-20-39	<0.06	Unit 6
699-84-35	0.03	Unit 6
699-41-40	0.0003	Unit 4
699-42-42B	0.0006	Unit 4

Cherry (1979) give a range of $K = 0.001$ to 1 m/d for silt and loess, and as low as $K = 1E-07$ m/d for clay. This range is partially based on a compilation of data by Davis (1969). Based on both the test data and the values reported in the literature, 0.0005 m/d is recommended as an initial K_h for Units 4 and 8, and 0.01 is recommended for Unit 6.

6.0 Boundary Conditions

Nearly all the boundaries of the sitewide conceptual model represent physical boundaries of the flow system. Perimeter boundaries define the edges of the flow system corresponding to the Columbia River on the north and east and the Yakima River and basalt ridges on the south and west. Boundary conditions are also needed for the top and bottom of the aquifer system. The top boundary consists of the water table and may include both natural areal recharge and local recharge from liquid waste disposal, irrigation, and artificial recharge. The bottom of the aquifer boundary generally is defined by the top of basalt and may include interflow with the underlying confined aquifer system, which may be either recharge or discharge.

6.1 Columbia River Boundary

The current approach is to represent the Columbia River as a prescribed-head boundary over the depth of the river and as a no-flow boundary from the bottom of the river to the bottom of the aquifer. It is unlikely that ground water in the unconfined aquifer system flows across this boundary. However, such flow is possible if a locally confined permeable unit extends beneath the river and is affected by stresses such as pumping. Definitions of hydrogeologic units in the conceptual model are being extended across the river to allow for possible simulations of such a scenario. For a general sitewide model, daily and seasonal changes in the river stage resulting from releases from upstream dams can be ignored, and a time-averaged river stage can be used for the prescribed-head value at the river. The prescribed-head values along the Columbia River can be interpolated between points where river stage is routinely measured.

Measurements of actual ground-water and/or contaminant flux to the river would be extremely valuable for model calibration. Flux predicted by the model may be compared to actual measured values to determine the accuracy of the model. The river may also be modeled as a prescribed flow boundary and other parameters adjusted to match the head distribution. However, because of the large flow of the Columbia River compared to the contribution from ground water, measurements of flow rate changes along the Hanford Reach caused by ground-water discharge are not feasible with any known technology. Estimates of ground-water discharge to the Columbia River have been made in past studies. Luttrell et al. (1992) applied a flow net analysis to calculate discharge in the area of the old Hanford Townsite. They estimated 6.6×10^6 m³/yr discharge to about a 1 km length of the river. An earlier estimate of 2.7×10^6 m³/yr for the same area was based on the sitewide flow model (Prater et al. 1984).

6.2 Yakima River Boundary

In past numerical models, the Yakima River has been represented by a prescribed-head boundary (Jacobson and Freshley 1990). Because the prescribed head values for the river are higher than the heads within the model area, this boundary is a source of recharge. The recharge rate is controlled by the hydraulic conductivity of model elements adjacent to the river and the difference between the head value defined for the river and the head at adjacent nodes. However, the model-calculated recharge at

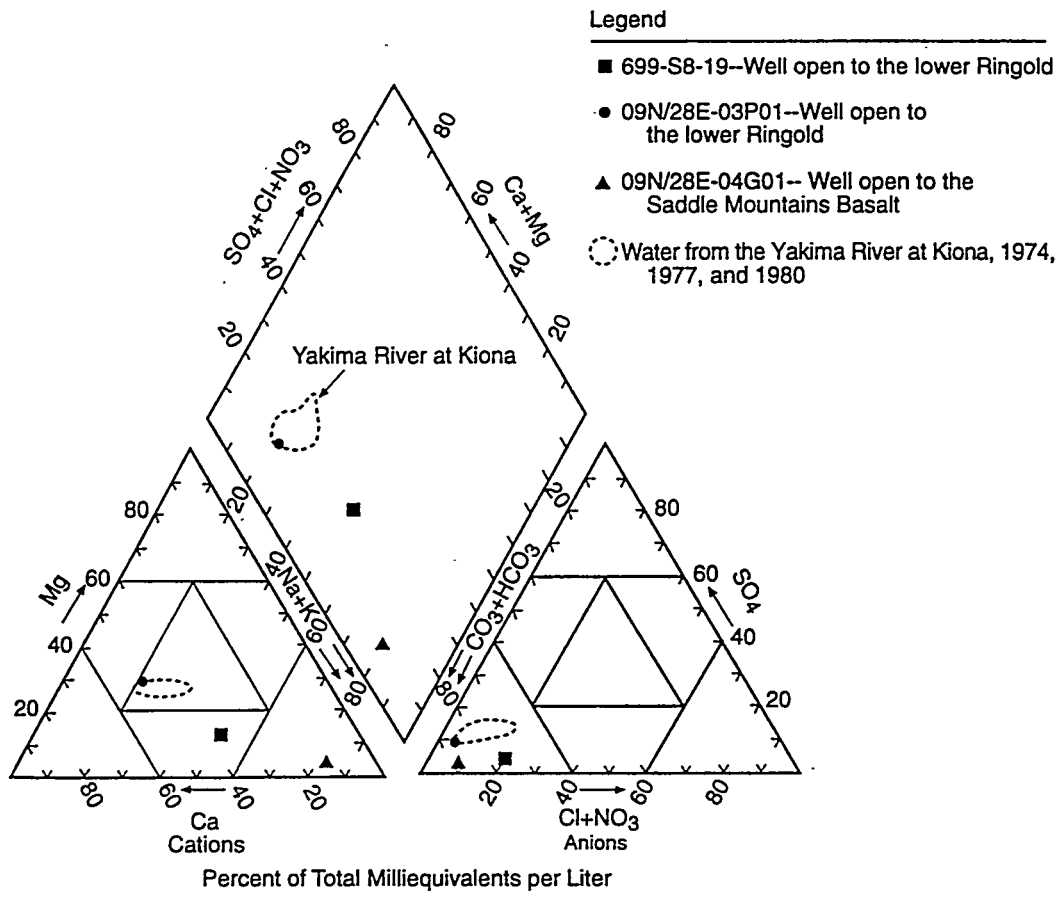
this boundary is highly uncertain because of a lack of wells and a corresponding lack of information concerning hydraulic properties and water-level elevations near the river. This causes uncertainty in the model predictions of ground-water flow within the area between the Yakima and Columbia rivers, an area which is becoming increasingly important as commercial development immediately south of the Hanford Site boundary continues.

As part of a study of ground-water chemistry of the Pasco Basin (Ebbert et al. 1993), the U.S. Geological Survey found evidence that the Yakima River recharges the unconfined aquifer in the reach adjacent to the Hanford Site. This conclusion was based on a comparison of the chemical composition of river water, ground water from a well (USGS number 09/28E-04G01) completed in the Saddle Mountains Basalt, and ground water from an offsite well (USGS number 09/28E-03P01) completed in the unconfined aquifer (Ringold Formation) near the river. Figure 6.1 shows a Piper diagram of the major-ion concentrations for water from these sources. An additional well (699-S8-19), which is open to the Ringold Formation on the Hanford Site, has also been plotted on the diagram. The offsite Ringold well (09/28E-03P01) plots near the normal range for Yakima River water. It is lower in relative concentrations of combined chloride and nitrate, and in combined sodium and potassium, than water from well 699-S8-19. Figure 6.1 also shows the location of the sampled wells in relation to the Yakima River.

To help define aquifer behavior in the vicinity of the Yakima River, river-stage monitoring has been conducted at a location just below Horn Rapids Dam. As reported in Thorne et al. (1993), water levels have been continuously monitored at Well 699-S24-19 for both the unconfined aquifer system and the basalt confined aquifer system. Water levels at this well do not show a direct response to changes in river stage. However, the water level of the unconfined aquifer interval does respond to the filling of a canal (the Horn Rapids Ditch) between the well and the river.

The section of the Yakima River below Horn Rapids dam flows through flood plain sediments that consist of moderately permeable stream channel deposits within fine-grained overbank and oxbow lake deposits. In this area, the unconfined aquifer may be somewhat isolated from the river by these fine-grained deposits near the river. Examination of drilling logs for private wells near the river shows that there is often fine-grained material near the water table, which sometimes acts as a locally confining unit. After water-bearing sediments are encountered, the water level in the well rises into the depth interval corresponding to the fine-grained material. The presence of low-permeability sediments near the river would also explain the lack of water-level response to the river stage at well 699-S24-19. However, because this well responds to filling of the canal, which is closer to the well, it is likely that the low-permeability sediments do not extend to the canal location. The lack of response could also be explained by recent silt deposits in the bed of the river.

The presence of low-permeability sediments along the Yakima River is also illustrated at the ACME Materials and Construction Inc. gravel pit located adjacent to the Yakima River near its confluence with the Columbia River. The southwestern corner of the gravel pit is within about 300 m of the river and the sediments have been removed down to a clay layer at a depth of about 12 to 18 m, well below the river level. Pumps remove water from the pit at a rate of more than 3800 m³/d. However, no inflow is observed on the river side of the pit. Instead, the water is entering from the north wall.



S9410005.3

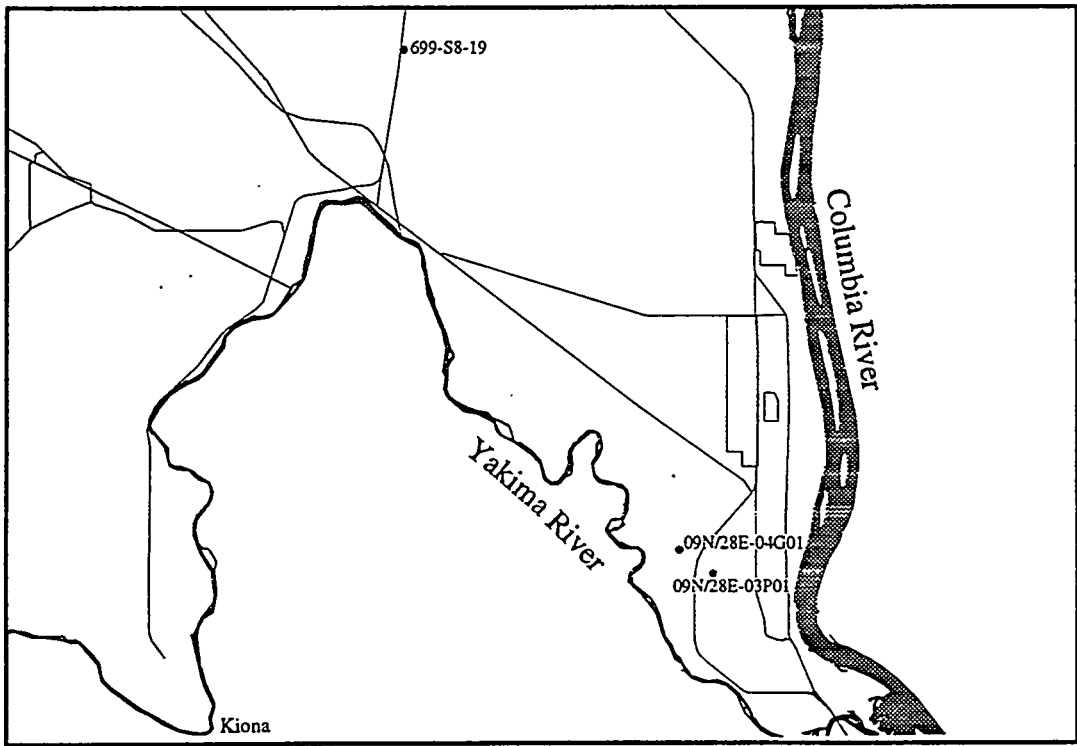


Figure 6.1. Major-Ion Composition of Water from the Ringold Formation, the Saddle Mountain Basalt, and the Yakima River at Kiona (modified from Ebbert et al. 1993)

6.3 Cold Creek Valley

The boundary of the model region crosses the mouth of the Cold Creek Valley at the northwestern corner of the Hanford Site. This is an area where the model boundary does not coincide with a physical boundary of the unconfined aquifer flow system. The unconfined aquifer sediments extend into the valley and are a conduit for recharge to the Hanford Site aquifer system. Actual recharge from Cold Creek Valley is not known. However, the U.S. Geological Survey has been conducting a study of the area, which may soon provide additional information.

Jacobson and Freshley (1990) used a prescribed-flux boundary with an assumed recharge of about 9100 m³/d at the mouth of the Cold Creek Valley in two of the cases they ran for the inverse calibration model. The result in both cases was unrealistically high head values calculated by the model in the vicinity of Cold Creek Valley. Therefore, either the prescribed recharge at this boundary was too large or transmissivities in the area were set too low. Better results were obtained by Jacobson and Freshley when using a prescribed-head boundary. However, uncertainty in the transmissivity distribution remains because it is not known if the recharge calculated by the model at this boundary, which depends on the head difference across the boundary and the transmissivity of the adjacent model elements, is realistic.

An hydraulic test was conducted at well 699-43-104 during the past year (see Appendix A). This test resulted in a relatively low transmissivity estimate of 25 m²/d and an equivalent hydraulic conductivity of about 2 m/d. However, these values may not be representative of the bulk of Cold Creek Valley sediments. Additional work needs to be done to better define the recharge boundaries at the mouth of Cold Creek and Dry Creek valleys.

6.4 Interflow with the Basalt Confined Aquifer System

Flow-system boundaries are formed by the contact between the unconfined aquifer system and basalt. At places where basalt subcrops above the water table, this contact may form either a perimeter boundary or an island of basalt within the model area. The basalt contact also forms the lower boundary of the unconfined aquifer system except in some areas where a mud unit may underlie the aquifer directly over basalt.

Some of the perimeter basalt contact boundaries (i.e., Rattlesnake Mountain) are recharge boundaries because of the infiltration of precipitation runoff and spring discharge from the upper slopes. There is also a potential for interflow (recharge or discharge) between the basalt confined aquifer system and the unconfined aquifer system at the lower boundary. Over most of the site, the amount of interflow is thought to be small because of the low hydraulic conductivity of the rock separating the two aquifer systems. However, areas of increased vertical communication have been previously identified in the Gable Mountain and Gable Butte area on the basis of chemistry data (Graham et al. 1984; Jensen 1987). Hydraulic head data for the uppermost confined basalt aquifer also indicates the potential for water to discharge from this aquifer upward into the unconfined system in the northeastern part of the Hanford Site (Spane and Raymond 1993).

Another potential area of increased vertical communication is in the vicinity of the Yakima River horn, where the river may have incised the upper basalt confining layers. A recent investigation (WHC 1993) identified a bimodal distribution of chloride in the unconfined aquifer in this area. Some wells yield concentrations of < 10 mg/L and other wells have > 20 mg/L. The lower concentration ground water is chemically similar to water from Rattlesnake Hills springs, suggesting that this ground water comes from subsurface discharge from the underlying basalts. The ground water with higher chloride concentrations may come from infiltration of surface flow, which is subject to greater evaporation.

The rate of groundwater movement between the confined and unconfined aquifer systems is difficult to quantify. Therefore, it is not known if ignoring this contribution has a significant effect on the accuracy of the ground-water flow model. Differences in ground-water chemistry and temperature offer two possible methods for identifying areas of enhanced intercommunication and possibly quantifying flow rates. The possible use of temperature logs for this purpose has been preliminarily investigated and results are presented in Appendix B.

6.5 Natural Areal Recharge

A prescribed-flux distribution may be associated with the upper aquifer boundary to represent the input of water from natural or artificial recharge. Past estimates of recharge have been summarized in earlier status reports (Thorne and Chamness 1992; Thorne et al. 1993). However, additional work has been conducted during the past year to improve the estimated distribution of natural recharge. A recharge map was developed by determining the combination of soil and vegetation types for locations across the Hanford Site. A recharge rate was then assigned to each combination on the basis of data from lysimeters, tracer studies, neutron probe measurements, and computer modeling. Estimated recharge rates were found to range from 0.26 to 12.7 cm/yr and the total volume of natural recharge from precipitation over the Hanford Site is estimated at 0.32 m³/s. Complete documentation of the newly estimated recharge distribution will be provided in a future report. A preliminary version of the recharge map was provided by Dresel et al. (1994).

6.6 Artificial Recharge

During the past 40 years, the volume of artificial recharge caused by wastewater discharged to disposal facilities on the Hanford Site has been greater than natural recharge and has significantly affected the ground-water flow system. The volume of artificial recharge is currently decreasing (Dresel et al. 1994). B Pond is currently the largest source of artificial recharge on the Hanford Site. However, until it was taken out of service in 1984, Gable Mountain Pond received a larger volume of discharge. Major ground-water mounds have occurred beneath B Pond, Gable Mountain Pond, and U Pond, and have affected sitewide ground-water flow patterns (Bierschenk 1959; Dresel et al. 1993). Wastewater is no longer being discharged to U Pond or Gable Mountain Pond, which have been decommissioned and are now dry. Other smaller-volume recharge sources exist in the 200, 100, and 300 Areas and may affect ground-water flow on a local scale. These sources could be important in simulations of contaminant transport if they are near, or coincident with, contaminant sources.

The City of Richland infiltration ponds, agricultural and lawn irrigation, and ground disposal of wastewater at a potato-processing plant are other sources of artificial recharge that may affect groundwater flow in the North Richland area and in the southern part of the Hanford Site (Liikala 1994).

7.0 Hydraulic Heads

The hydraulic head distribution for the unconfined aquifer on the Hanford Site and the surrounding area is determined each year by measuring water levels at more than 600 wells. Results of the measurements made in 1993 are presented in Dresel et al. (1994). Additional water-level data for the North Richland area are provided in Liikala (1994). The annual water-level measurements provide an extensive data base that can be used to define initial head conditions for numerical modeling and for a comparison of modeling runs with historical data.

Most of the wells in the current unconfined aquifer monitoring network are completed in the upper part of the aquifer, within 7 m of the water table. Three-dimensional modeling will require more extensive information on the vertical distribution of hydraulic head. Therefore, a listing of wells completed at greater depths and wells with individual piezometers open to different depth intervals has been compiled (Thorne et al. 1993). Water-level measurements in these wells and piezometers are planned and will provide data on vertical hydraulic head distributions.

8.0 Contaminant Distributions

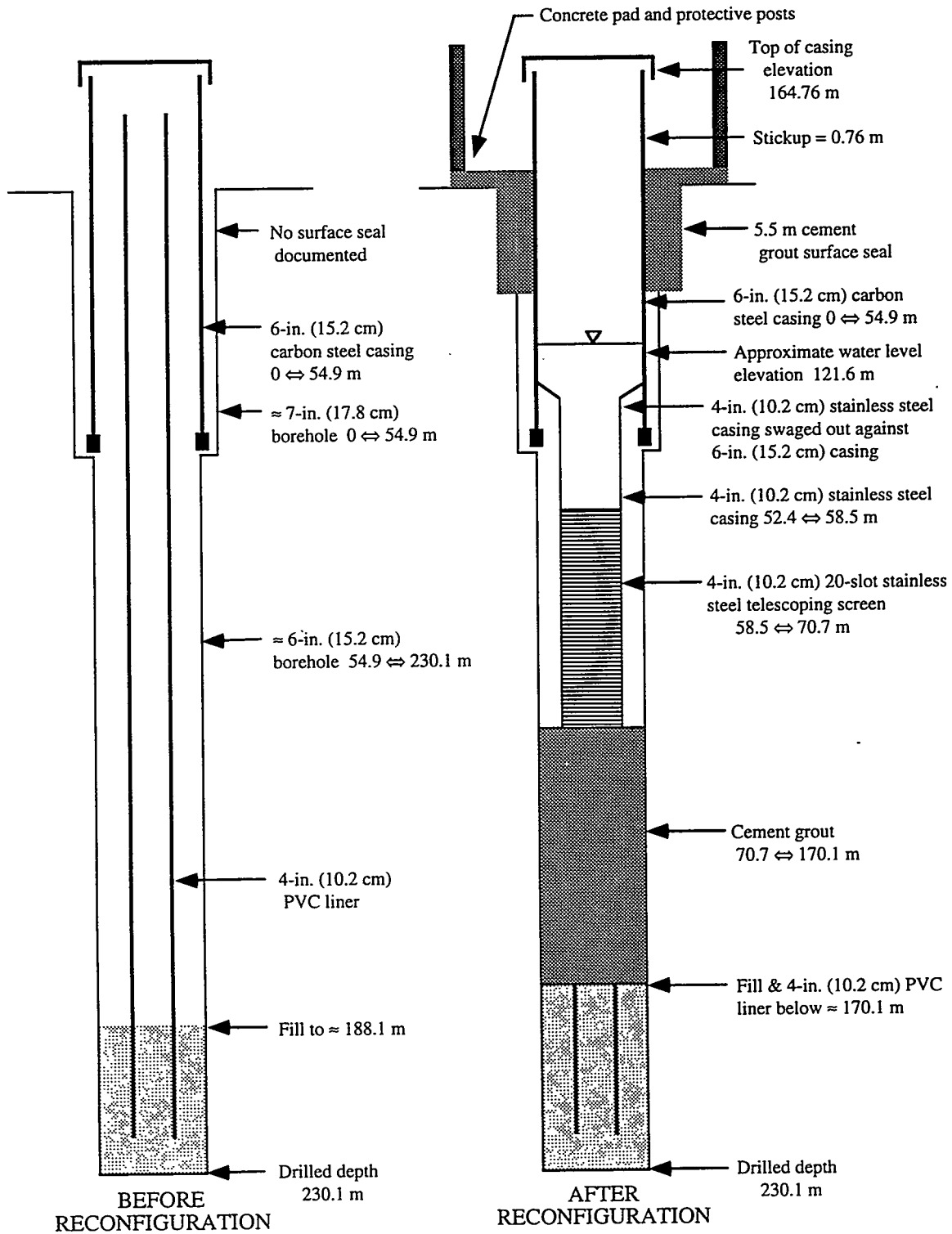
Information on the distributions of contaminants within the unconfined aquifer is needed for setting initial conditions for the numerical transport model. Contaminants also act as tracers for the movement of ground water within the flow system. For verification purposes, the historical movement of contaminant plumes can be compared to ground-water flow directions predicted by the flow model and to contaminant distributions predicted by the transport model.

The concentrations of both chemical and radiological contaminants are measured in hundreds of Hanford Site wells each year. Contaminant distributions measured during 1993 and information on sampling and analysis techniques are provided in Dresel et al. (1994). Like the hydraulic-head measurement network, the sampling network is composed mainly of wells completed in the upper part of the unconfined aquifer system, generally less than 7 m (20 ft) below the water table. A limited number of wells completed in the upper basalt confined aquifer system are also sampled each year (Evans et al. 1992).

Two existing "Golder" wells, 699-18-21 and 699-31-11, were reconfigured in 1993 to provide access to an intermediate depth interval of the unconfined aquifer. Details of the well reconfiguration were provided in Thorne et al. (1993). However, a correction should be noted for the new configuration of well 699-18-21. The as-built diagram presented in Thorne et al. (1993) showed the screened interval from 173.7 ft to 219.3 ft (52.9 m to 66.8 m). The actual screened interval is from 192 ft to 232 ft (58.5 m to 70.7 m) as shown in Figure 8.1.

Analysis results of water samples collected from well 699-31-11 and analyzed for tritium and iodine-129 were reported in Thorne et al. (1993). Samples were collected from well 699-18-21 during FY 94 and results are presented in this report. The analysis results for well 699-18-21, which is open to a depth interval 16.4 to 28.6 m below the current water table, were about 155,000 pCi/L for tritium and 0.2 pCi/L for iodine-129. These concentrations are consistent with those found in nearby sampling network wells completed at the top of the aquifer. The tritium concentration is about 25% higher than the concentration reported for well 699-20-20, which is the nearest sampling network well (Dresel et al. 1994). Well 699-18-21 is completed at the bottom of Unit 1, an extensive sand and gravel unit that is found below the water table mainly in the western half of the Hanford Site. Nearby sampling network wells are completed at the top of the saturated zone in Unit 1.

One objective of the sampling at the reconfigured wells was to determine if contaminated water could migrate vertically downward along the existing well casing during pumping, resulting in false indications of contaminants at depth. Therefore, samples for tritium were taken three times during development pumping. A plot of the tritium results in relation to pumped volume is shown in Figure 8.2. The increasing trend may indicate vertical leakage along the casing. The results of samples taken at well 699-31-11 during development indicated a decrease in tritium concentration over time (Thorne et al. 1993). According to the geologic log (PSPL 1982), no obvious locally confining units are present above the screened interval at this location.



Note: Not to scale

Figure 8.1. Corrected As-Built Diagram for the Reconfigured Well 699-18-21 (Golder S-12)

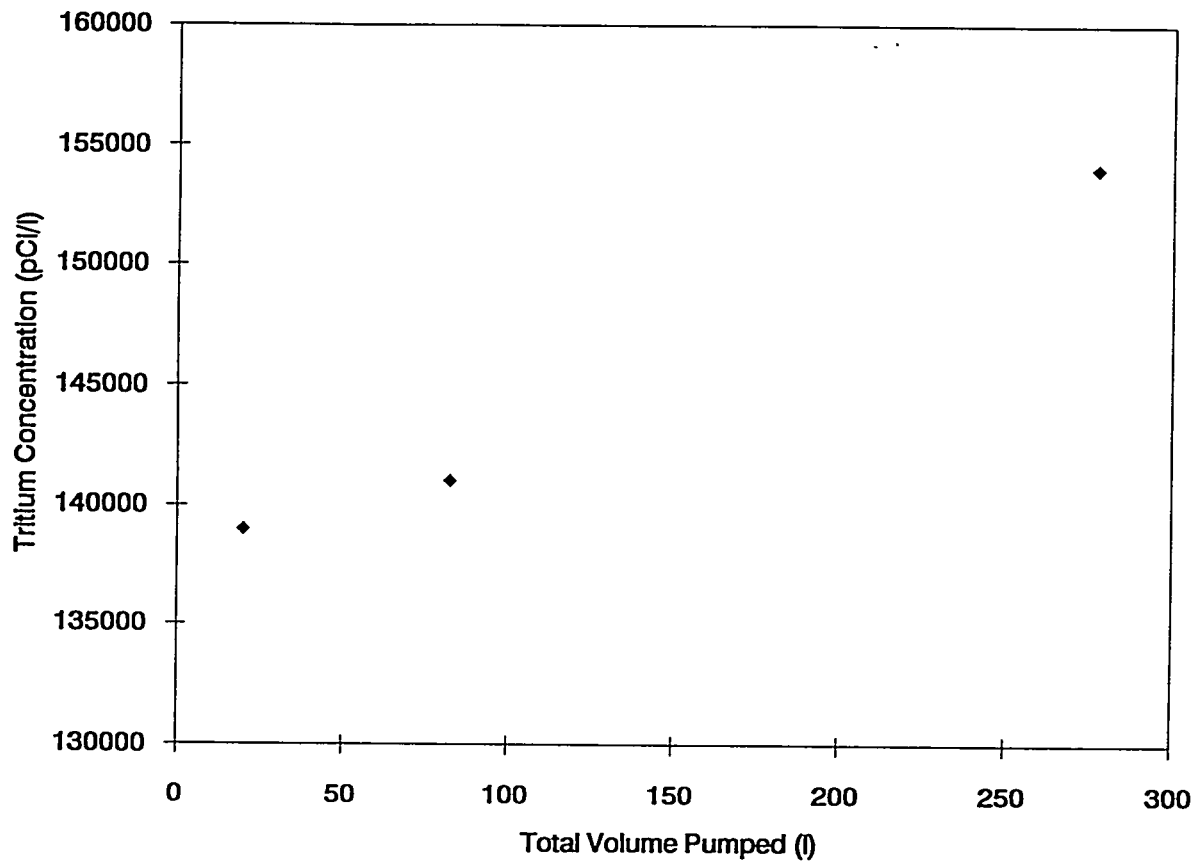


Figure 8.2. Tritium Concentration Trend During Development Pumping of the Reconfigured Golder Well 699-18-21

9.0 References

- Bauer, H. H., and J. J. Vaccaro. 1990. *Estimates of Ground-Water Recharge to the Columbia Plateau Regional Aquifer System, Washington, Oregon, and Idaho for Predevelopment and Current Land Use Conditions*. Water Resources Investigation Report 88-4108, U.S. Geological Survey, Tacoma, Washington.
- Bauer, H. H., J. J. Vaccaro, and R. C. Lane. 1985. *Maps Showing Ground-Water Levels in the Columbia River Basalt and Overlying Materials, Spring 1983, Southeastern Washington*. Water Resources Investigation Report 84-4360, U.S. Geological Survey, Tacoma, Washington.
- Bierschenk, W. H. 1959. *Aquifer Characteristics and Ground-Water Movement at Hanford*. HW-60601, General Electric Company, Hanford Atomic Products Operation, Richland, Washington.
- Cearlock, D. B., K. L. Kipp, and D. R. Friedrichs. 1975. *The Transmissivity Iterative Calculation Routine - Theory and Numerical Implementation*. BNWL-1706, Pacific Northwest Laboratory, Richland, Washington.
- Chamness, M. A., and J. K. Merz. 1993. *Hanford Wells*. PNL-8800, Pacific Northwest Laboratory, Richland, Washington.
- Connelly, M. P., B. H. Ford, and J. W. Lindberg. 1992a. *Hydrogeologic Model for the 200 East Groundwater Aggregate Area*. WHC-SD-EN-TI-019, Westinghouse Hanford Company, Richland, Washington.
- Connelly, M. P., B. H. Ford, and J. V. Borghese. 1992b. *Hydrogeologic Model for the 200 West Groundwater Aggregate Area*. WHC-SD-EN-TI-014, Westinghouse Hanford Company, Richland, Washington.
- Connelly, M. P. 1994. *Capture Zone Analyses for the 200-ZP-1 and 200-UP-1 Pilot Scale Pump-and-Treat Tests*. WHC-SD-EN-TI-252, Westinghouse Hanford Company, Richland, Washington.
- Cushing, C. E. (ed.). 1994. *Hanford Site National Environmental Policy Act (NEPA) Characterization*. PNL-6415, Rev. 6, Pacific Northwest Laboratory, Richland, Washington.
- Davis, S. N. 1969. "Porosity and Permeability of Natural Materials." In *Flow Through Porous Media*, ed. R. J. M. DeWiest, pp. 54-89. Academic Press, New York.
- Deju, R. A. 1974. *The Hanford Field Testing Program*. ARHC-00004-201, Atlantic Richfield Hanford Company, Richland, Washington.
- DOE (see U.S. Department of Energy)

- Evans, J. C., R. W. Bryce, and D. J. Bates. 1992. *Hanford Site Ground-Water Monitoring for 1991*. PNL-8284, Pacific Northwest Laboratory, Richland, Washington.
- Freeze, R. A., and J. A. Cherry. 1979. *Groundwater*. Prentice-Hall, Inc., Englewood Cliffs, New Jersey.
- Freshley, M. D., and P. D. Thorne. 1992. *Ground-Water Contribution to Dose From Past Hanford Operations*. PNWD-1974 HEDR, Pacific Northwest Laboratory, Richland, Washington.
- Gee, G. W., and P. R. Heller. 1985. *Unsaturated Water Flow at the Hanford Site: A Review of Literature and Annotated Bibliography*. PNL-5428, Pacific Northwest Laboratory, Richland, Washington.
- Graham, M. J., G. V. Last, and K. R. Fecht. 1984. *An Assessment of Aquifer Intercommunication in the B Pond, Gable Mountain Pond Area*. RHO-RE-ST-12P, Rockwell Hanford Operations, Richland, Washington.
- Hartman, M. J., and K. A. Lindsey. 1993. *Hydrogeology of the 100-N Area, Hanford Site, Washington*. WHC-SD-EN-EV-027, Westinghouse Hanford Company, Richland, Washington.
- Jacobson, E. A., and M. D. Freshley. 1990. *An Initial Inverse Calibration of the Ground-Water Flow Model for the Hanford Unconfined Aquifer*. PNL-7144, Pacific Northwest Laboratory, Richland, Washington.
- Jensen, E. J. 1987. *An Evaluation of Aquifer Intercommunication Between the Unconfined and Rattlesnake Ridge Aquifers on the Hanford Site*. PNL-6313, Pacific Northwest Laboratory, Richland, Washington.
- Kipp, K. L., and R. D. Mudd. 1973. *Collection and Analysis of Pump Test Data for Transmissivity Values*. BNWL-1709, Pacific Northwest Laboratory, Richland, Washington.
- Liikala, T. L. 1994. *Hydrogeology Along the Southern Boundary of the Hanford Site Between the Yakima and Columbia Rivers, Washington*. PNL-10094, Pacific Northwest Laboratory, Richland, Washington.
- Lindberg, J. W. 1993a. *Geology of the 100-B/C Area, Hanford Site, South-Central Washington*. WHC-SD-EN-TI-133, Westinghouse Hanford Company, Richland, Washington.
- Lindberg, J. W. 1993b. *Geology of the 100-K Area, Hanford Site, South-Central Washington*. WHC-SD-EN-TI-155, Westinghouse Hanford Company, Richland, Washington.
- Lindsey, K. A. 1991. *Revised Stratigraphy for the Ringold Formation, Hanford Site, South-Central Washington*. WHC-SD-EN-EE-004 Rev. 0, Westinghouse Hanford Company, Richland, Washington.

- Liikala, T. L., and R. L. Aaberg. 1988. *Geohydrologic Characterization of the Area Surrounding the 183-H Solar Evaporation Basins*. PNL-6728, Pacific Northwest Laboratory, Richland, Washington.
- Liikala, T. L. 1994. *Hydrogeology Along the Southern Boundary of the Hanford Site Between the Yakima and Columbia Rivers, Washington*. PNL-10094, Pacific Northwest Laboratory, Richland, Washington.
- Lindberg, J. W., and F. W. Bond. 1979. *Geohydrology and Ground-Water Quality Beneath the 300 Area, Hanford Site, Washington*. PNL-2949, Pacific Northwest Laboratory, Richland, Washington.
- Lindberg, J. W. 1993a. *Geology of the 100-B/C Area, Hanford Site, South-Central Washington*. WHC-SD-EN-TI-133, Westinghouse Hanford Company, Richland, Washington.
- Lindberg, J. W. 1993b. *Geology of the 100-K Area, Hanford Site, South-Central Washington*. WHC-SD-EN-TI-155, Westinghouse Hanford Company, Richland, Washington.
- Lindsey, K. A. 1991. *Revised Stratigraphy for the Ringold Formation, Hanford Site, South-central Washington*. WHC-SD-EN-EE-004 Rev. 0, Westinghouse Hanford Company, Richland, Washington.
- Lindsey, K. A. 1992. *Geology of the Northern Part of the Hanford Site: An Outline of Data Sources and the Geologic Setting of the 100 Areas*. WHC-SD-EN-TI-011, Rev. 0, Westinghouse Hanford Company, Richland, Washington.
- Lindsey, K. A., B. N. Bjornstad, and M. P. Connelly. 1991. *Geologic Setting of the 200 West Area: An Update*. WHC-SD-EN-TI- 008, Westinghouse Hanford Company, Richland, Washington.
- Lindsey, K. A. and G. K. Jaeger. 1993. *Geologic Setting of the 100-HR-3 Operable Unit, Hanford Site, South-Central Washington*. WHC-SD-EN-TI-132, Westinghouse Hanford Company, Richland, Washington.
- Lindsey, K. A., B. N. Bjornstad, J. W. Lindberg, and K. M. Hoffman. 1992. *Geologic Setting of the 200 East Area: An Update*. WHC-SD-EN-TI-012, Westinghouse Hanford Company, Richland, Washington.
- Luttrell, S. P., D. R. Newcomer, S. S. Teel, and V. R. Vermeul. 1992. *Hydrogeologic Controls on Ground-Water and Contaminant Discharge to the Columbia River Near the Hanford Townsite*. PNL-8167, Pacific Northwest Laboratory, Richland, Washington.
- Newcomb, R. C., J. R. Strand, and F. J. Frank. 1972. *Geology and Ground-Water Characteristics of the Hanford Reservation of the U.S. Atomic Energy Commission, Washington*. Prof. Paper 717, U.S. Geological Survey, Washington, D.C.
- Peterson, R. E. 1992. *Hydrologic and Geologic Data Available for the Region North of Gable Mountain, Hanford Site, Washington*. WHC-SD-EN-TI-006, Westinghouse Hanford Company, Richland, Washington.

Prater, L. S., J. T. Reiger, C. S. Cline, E. J. Jensen, and T. L. Liikala. 1984. *Ground-Water Surveillance at the Hanford Site for CY-1983*. PNL-5041, Pacific Northwest Laboratory, Richland, Washington.

Puget Sound Power and Light (PSPL). 1982. *Skagit/Hanford Nuclear Project, Preliminary Safety Analysis Report*. Appendix 20, Amendment 23, Puget Sound Power and Light Company, Bellevue, Washington.

PSPL (see Puget Sound Power and Light)

Reidel, S. P., K. A. Lindsey, and K. R. Fecht. 1992. *Field Trip Guide to the Hanford Site*. WHC-MR-0391, Westinghouse Hanford Company, Richland, Washington.

Spane, F. A., Jr., and R. G. Raymond. 1993. *Preliminary Potentiometric Map and Flow Dynamic Characteristics for the Upper-Basalt Confined Aquifer System*. PNL-8869, Pacific Northwest Laboratory, Richland, Washington.

Spane, F. A., Jr. 1993. *Selected Hydraulic Test Analysis Techniques for Constant-Rate Discharge Tests*. PNL-8539, Pacific Northwest Laboratory, Richland, Washington.

Swanson, L. C. 1992. *Phase 1 Hydrogeologic Summary of the 300-FF-5 Operable Unit, 300 Area*. WHC-SD-EN-TI-052, Westinghouse Hanford Company, Richland, Washington.

Swanson, L. C. 1994. *1994 Characterization Report for the State Approved Land Disposal Site*. WHC-SD-CO18H-RPT-003, Westinghouse Hanford Company, Richland, Washington.

Thorne, P. D., and M. A. Chamness. 1992. *Status Report on the Development of a Three-Dimensional Conceptual Model for the Hanford Site Unconfined Aquifer System*. PNL-8332, Pacific Northwest Laboratory, Richland, Washington.

Thorne, P. D., M. A. Chamness, F. A. Spane, V. R. Vermeul, and W. D. Webber. 1993. *Three-Dimensional Conceptual Model for the Hanford Site Unconfined Aquifer System, FY93 Status Report*. PNL-8971, Pacific Northwest Laboratory, Richland, Washington.

Thorne, P. D., and D. R. Newcomer. 1992. *Summary and Evaluation of Available Hydraulic Property Data for the Hanford Site Unconfined Aquifer System*. PNL-8337, Pacific Northwest Laboratory, Richland, Washington.

U.S. Department of Energy (DOE). 1988. *Consultation Draft, Site Characterization Plan, Reference Repository Location, Hanford Site, Washington*. DOE/RW-0164, Vol. 1 and 2, U.S. Department of Energy, Richland, Washington.

WHC (see Westinghouse Hanford Company)

Westinghouse Hanford Company (WHC). 1993. *Westinghouse Hanford Company Operational Groundwater Status Report, 1990-1992*. WHC-EP-0595, Westinghouse Hanford Company, Richland, Washington.

Appendix A

Analyses of Constant-Rate Discharge Tests Conducted to Support the Three-Dimensional Conceptual Model

Appendix A

Analyses of Constant-Rate Discharge Tests Conducted to Support the Three-Dimensional Conceptual Model

This appendix provides detailed information on the analyses of constant-rate discharge tests conducted during the past year to support development of the Hanford sitewide three-dimensional conceptual model. Constant-rate tests were conducted at wells 699-S19-11, 699-S14-20, 699-4E-6, 699-18-21, 699-31-11, and 699-43-104. These wells were selected for testing based on location and the lack of previous reliable hydraulic tests at the well.

Two of the wells, 699-18-21 and 699-31-11, are "Golder" wells that were reconfigured during 1993 (Thorne et al. 1993). These wells had previously been drilled to basalt for seismic measurements and were completed with a 4-in. (10.2-cm) plastic liner that did not allow access to the aquifer. The plastic liners were removed and screens were placed to provide access to a selected depth interval.

A.1 Test Methods and Equipment

To conduct a constant-rate discharge test, water is removed from a well at a constant flow rate and the associated water-level drawdown is measured over time at the pumping well and, if available, at one or more nearby observation wells. When pumping is stopped, recovery water levels may also be measured and analyzed.

A submersible pump was used to remove water from each of the wells at a nearly constant rate. Flow rates were checked by monitoring a flow meter and flow was adjusted with a gate valve to maintain a nearly constant rate. Pressure transducers manufactured by Keller Inc. were used to monitor water levels in the pumping well and any nearby observation wells during the test. The transducers were vented at the surface to automatically compensate for atmospheric pressure fluctuations. Flow rates were measured with turbine flow meters manufactured by Omega Engineering Inc. Measurements from the transducers and flow meter were automatically recorded by a Campbell Scientific Inc. model CR-10 data logger. Water levels were also measured periodically with an e-tape and flow meter measurements were checked by measuring the time required to fill a container of known volume.

All of the tested wells were approved for discharge of purge water to the ground. Therefore, the water was discharged to ground at a point at least 100 m from the pumped well to minimize the possible effects of infiltration.

A.2 Barometric Pressure Effects

Although the pressure transducers were vented to compensate for changes in barometric pressure, changes in the water level in a well can also result from barometric fluctuations. This response is strongest for confined aquifers. However, wells in unconfined aquifers also may show some response to barometric changes (Weeks 1979). To determine the significance of barometric effects, water-level changes were monitored during a baseline period and compared to barometric pressure change. The barometric efficiency was then calculated according to the method presented by Clark (1967). If barometric changes were significant enough to affect the test analysis, the barometric efficiency value was used to correct the water levels observed during testing.

A.3 Analysis Methods

The mathematical solution for transient drawdown, s , in an aquifer resulting from radial flow of compressible ground water to a well pumped at a constant rate was given by Theis (1935) as:

$$s = \frac{Q}{4\pi T} W(u)$$

where: T = transmissivity of the aquifer
 Q = constant discharge rate.

The dimensionless well function, $W(u)$, in this equation is defined as:

$$W(u) = \int_u^{\infty} \frac{e^{-u}}{u} du$$

where: $u = \frac{r^2 S}{4Tt}$

and where: r = radial distance to the pumping well
 S = storativity of the aquifer.

The Theis equation is based on several assumptions including: 1) the aquifer is confined, homogeneous, isotropic, and of infinite lateral extent; 2) the well is a line-sink (i.e., has no storage); 3) the well completely penetrates the aquifer; and 4) flow is laminar. Although all of these conditions are rarely met, the effect on hydraulic property determination is often negligible. Other equations have also been presented for cases where one or more of these assumptions are not met. The Boulton (1963) and Neuman (1974 and 1975) equations account for delayed yield from unconfined aquifers. The image well method (Ferris et al. 1962) may be used for analysis of tests in bounded aquifers. Corrections for the effects of vertical flow gradients caused by partially penetrating wells have been presented by Hantush (1962), Dagan (1967), Kipp (1973), and Neuman (1974).

Type-Curve Matching Methods

Because $W(u)$ and $1/u$ are proportional to s and t , the Theis equation can be plotted as $\log[W(u)]$ versus $\log(1/u)$ to construct a dimensionless "type curve." The type curve can then be matched to test data plotted as $\log(s)$ versus $\log(t)$. Coordinates of corresponding "match points" on the type curve and data plot provide values of $W(u)$, u , s , and t , which are used with the equations above to calculate values for T and S , respectively (Theis 1935).

Unconfined aquifers produce ground water from both elastic storage and gravity drainage because the water table is not fixed during testing. This causes the drawdown response during pumping tests to depart from that predicted by the Theis equation. Walton (1960) states that unconfined aquifer constant-rate discharge tests conducted within fully penetrating wells are characterized by the presence of three distinct segments on a time-drawdown curve. In the first segment, the aquifer reacts as would a confined aquifer, with ground water produced through expansion of water and compression of the aquifer matrix. Drawdowns during this segment follow that predicted using the Theis equation, with aquifer storage equal to its elastic component (S). During the second segment of the drawdown curve, the rate of drawdown decreases as gravity drainage, which induces a vertical ground-water flow component, becomes important. Gravity drainage (also referred to as delayed yield) within the unconfined aquifer causes the time-drawdown curve to deviate significantly from that predicted by the Theis equation because the gravity drainage/vertical ground-water flow components "reflect the presence of recharge in the vicinity of the pumped well" (Walton 1960). During the third segment, the vertical flow component becomes insignificant and radial flow conditions are once again predominant within the aquifer. Drawdowns during the third segment once again follow that predicted using the Theis equation, with aquifer storage equal to its combined elastic component (S) and specific yield (S_y).

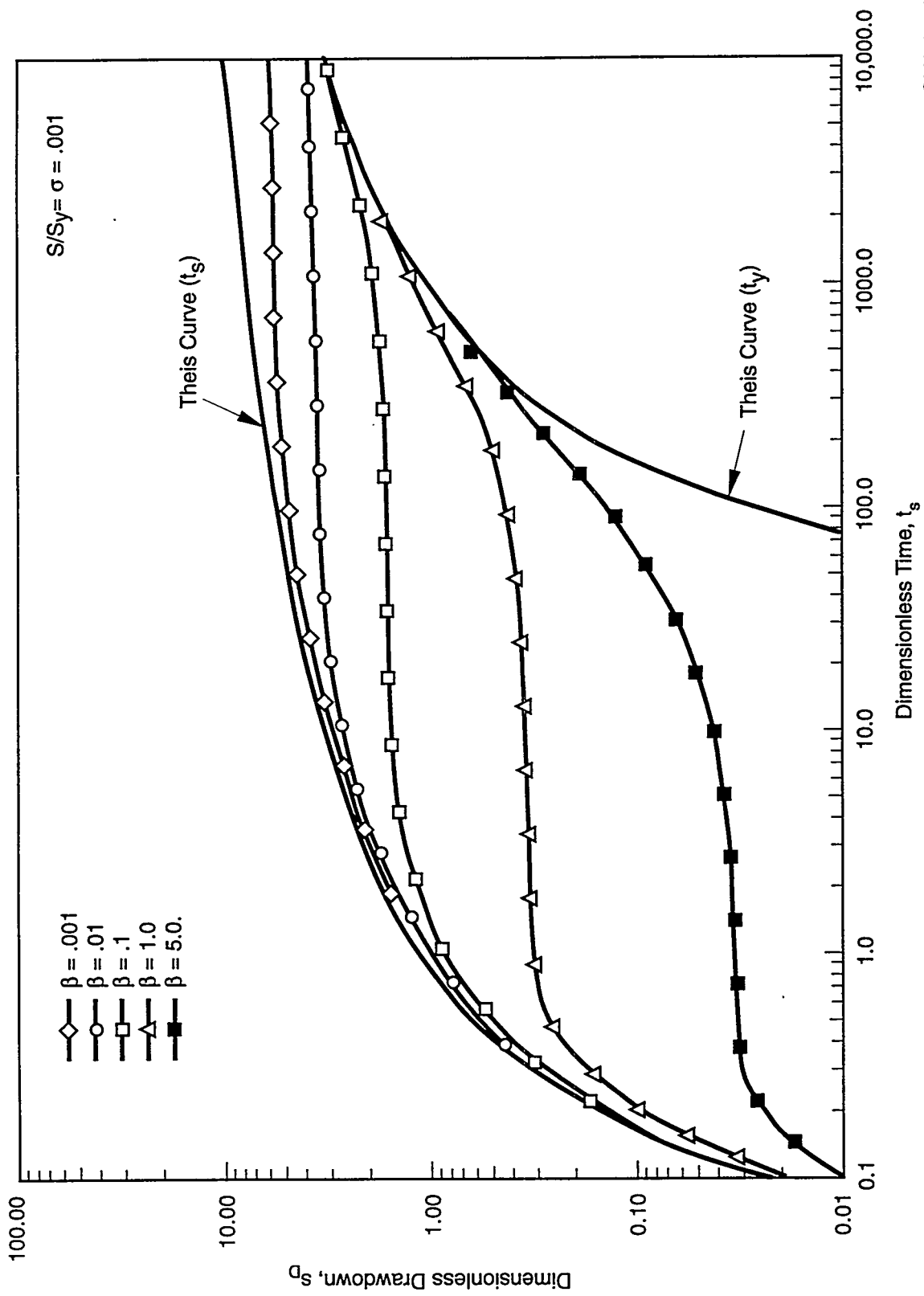
Because of the vertical flow that takes place within an unconfined aquifer, differences between vertical and horizontal hydraulic conductivity become important. Figure A.1 shows typical dimensionless unconfined aquifer responses for various β (β) values and a ratio of $S/S_y = 0.001$:

where $\beta = (K_v/K_h)(r/b)^2$

and where K_h = horizontal hydraulic conductivity
 K_v = vertical hydraulic conductivity.

The relative degree of separation between the first and third segments of flow depends on the ratio S/S_y (or σ). Therefore, a universal set of type curves for drawdown in an unconfined aquifer cannot be developed because a separate set of type curves, similar to that shown in Figure A.1, exists for each value of σ .

Neuman (1975) developed type curves, however, that can be used separately to describe the first and second segments of unconfined aquifer flow (Neuman Type A), and the second and third segments of unconfined aquifer response (Neuman Type B). Neuman Type A curves are expressed with respect



S9410005.4

Figure A.1. Dimensionless Type Curves Showing the Entire Response for Constant-Rate Discharge Tests in Unconfined Aquifers With $\sigma = 10^{-3}$

to the dimensionless time parameter (t_x), while Neuman Type B curves use the dimensionless time parameter (t_y); where, t_x and t_y are defined as:

$$t_x = (Tt)/(r^2 S)$$

$$t_y = (Tt)/(r^2 S_y)$$

The standard type-curve analysis procedure for unconfined aquifer tests is to match the observed drawdown response at an observation well to a family of either Neuman Type A or Neuman Type B curves. The shape of the observed response curve indicates which of the three segments of the unconfined aquifer response are present and whether Type A or Type B curves should be used. In some cases, the test data include all three segments and matches can be made to both the Type A and Type B curves. Matching late-time test data with Neuman Type B curves allows the determination of β , T , and S_y ; whereas, matching early-time test data with Neuman Type A curves allows the independent determination of β , T , and S . Values of β and T determined from the two separate matches should be approximately the same. Based on the value of β corresponding to the type-curve selected in the curve-matching process, the vertical anisotropy ($K_D = K_v/K_h$) can also be determined from Equation 8, provided that the observation well distance, r , and aquifer thickness, b , are known.

Neuman (1974, 1975) also considered the case where either the pumping or observation wells partially penetrate an unconfined aquifer. In this situation, the number of independent dimensionless parameters in the equation for drawdown increases from three for the fully penetrating case to seven. As stated by Neuman (1975, p. 337), "This large number of dimensionless parameters makes it practically impossible to construct a sufficient number of type curves to cover the entire range of values needed for field application." However, if the aquifer thickness and depth of penetration of both the pumping and observation wells are known, it is possible, through use of a computer program, to calculate type curves for each particular field case. Curve-matching analyses can then be performed in the same manner as for the fully penetrating well case.

Type-curve matching methods are, however, generally applicable only to data from observation wells. Errors may be introduced by applying type-curve matching methods for analysis of pumping well data. This is because friction loss at the pumping well may cause an additional component of drawdown independent of the aquifer response. The additional drawdown causes the data to be shifted vertically on the log-log plot employed in type-curve matching and introduces error in the calculated transmissivity and storativity values. Attempts have been made to determine the friction loss component through step-drawdown tests and then correct the drawdown measurements prior to type-curve matching. However, the semilog straight-line method described below is considered a more reliable technique for analyzing data from a pumping well.

Semilog Straight-Line Method

Cooper and Jacob (1946) presented a method for analyzing constant-rate discharge tests by fitting a straight line to drawdown data plotted versus the log of time. They showed that the Theis equation could be approximated by

$$s = \frac{Q}{4\pi T}(-0.5772 - \ln u)$$

for small values of u . Therefore, the slope of a straight line fitted to the data is inversely proportional to transmissivity. Storativity can also be determined from the intercept of the straight line with the y-axis. However, the storativity result is usually not accurate for pumping well data. This is because of the vertical shift of drawdown data caused by friction losses and other pumping well effects.

As indicated by Cooper and Jacob (1946), semilog straight-line methods are only valid for small values of the parameter u , which corresponds to relatively large values of time. It is generally accepted that the method is valid when $u < 0.01$. However, in some cases the error introduced by using data corresponding to somewhat larger values of u in straight-line analysis is minor (Chapuis 1992). The semilog method may be applied to drawdown or recovery data and is not affected by friction losses at the well. However, this method is only applicable to data that reflect infinite-acting radial flow in the aquifer. The method is often misapplied to data that are affected by boundaries, delayed yield, aquifer leakage, or other non-ideal well and formation conditions. Use of the derivative diagnostic technique described below is helpful in identifying ranges of data that can be analyzed with the semilog straight-line method.

Derivative Diagnostic Technique

The key to determining correct aquifer hydraulic properties using the semilog straight-line technique is determining which data segment represents infinite-acting radial flow as assumed by the Theis equation. Often, more than one straight-line segment will appear on a semilog plot due to nonideal aquifer conditions. Therefore, it is important to recognize when nonideal well or aquifer effects are significant. These effects may be discerned by preparing a diagnostic plot of the test data and comparing it to characteristic curves associated with various nonideal conditions. Log-log plots of water level versus time have traditionally been used for diagnostic purposes and, more recently, the derivative of the water-level or pressure change has also been used (Bourdet et al. 1984, Spane 1993) as a diagnostic tool.

A log-log plot of the water-level response versus time is prepared and the derivative of the semilog plot is then calculated and graphed on the log-log plot with the water-level data. For recovery data, the "Agarwal equivalent time function" (Agarwal 1980) or some other superposition function is used in calculating the derivative. This accounts for the effects of the pumping period and causes the recovery data to fall on a straight line (constant derivative) on the semilog plot. The effects of various aspects of the well-aquifer system show up on the derivative plot and can be easily correlated with features of the log-log plot that have traditionally been used to diagnose test behavior.

Figure A.2 shows log-log drawdown and derivative responses that are characteristic of some commonly encountered aquifer conditions. The early data, occurring before the straight-line approximation is valid or where wellbore storage is dominant produces a steep upward trending derivative. The derivative normally decreases during transition from wellbore storage to radial flow, and stabilizes at a constant value when radial infinite-acting flow conditions are established. The stable derivative reflects the straight line on the semi-log plot for infinite-acting radial flow. Delayed yield and double-porosity aquifers may show two stable derivative sections at the same vertical position, separated by a "valley" representing the transition from one storage value to the other. Pressure derivative plots are also useful in identifying boundary effects. A linear no-flow boundary will result in a doubling of the magnitude of the derivative. If radial flow is established before the influence of the boundary is seen, a

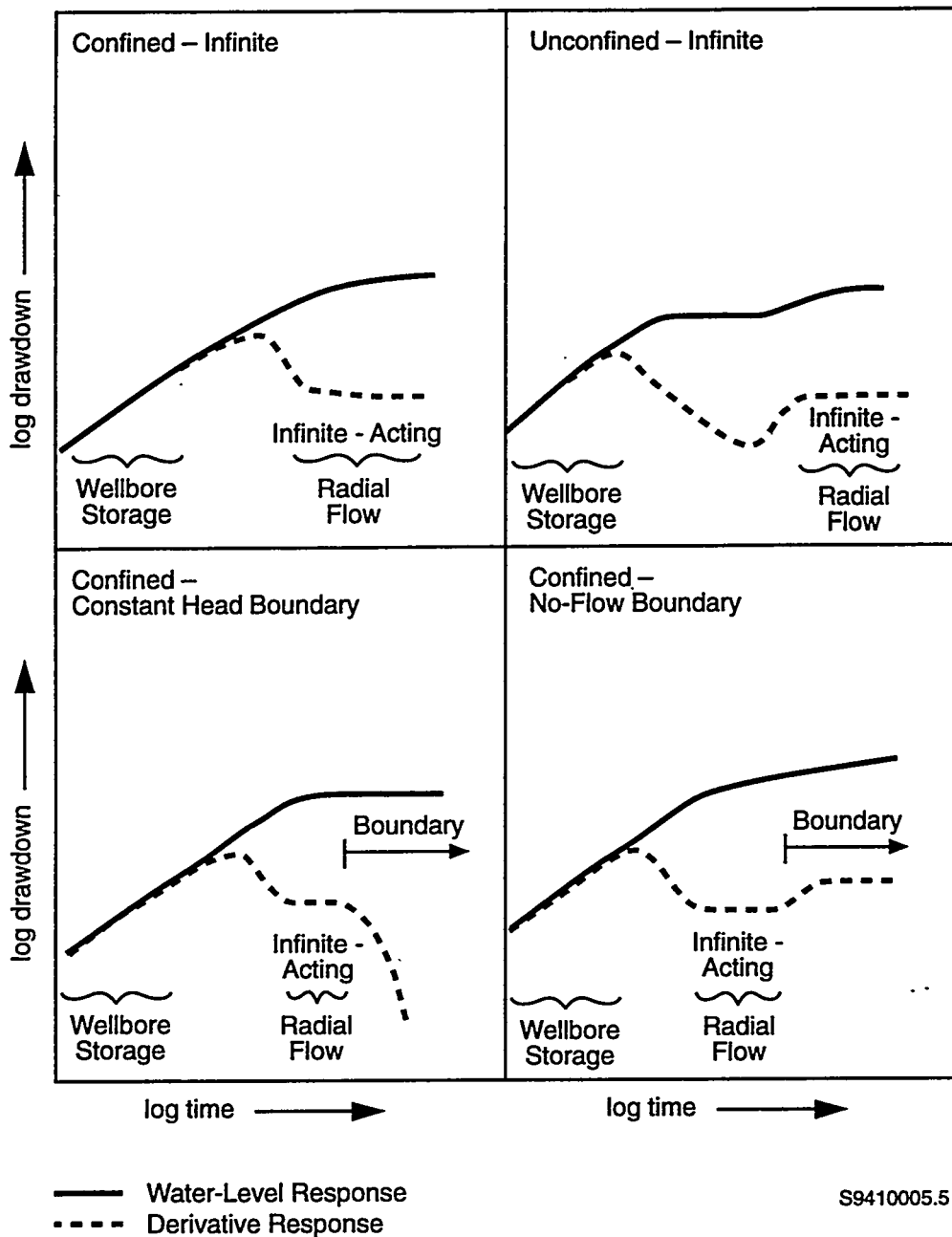


Figure A.2. Characteristic Log-Log Drawdown and Derivative Responses for Various Well and Aquifer Conditions

stable derivative will occur for a time followed by an upward shift to twice the original value. Constant-head boundaries show up as a downward trend in the derivative, which may be preceded by a stable derivative if radial flow conditions occur before the boundary effect becomes dominant.

Step Drawdown Tests

Step drawdown or, more accurately, step discharge tests are performed to determine the head loss associated with turbulent flow at the pumping well. Based on the Cooper and Jacob (1946)

approximation, a well that has been pumped for a sufficient length of time to meet the $u < 0.01$ criterion should display drawdown (s_w) proportional to the flow rate. This can be expressed as

$$s_w = BQ$$

where B is the proportionality constant. However, turbulent flow at the well causes drawdown to deviate from this relationship because Darcy's Law does not apply. Jacob (1946) proposed the following relationship to describe drawdown in this case

$$s_w = BQ + CQ^2$$

where C is a coefficient describing the effect of turbulent flow.

Bierschenk (1964) developed a method of determining the B and C coefficients by plotting specific capacity (s_w/Q) versus Q and fitting a straight line to the data. The coefficients are then determined by dividing the equation above by Q to obtain

$$s_w/Q = B + CQ$$

The slope of the fitted line is the turbulent flow coefficient and the intercept is the laminar flow coefficient.

After the B and C parameters have been determined, drawdown data at the pumping well can be corrected for the effect of turbulence by subtracting CQ^2 . However, it should be noted that a significant portion of friction loss at the pumping well may also be caused by laminar flow that is not accounted for by this procedure (Driscoll 1986).

Drawdown data during the second and later steps of the test are affected by earlier steps and cannot generally be analyzed for hydraulic properties by directly applying constant-rate analysis techniques. However, Agarwal (1980) presented an equivalent time function based on the principle of superposition that normalizes drawdown data from later steps. A plot of step drawdown versus Agarwal equivalent time is identical to a plot of constant-rate drawdown versus time (for the step) for a constant discharge rate equal to the rate change at the beginning of the step.

A.4 Analysis and Results for Well 699-S19-11

Well 699-S19-11 is completed with 6-in. (15.2 cm) inside diameter steel casing perforated over the depth interval 28.7 - 35.0 m. The depth to water is approximately 27.6 m. Over the perforated interval, the aquifer is composed of gravel and cobbles to sand and gravel. The well partially penetrates the aquifer and the aquifer thickness is unknown.

Prior to conducting the constant-rate test, water levels were monitored for more than three days. Figure A.3 shows the change in water level during this period compared to the change in barometric pressure. These pre-test data were used to determine the influence of barometric pressure on the water level and to determine if any long-term water-level trends were present. The Clark (1967) method was

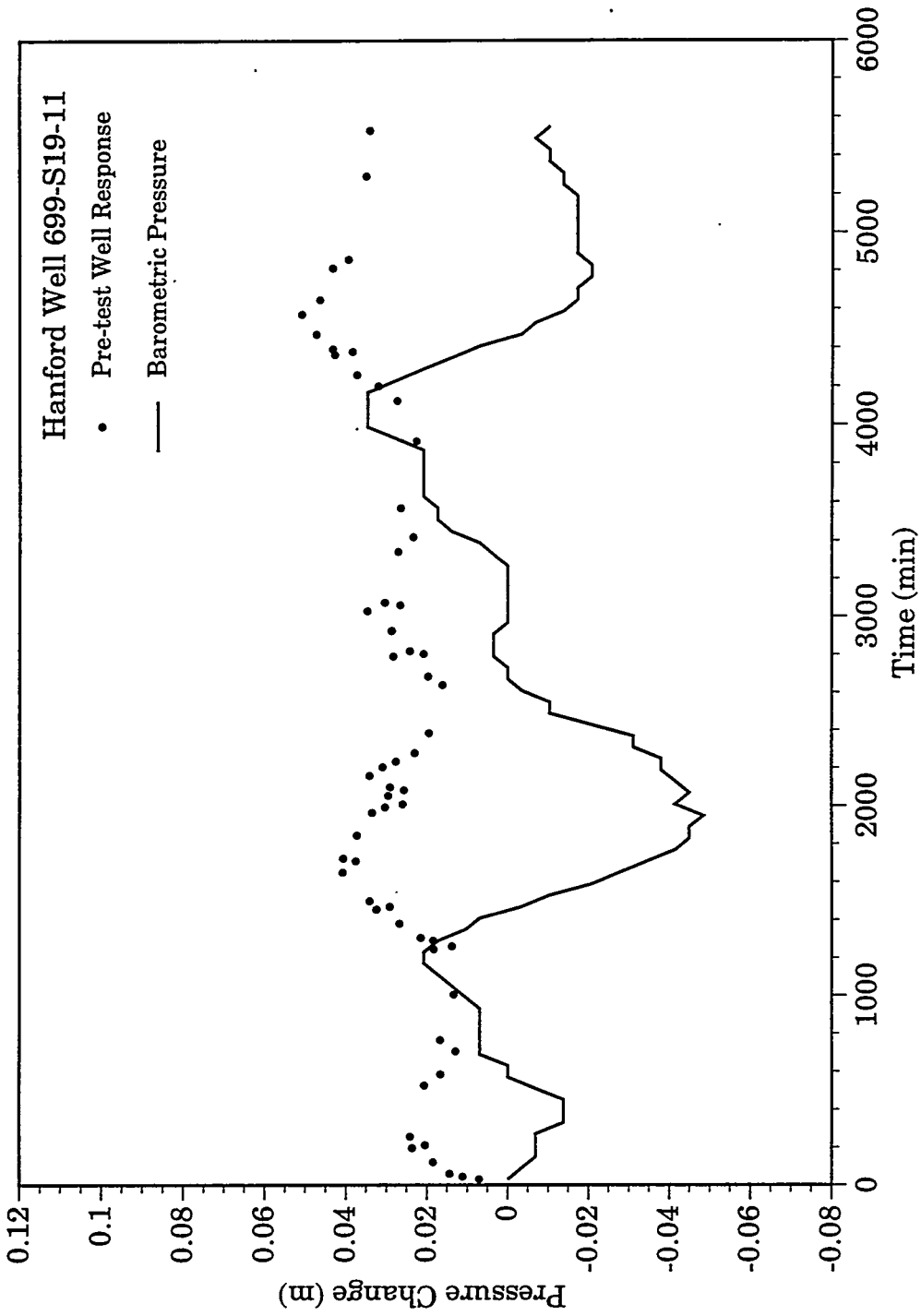


Figure A.3. Baseline Comparison of Water-Level and Barometric Pressure Data for Well 699-S19-11

applied to determine a barometric efficiency of 0.42 for the well. Although a slight trend appears to affect the pre-test data, it is not significant enough to affect the test results and was not removed. Pre-test water-level data corrected for barometric effects are plotted in Figure A.4.

A constant-rate discharge test was conducted for 1830 min during June 20-21, 1994. Following the pumping period, recovery was monitored for a similar time period. The average pumping rate was 163 L/min. A log-log diagnostic plot of the drawdown and derivative data is shown in Figure A.5. Derivatives were calculated using the computer program presented in Spane and Wurstner (1992). These data have been corrected for barometric pressure effects. Although the derivative continues to decline throughout the pumping period, it is nearly stable after about 200 min. Noise in the later-time derivative is accentuated because of the low value of the derivative on the log scale. The data after 200 min appears to be near radial flow conditions and these data were used for the semilog straight-line analysis shown in Figure A.6. Transmissivity calculated from the straight line fit is 490 m²/d.

A log-log diagnostic plot of recovery and derivative data is shown in Figure A.7. The data were also corrected for barometric pressure effects. They are plotted versus the equivalent time function of Agarwal (1980) to account for the effect of the pumping period. Although declining slightly, the derivative response is relatively flat during the equivalent time period of 30 to 300 min. At later times the derivative is less stable, possibly because of incompletely corrected barometric or other external stresses. The data between 30 and 300 min equivalent time were used for the semilog straight-line analysis shown in Figure A.8. Transmissivity calculated from the straight line fit is 610 m²/d, which is within 20% of the value calculated from the drawdown data.

The semilog straight-line analysis method used to analyze pumping and recovery data from this test assumes a fully penetrating pumping well and confined aquifer conditions. Analysis results may have been affected by the partially penetrating condition of the well and the unconfined aquifer. However, the drawdown (or recovery) curve for a partially penetrating well in an unconfined aquifer parallels the curve for a fully penetrating, confined aquifer well during the third (radial flow) segment of the unconfined aquifer response. Data at relatively late dimensionless times are, therefore, expected to approach the correct straight-line slope for calculating transmissivity of the entire aquifer. The recovery data is expected to be less affected by flow-rate variations than the drawdown data. Therefore, the best estimate for transmissivity from this test is 600 m²/d. Storativity could not be determined because of the lack of observation well data. Equivalent hydraulic conductivity, based on an assumed aquifer thickness of 15 m is 40 m/d. However, the actual aquifer thickness is unknown and the hydraulic conductivity may be higher or lower depending on actual aquifer thickness.

A.5 Analysis and Results for Wells 699-S14-20A, B, and C

Three wells are present at this site. The pumping well, 699-S14-20B, is completed with 12-in. (30.5-cm) diameter casing. Observation well 699-S14-20A, located at a radial distance of 2.77 m from the pumping well, is completed with 8-in. (20.3-cm) diameter casing. Observation well 699-S14-20C, located at a radial distance of 3.20 m from the pumping well, is completed with 6-in. (15.2-cm) diameter casing. All three wells extend to the top of basalt and appear to be perforated over almost the entire saturated depth interval from 27.5 to 48.8 m. Documentation of the perforation depths for the B and C wells was not available. Therefore, a downhole camera survey was conducted to determine the

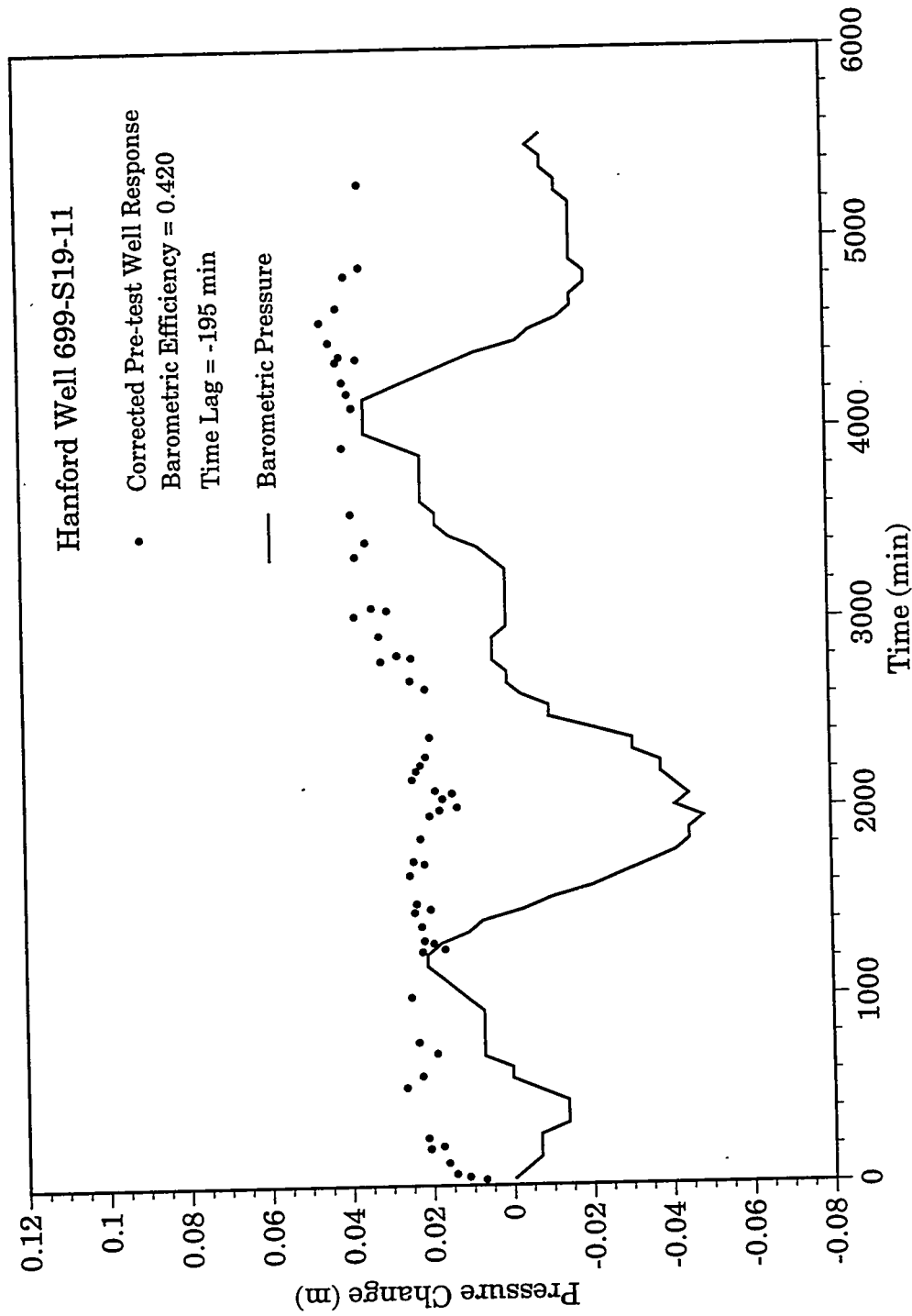


Figure A.4. Baseline Water-Level Data at Well 699-S19-11 Corrected for Barometric Fluctuations

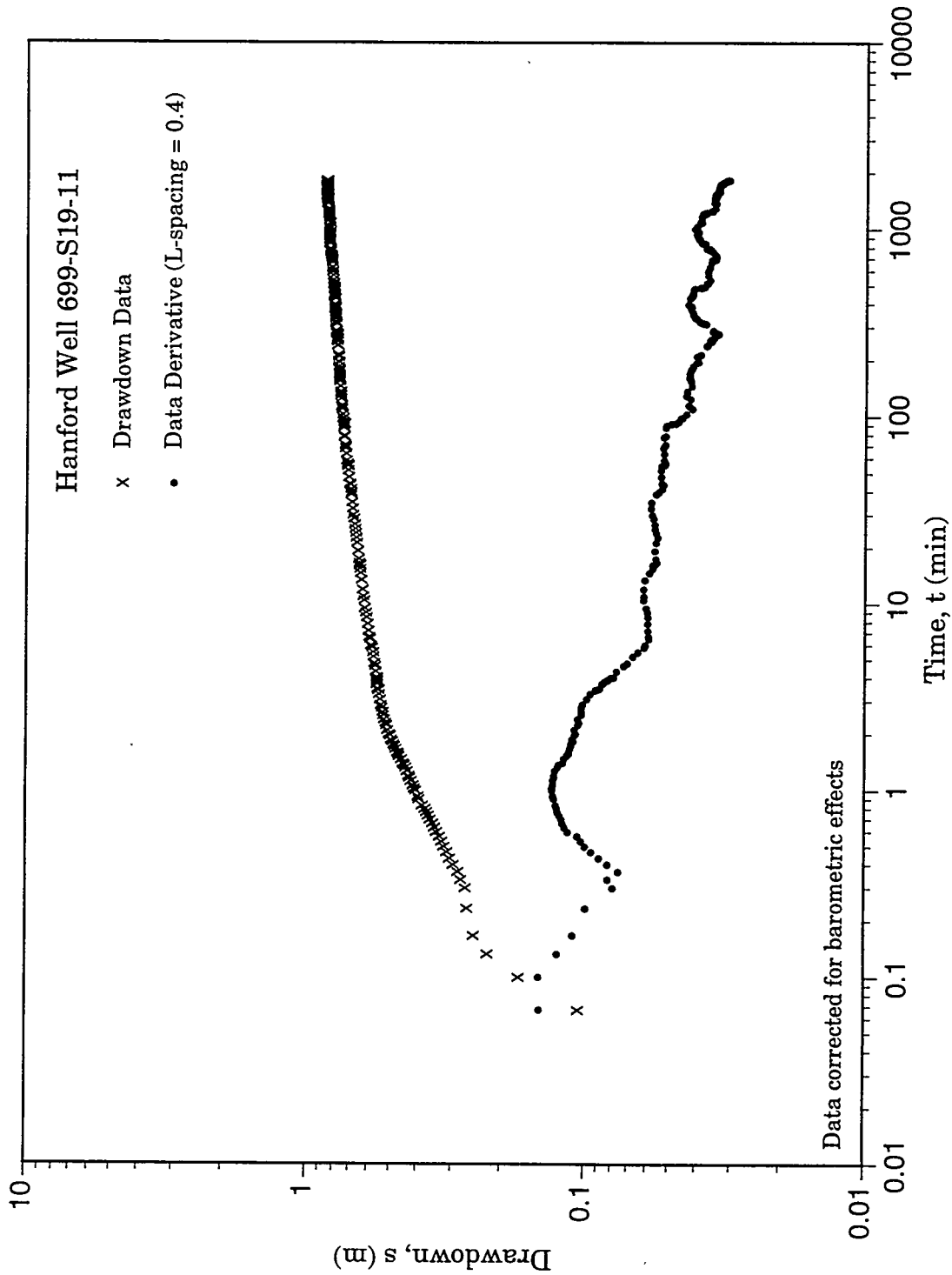


Figure A.5. Log-Log Diagnostic Plot of Drawdown and Drawdown Derivative at Well 699-S19-11

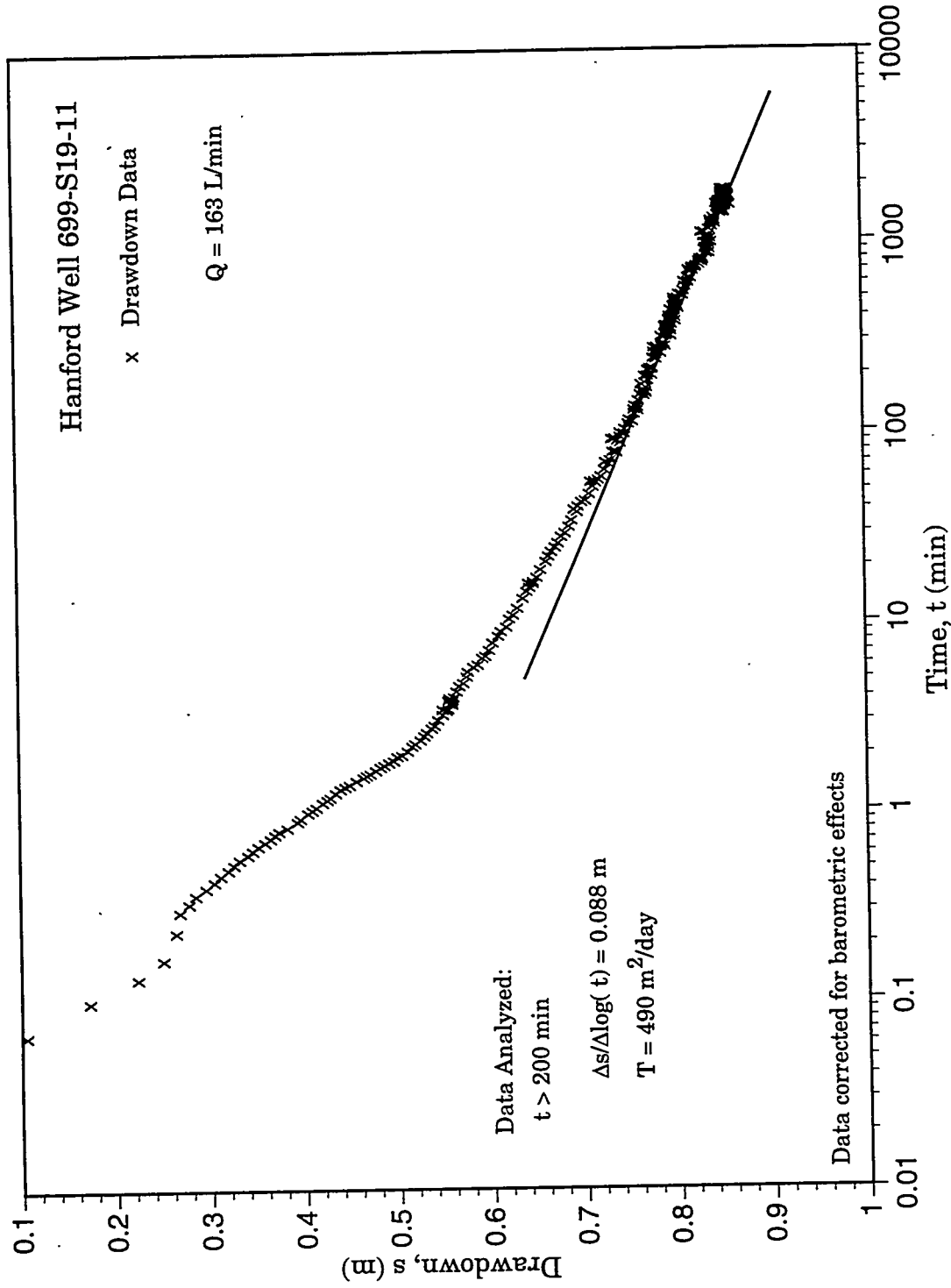


Figure A.6. Semilog Straight-Line Analysis for Drawdown Data from Well 699-S19-11

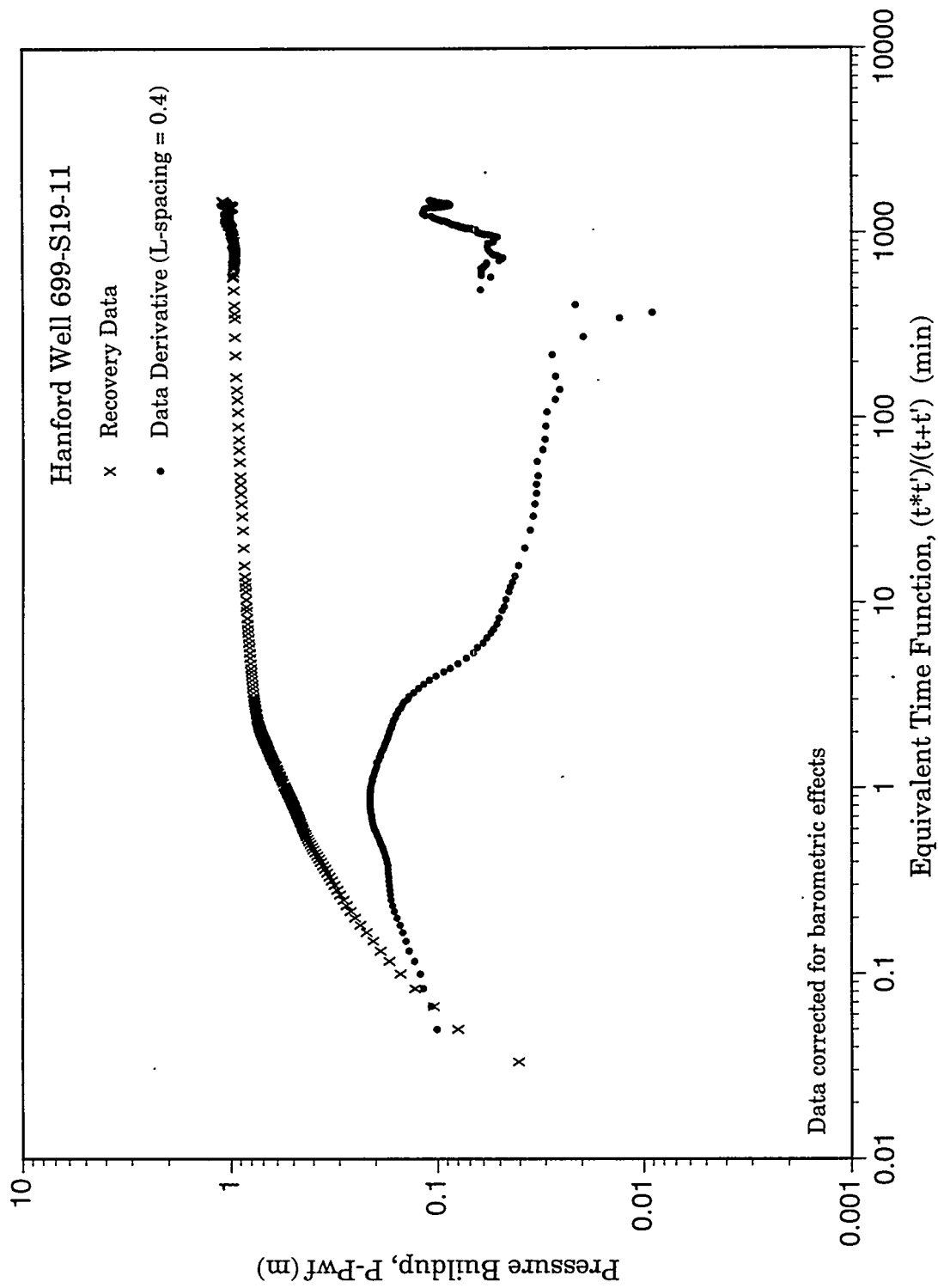


Figure A.7. Log-Log Diagnostic Plot of Recovery and Recovery Derivative at Well 699-S19-11

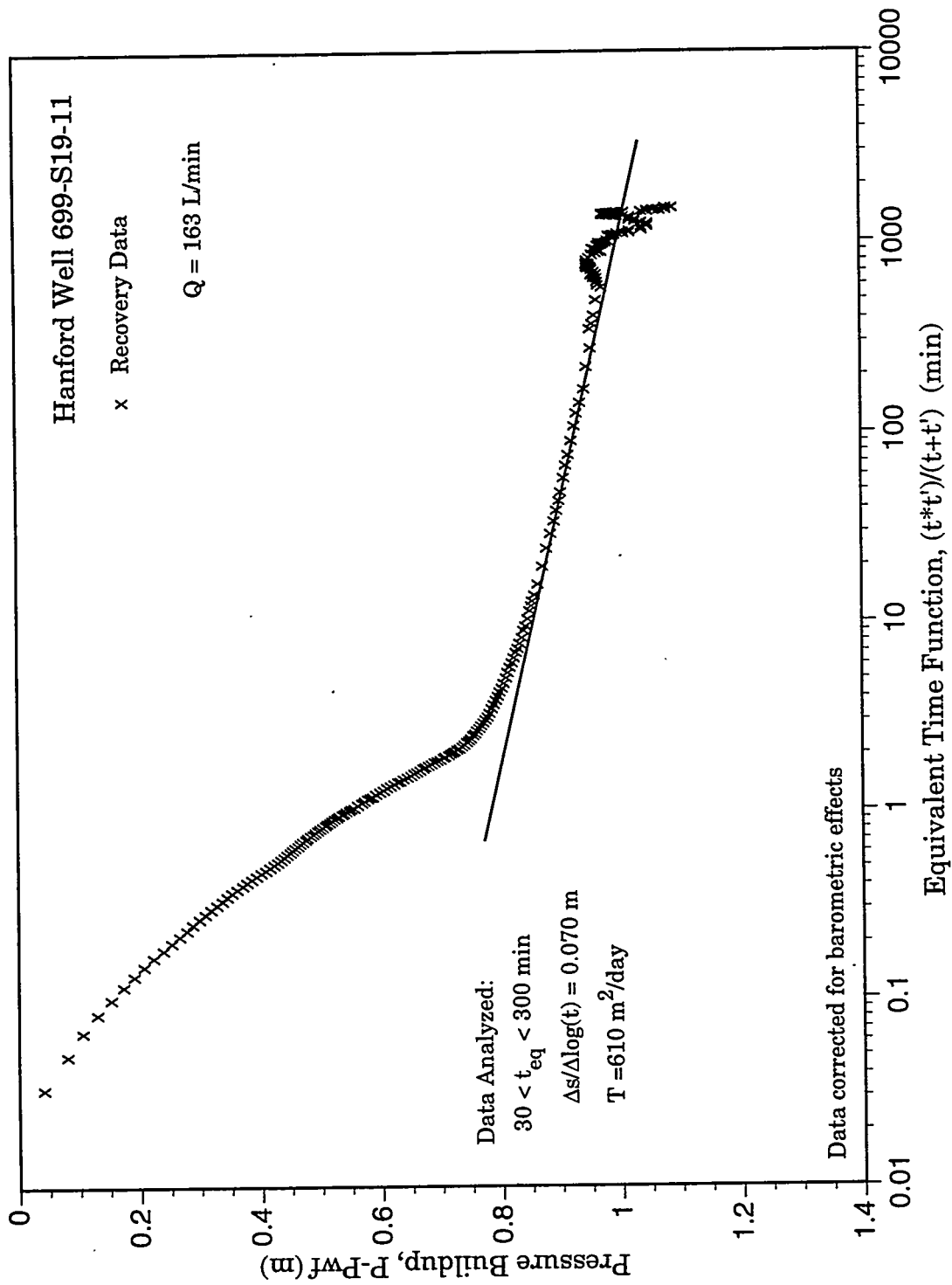


Figure A.8. Semilog Straight-Line Analysis for Recovery Data from Well 699-S19-11

perforated depths and the condition of these wells. Well A was originally drilled about 3 m into basalt. However, the bottom part of the well is filled and a screen has been placed inside the perforated casing. Well A is used for annual ground-water sampling and is known to produce very little water. It is rapidly dewatered when pumped at less than 20 L/min and takes several hours to recover. The other wells at this location produce more water. Well B was pumped at 166 L/min and showed less than 6.5 m drawdown. It is not known whether the difference in behavior of the wells is caused by formation heterogeneity or well completion problems.

Water levels were monitored at each of the wells for over 6 days prior to conducting the pumping test. Figures A.9 through A.11 show the change in water levels at each of the wells during this period compared to the change in barometric pressure. Barometric efficiencies of 0.19, 0.19, and 0.22 were calculated for wells A, B, and C, respectively, by applying the Clark (1967) method. Barometric pressure changes did not significantly affect water-levels in any of the wells during the test. A slight upward trends appears in the pre-test data for well A (Figure A.9). However, it was too small to affect the test results and was not removed. The pre-test data for well C show a downward trend of 0.0094 m/d, which appears to be a result of instrument drift because the trend was not observed in e-tape measurements. This trend was removed from the test data prior to analysis.

A constant-rate discharge test was conducted at well B for 2790 min during July 6-8, 1994. The average pumping rate was 166 L/min. Water level responses were measured at the observation wells during pumping. Recovery data was not analyzable because of an apparent leak in the pump foot-valve. Water leaking back into the well caused an anomalous response.

A log-log diagnostic plot of drawdown and derivative data for well A is shown in Figure A.12. The derivative shows a dip at about 500 min that corresponds to a change in slope on the semilog data plot (Figure A.13). The data from about 500 to 1300 min are near a straight line on the semilog plot, although the derivative fluctuates. The derivative then shows a sharp decrease that may reflect flow-rate changes at the pumping well. Data between 500 and 1300 min were analyzed using the semilog straight-line technique (Figure A.13). The resulting transmissivity value was 670 m²/d. However, it is not clear that this is the best data range to analyze.

The log-log plot of drawdown and derivative for the pumping well (well B) is shown in Figure A.14. The derivative shows a valley that is characteristic of delayed yield effects. The derivative then continues to increase, although it is noisy, and does not display the stable constant derivative that would indicate infinite-acting radial flow. This derivative pattern could be caused by either the early part of the third segment of delayed yield, before radial flow conditions are achieved, or by an impermeable boundary effect. Because of the lack of radial flow conditions, as indicated by the changing derivative, analysis using the semilog straight-line technique is not valid and was not attempted.

A log-log diagnostic plot of drawdown and derivative data for well C is shown in Figure A.15. The derivative shows a similar pattern to that for well B and radial flow conditions are not indicated. Therefore, analysis using the semilog straight-line technique is also not valid for well C.

Figure A.16 shows a composite plot of the drawdown data for all three wells. The data are plotted versus the parameter t/r^2 to normalize for differences in well radius. According to the Neuman (1975) equations, the well responses should fall on different β curves, which converge at late time. Drawdown at the pumping well, well B, is about an order of magnitude greater than would be indicated

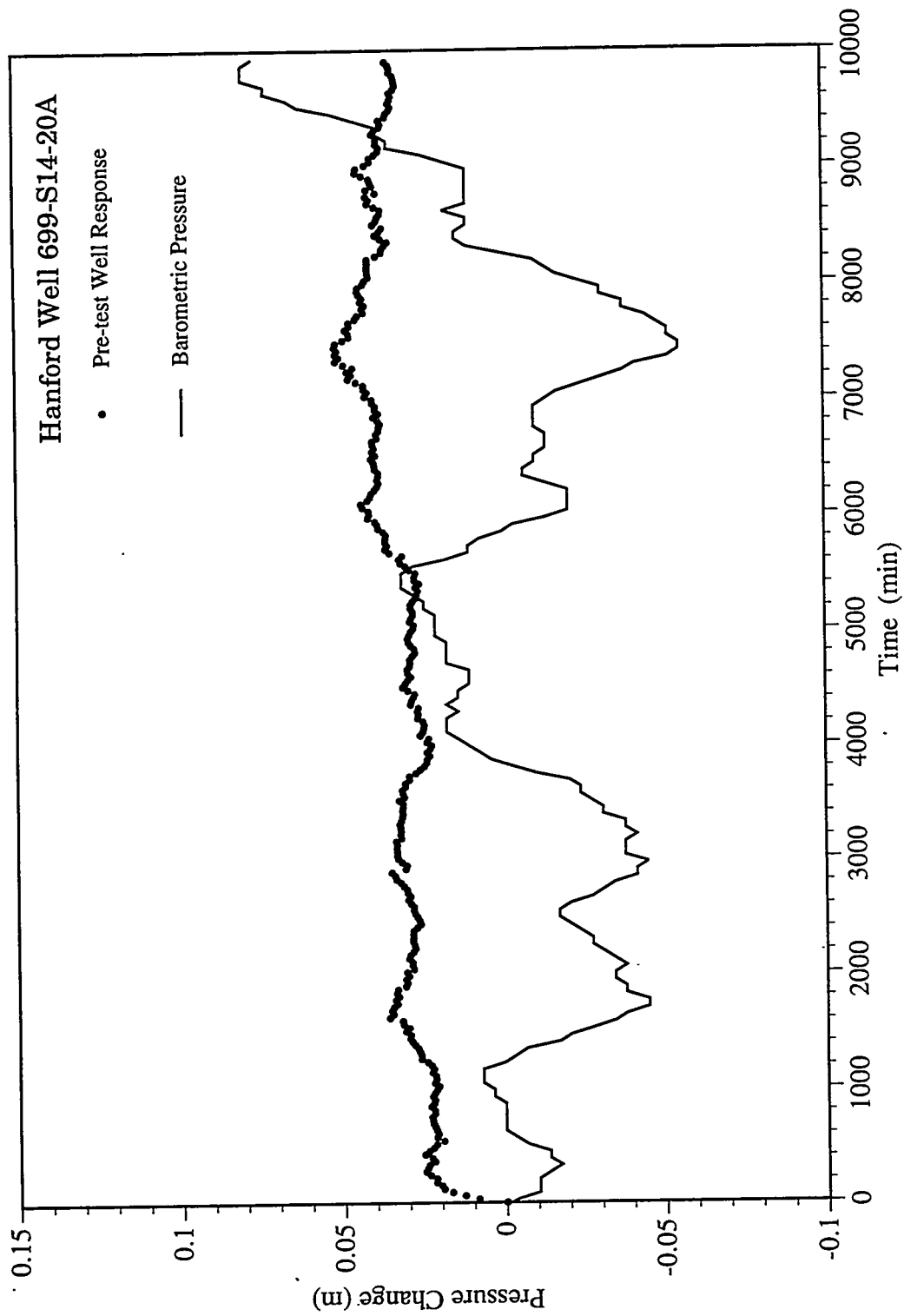


Figure A.9. Baseline Comparison of Water-Level and Barometric Pressure Data for Well 699-S14-20A

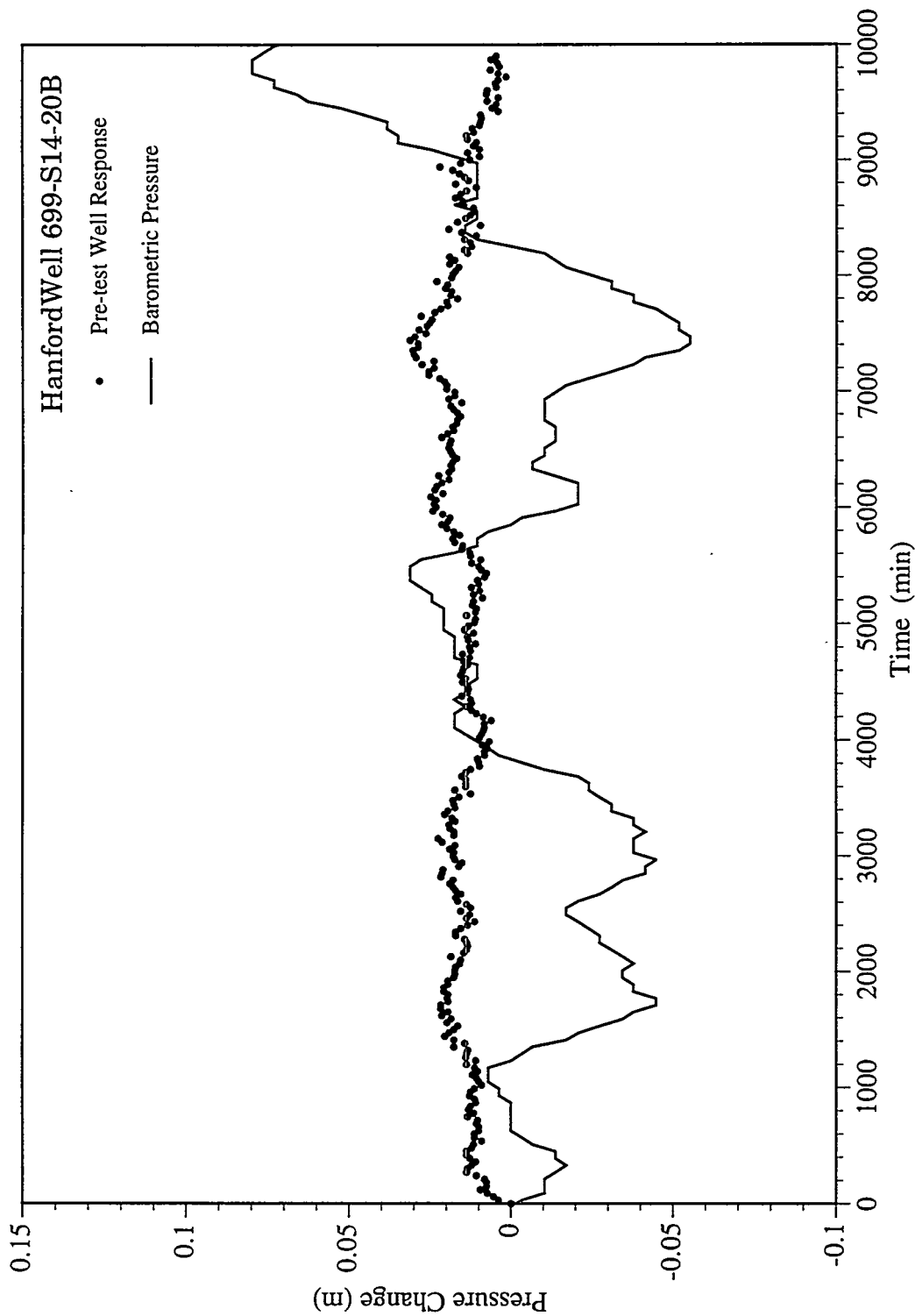


Figure A.10. Baseline Comparison of Water-Level and Barometric Pressure Data for Well 699-S14-20B

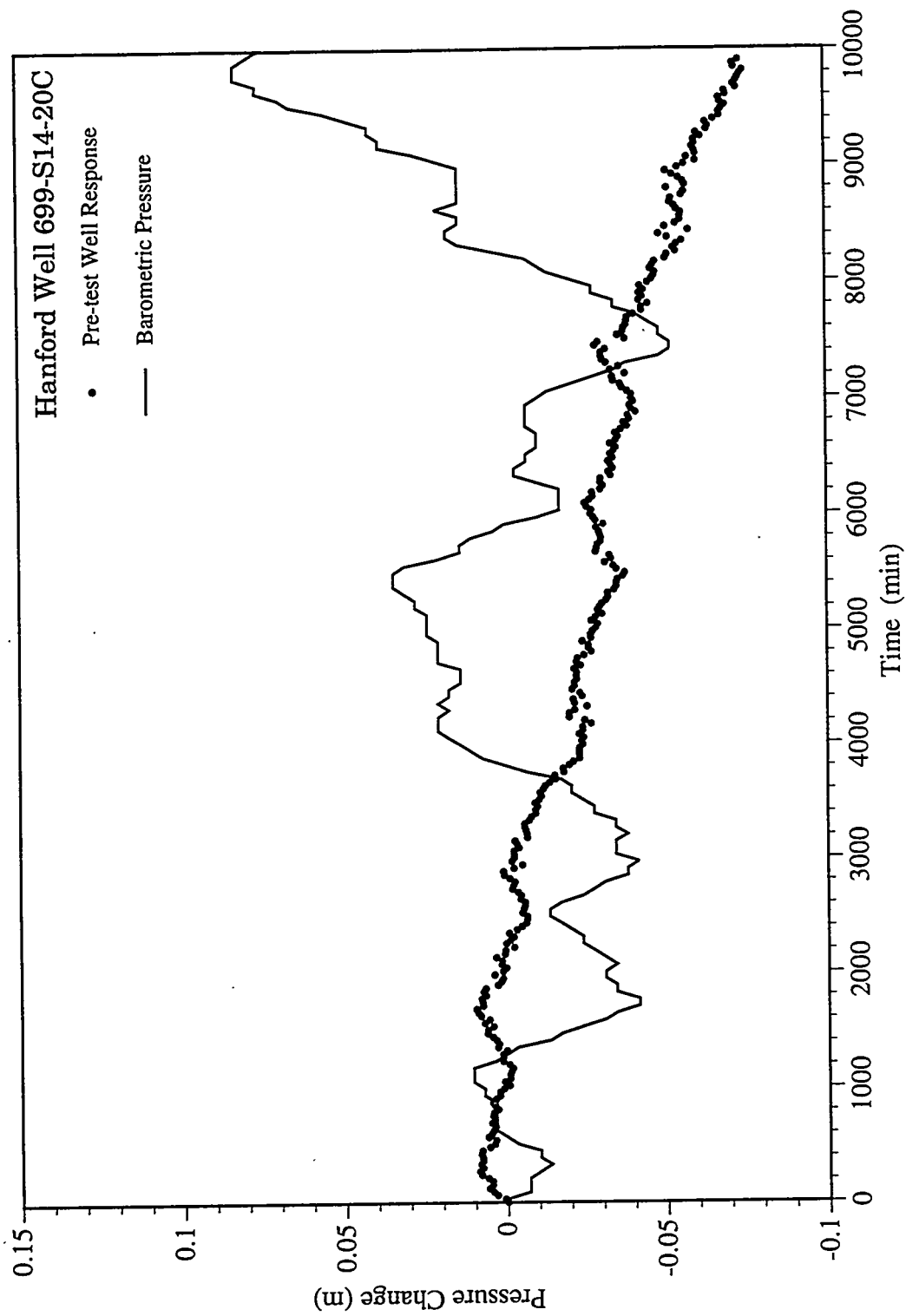


Figure A.11. Baseline Comparison of Water-Level and Barometric Pressure Data for Well 699-S14-20C

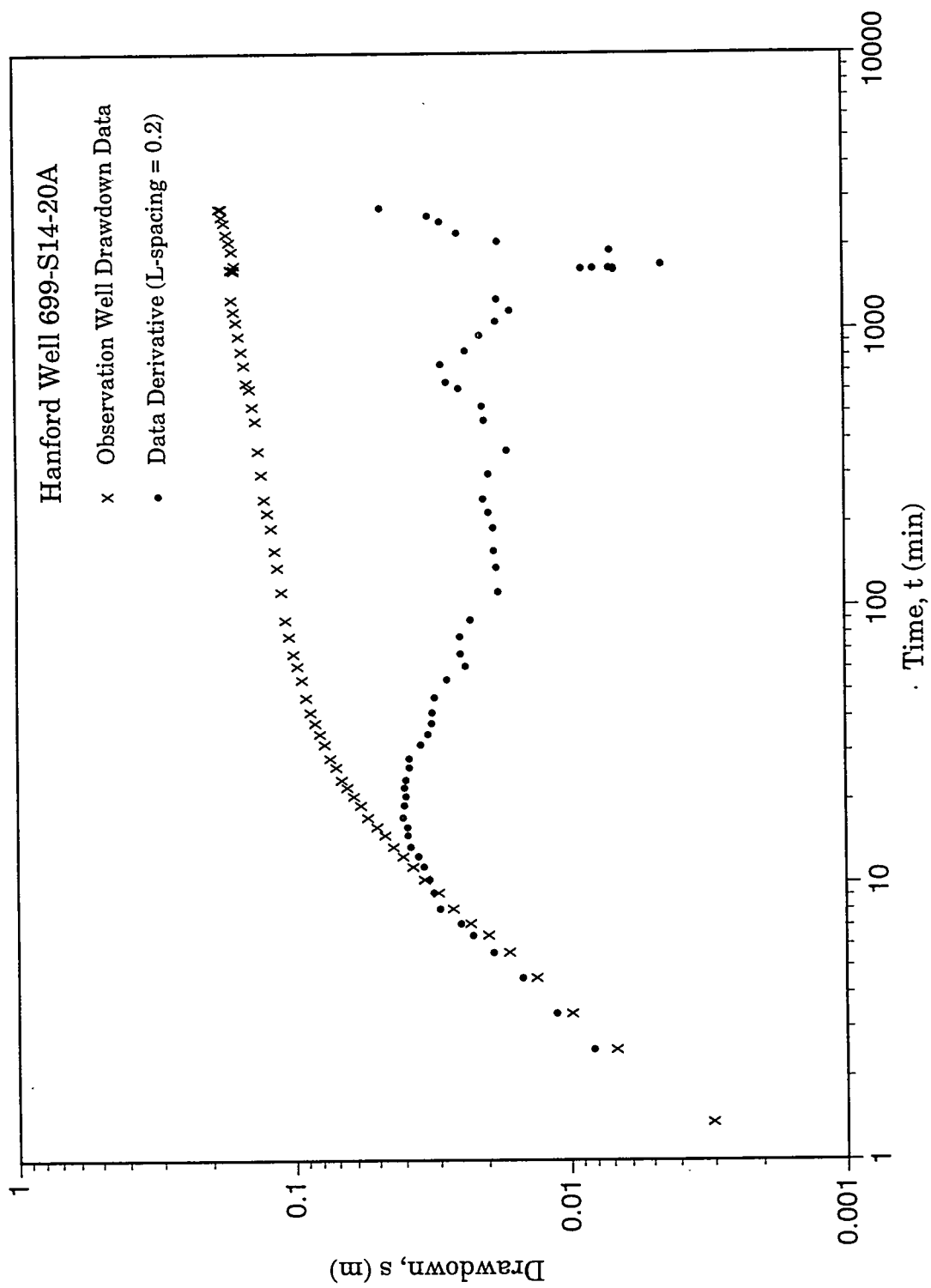


Figure A.12. Log-Log Diagnostic Plot of Drawdown and Drawdown Derivative at Well 699-S14-20A

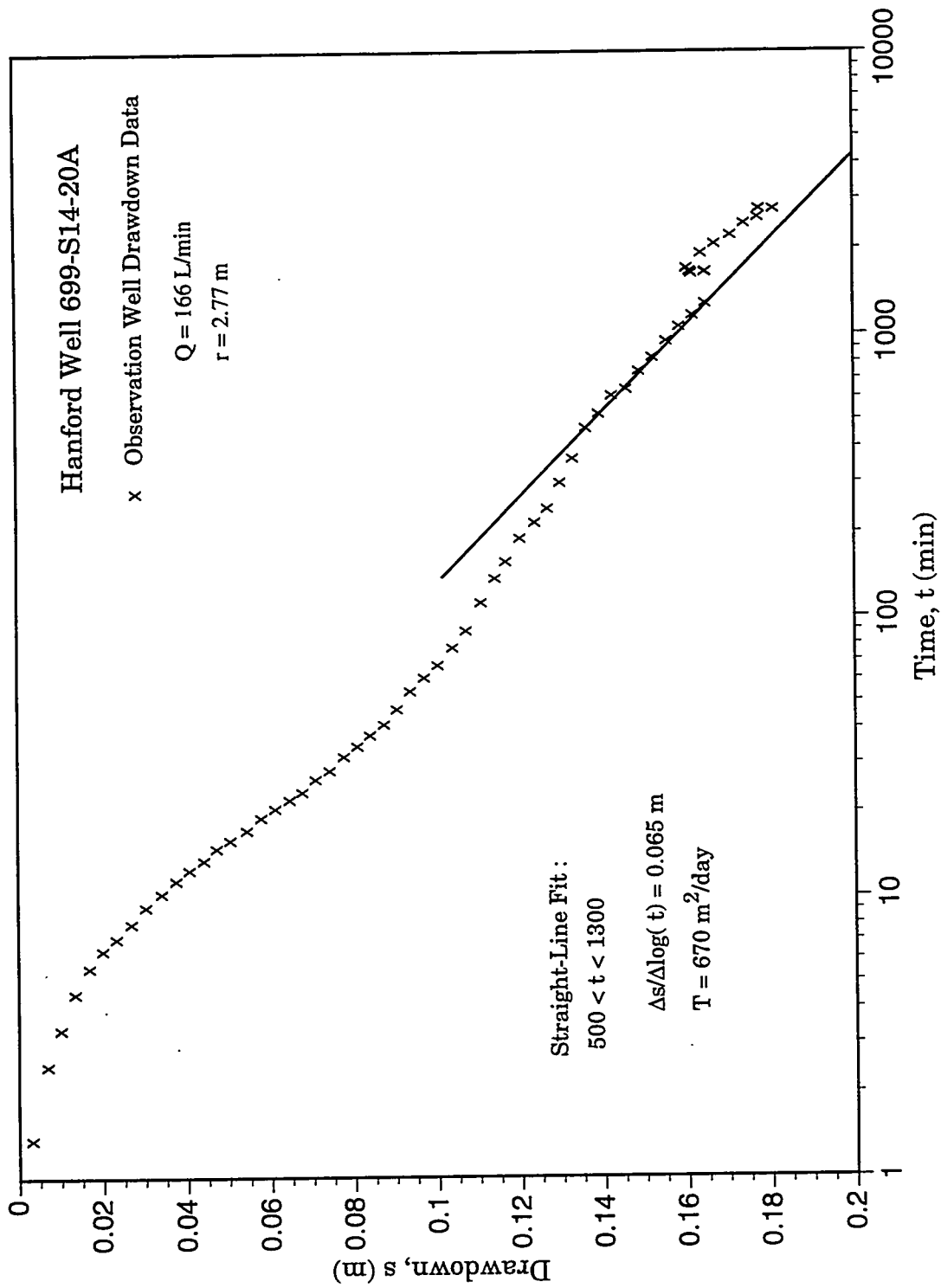


Figure A.13. Semilog Straight-Line Analysis for Drawdown Data from Well 699-S14-20A

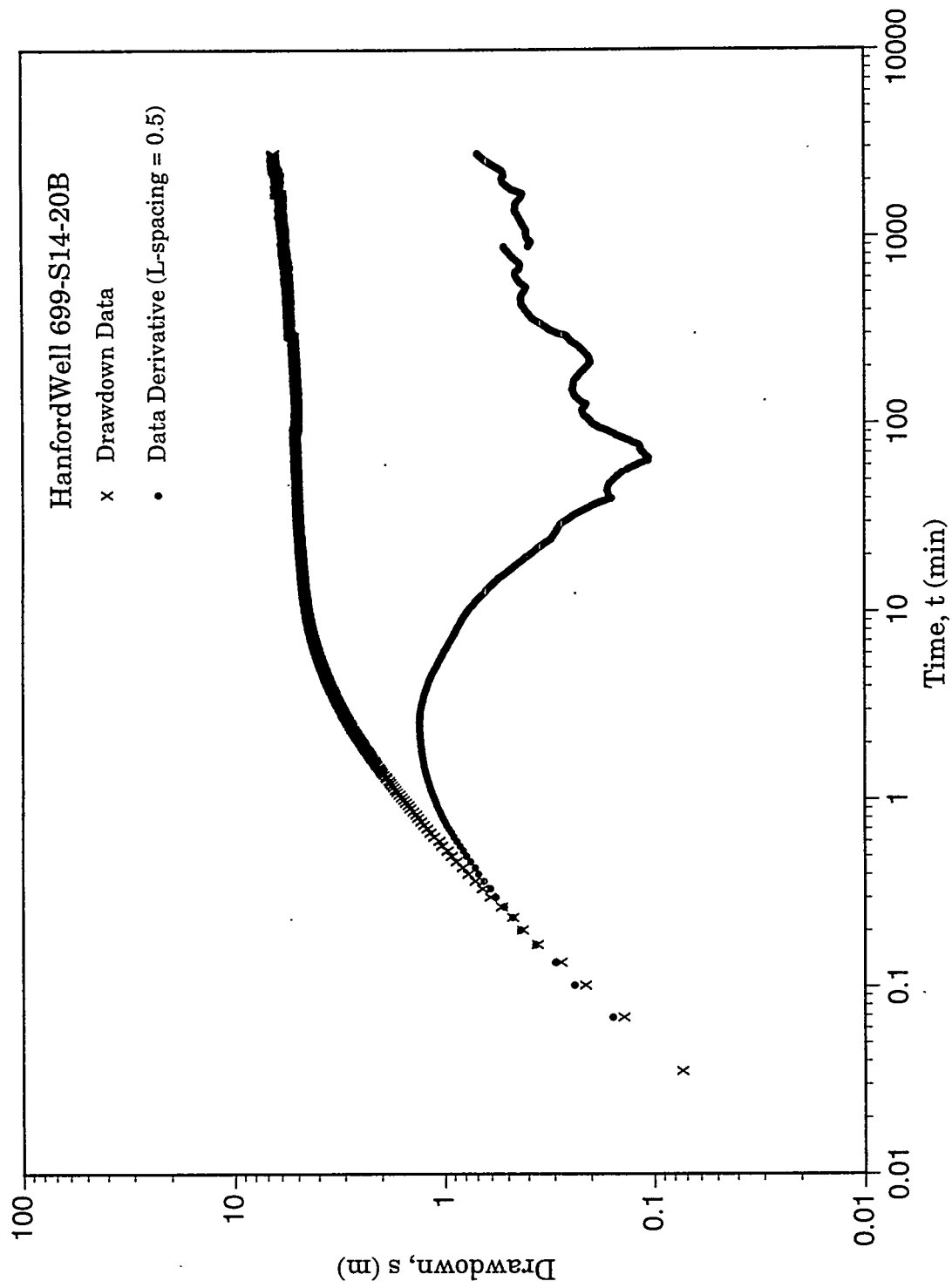


Figure A.14. Log-Log Diagnostic Plot of Drawdown and Drawdown Derivative at Well 699-S14-20B

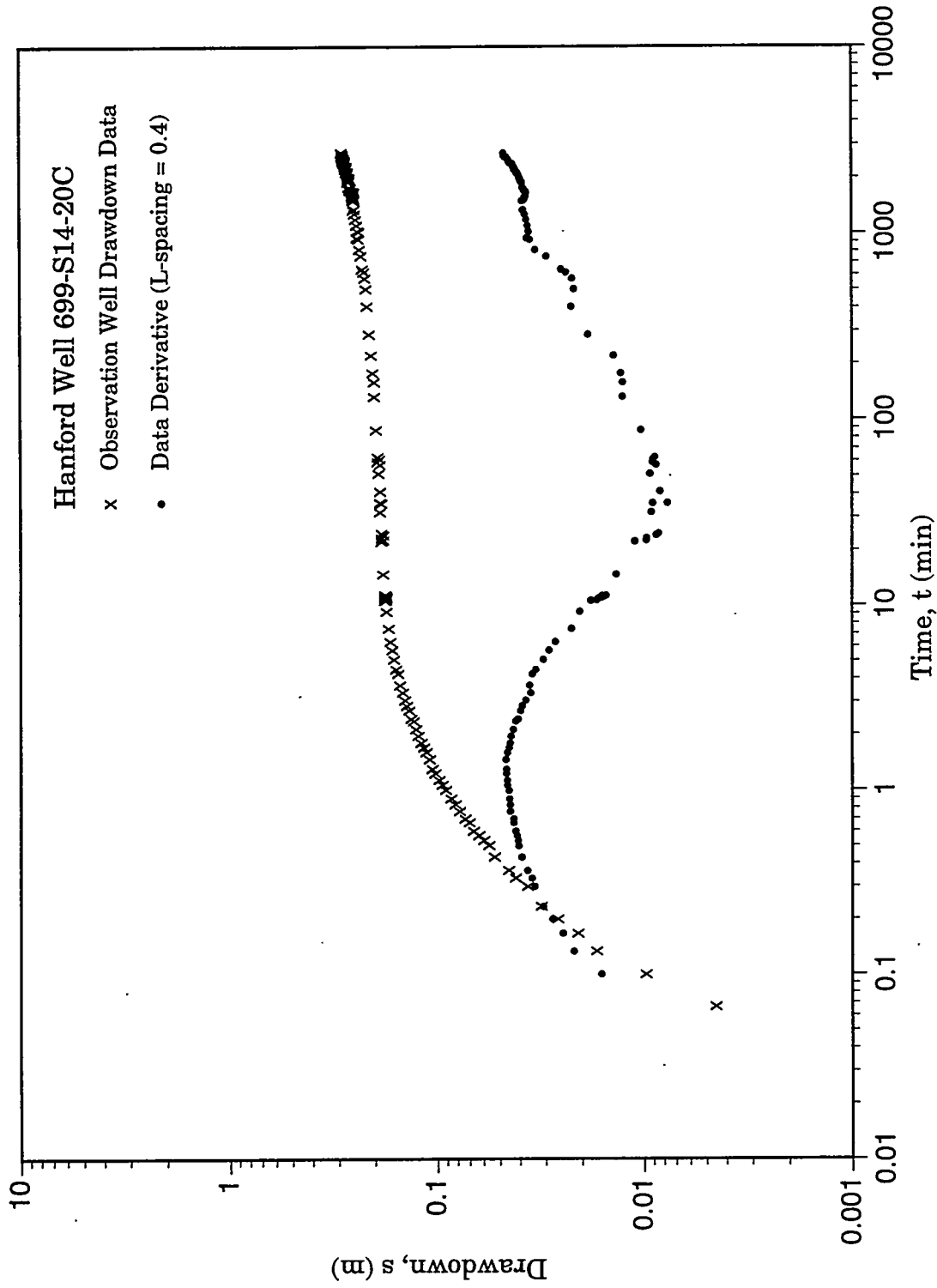


Figure A.15. Log-Log Diagnostic Plot of Drawdown and Drawdown Derivative at Well 699-S14-20C

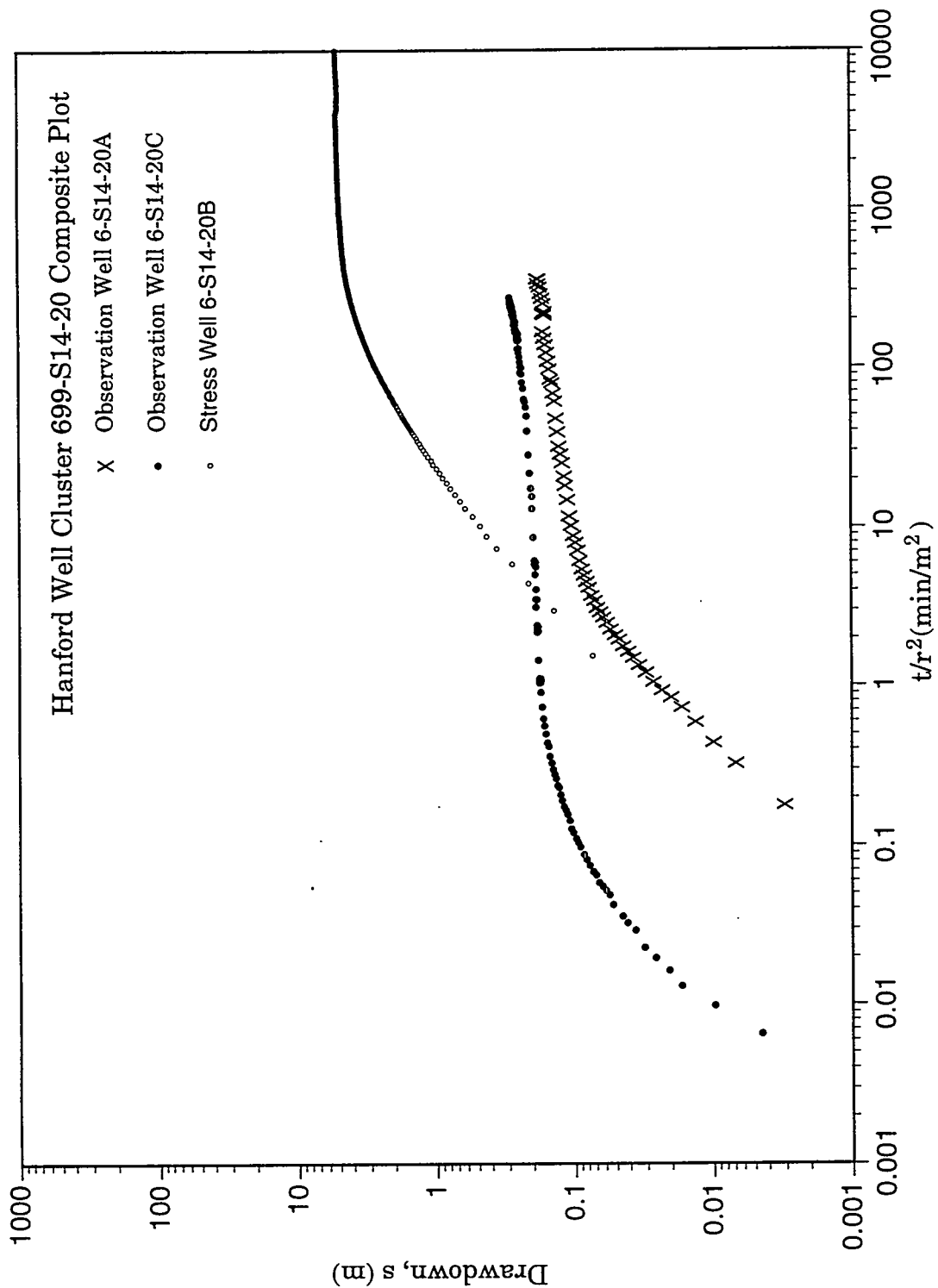


Figure A.16. Composite Log-Log Plot of Drawdown at Wells 699-S14-20A, B, and C

by extrapolating the drawdown at the observation wells. Increased drawdown at the pumping well may result from friction losses. At the end of the pumping period, the drawdown at well C is about twice that observed at well A. Well A may be affected by completion problems or aquifer heterogeneity. This well appears to be in a lower conductivity area or somehow isolated from the aquifer because it produces water poorly. Well C is the most promising for type curve analysis and shows the shape characteristic of delayed yield.

Figure A.17 shows the type-curve analysis of the data from well C using an unconfined aquifer curve generated according to Neuman (1975). Full aquifer penetration by both the pumping and observation wells was assumed. A σ (S/S_y) value of 0.02 and K_v/K_h of 0.2 provided the best fit. Transmissivity of 450 m²/d was calculated from this analysis. Storativity and specific yield values of 5E-03 and 0.25, respectively, were also calculated.

The best estimates of hydraulic properties for the tested interval are $T=450$ m²/d, $S=5E-03$, and $S_y=0.25$. These values are based on the unconfined aquifer type-curve analysis of data from observation well C. The best estimate of equivalent hydraulic conductivity is $K_h=21$ m/d, based on a test interval thickness of 21.3 m. The straight-line analysis of data from well A resulted in a nearly identical T value. However, the behavior of well A during sample collection activities and the derivative responses observed at wells B and C may indicate that the aquifer is heterogeneous. A boundary with less permeable materials may exist near the pumped well.

A.6 Analysis and Results for Well 699-4-E6

Well 699-4-E6 is a 9-in. (22.9-cm) diameter borehole with a well screen placed between the depths of 20.3 and 26.4 m. The measured depth to water prior to the test was 20.8 m and the depth to the bottom of the well was 26.8 m. The aquifer at the screened interval is reported to consist of sand and gravel with cobbles and minor amounts of silt.

A constant-rate test was attempted on July 13, 1994. Pumping was conducted at a rate of 220 L/min, the maximum rate possible with the available pump. However, this rate did not result in sufficient drawdown for a transient test analysis and pumping was terminated after 21 min. A drawdown of less than 0.04 m was observed during the first 5 min of pumping. The well then maintained this level during the remainder of the pumping period.

To obtain a limiting value for the minimum possible transmissivity at this well, a type curve was generated using the method of Neuman (1975). Unconfined aquifer conditions and 50% aquifer penetration were assumed. Storativity of 0.001 and specific yield of 0.2 were also assumed, as was $K_v/K_h = 0.5$. The observed drawdown data and the type curve predicted drawdown based a transmissivity of 10,000 m²/d are shown in Figure A.18. The observed drawdown at the end of the pumping period is slightly less than the predicted drawdown based on these assumptions. The transmissivity of 10,000 m²/d is regarded as a minimum limiting value because part of the observed drawdown may have been caused by friction losses at the pumped well. Based on the assumed aquifer thickness of 11.2 m, the equivalent minimum K_h is 890 m/d. The actual transmissivity and hydraulic conductivity of this interval may be higher than these minimum values.

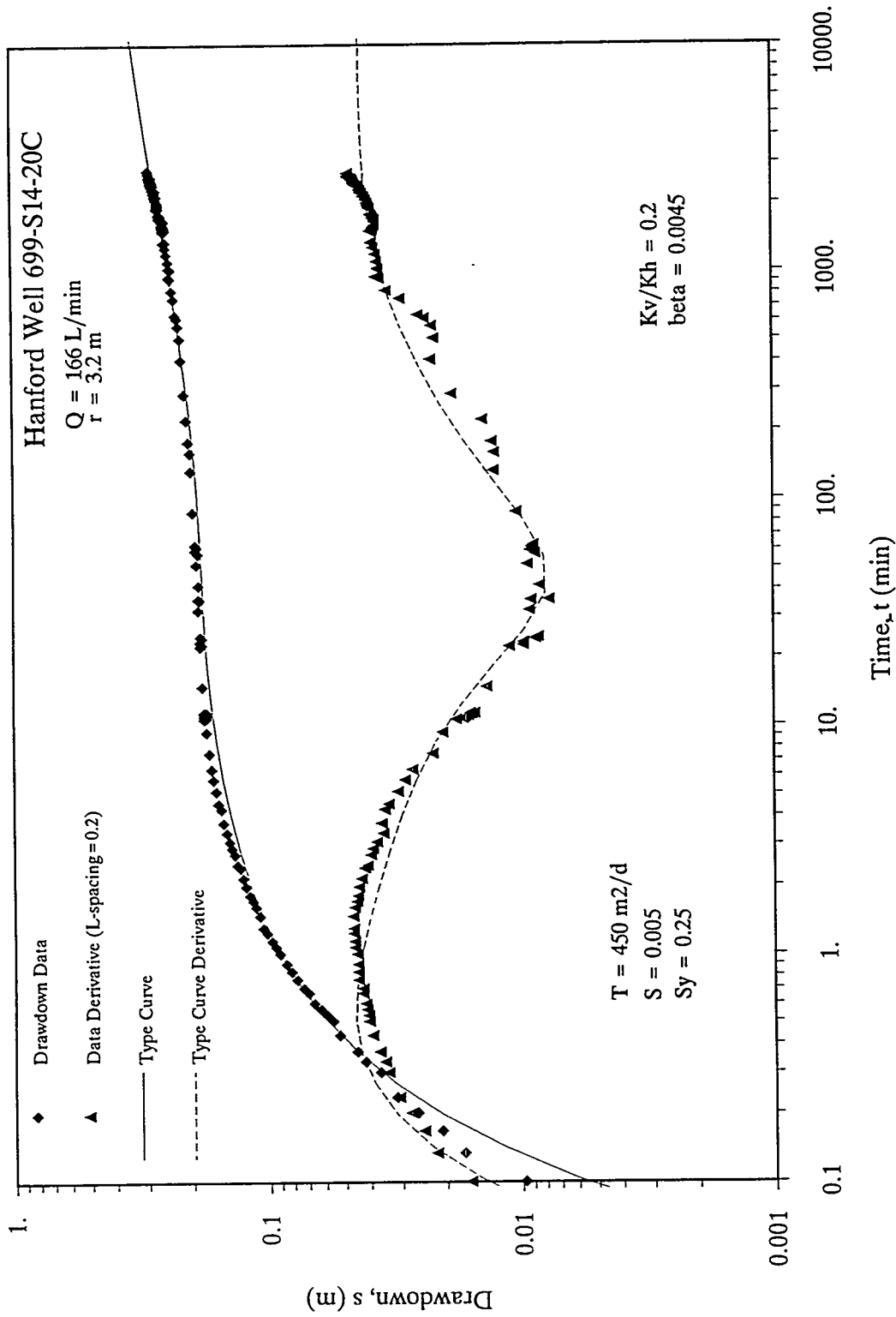


Figure A.17. Unconfined Aquifer Type-Curve Analysis of Drawdown at Well 699-S14-20C

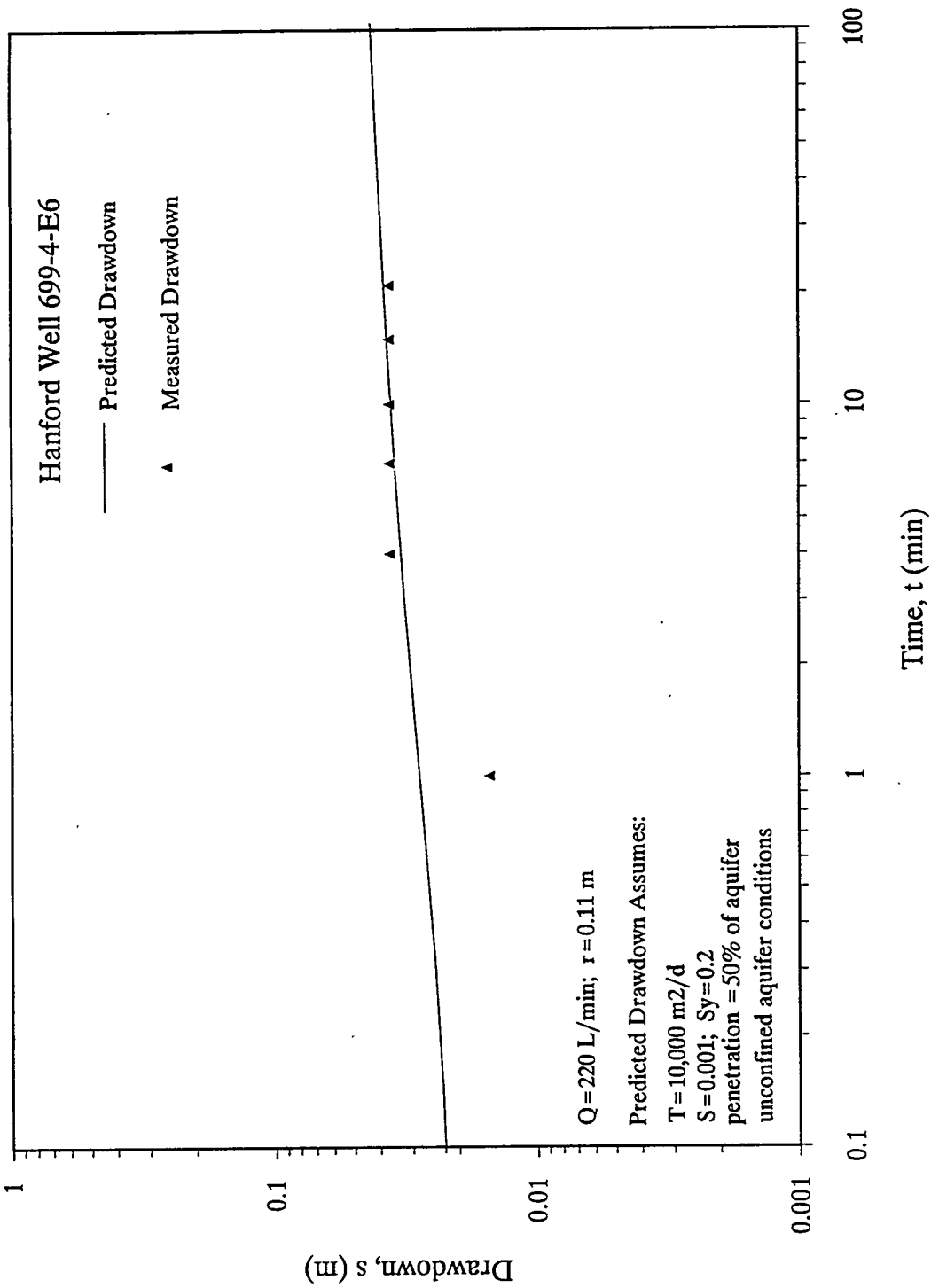


Figure A.18. Type-Curve Approximation for Drawdown at Well 699-4-E6

A.7 Analysis and Results for Well 699-18-21

Well 699-18-21 is a "Golder" well that was reconfigured during 1993 to provide access to the unconfined aquifer (Thorne et al. 1993). A 4-in. (10.2-cm) diameter stainless steel screen was placed over the depth interval from 58.5 to 70.7 m. The deeper section of the borehole was filled with cement grout. Depth to water is approximately 42.1 m. The interval from the water table to a silt layer at 74.7 m depth is composed of gravel and sandy gravel with some silty gravel and silty sand layers.

Step drawdown tests were performed at this well and at the other reconfigured "Golder" well, 699-31-11, to determine the effects of well friction loss. These wells had been drilled using mud rotary drilling, which may have caused a plugging of the aquifer at the borehole wall.

Three constant-rate discharge steps were conducted during May 5 to 6, 1994. Information on each of the flow rate steps is summarized below:

	Step 1	Step 2	Step 3
flow rate (L/min)	48.8	115.1	176.8
time period (min)	0-30	30-90	90-952
maximum drawdown (m)	0.18	0.57	1.04

Prior to conducting the step drawdown test, water levels were monitored for 5.8 days. Figure A.19 shows the change in water level during this period compared to the change in barometric pressure. These pre-test data were used to determine the influence of barometric pressure on the water level and to determine if any long-term water-level trends were present. A barometric efficiency of less than 5% was determined by applying the method of Clark (1967). Although a slight trend appears to affect the pre-test data, it is not significant enough to affect the test results. The total water-level change caused by this trend during the pumping period is less than 0.002 m. Water-level changes caused by barometric pressure fluctuations are also insignificant. Therefore, test data were not corrected for the trend or for barometric pressure effects.

Data from the third flow-rate step were analyzed to determine hydraulic properties because of the longer duration of this step. A log-log diagnostic plot of water-level and derivative data for the third step is shown in Figure A.20. Because of noise and the high data frequency, the data were smoothed using a 5-point moving average prior to calculating the derivative. Smoothed data are plotted in Figure A.20 and unsmoothed data are shown in the semilog plot (Figure A.21). The data have been plotted against the Agarwal (1980) equivalent time function, which accounts for the effects of the earlier flow rate steps. Noise in the drawdown data is accentuated in the derivative. However, the general trend of the derivative is horizontal after an equivalent time of about 20 min. Therefore, the data after 20 min appears to reflect radial flow conditions and these data were used for the semilog straight-line analysis shown in Figure A.21. Transmissivity calculated from the straight-line fit is 3100 m²/d. Although assumptions in the semilog straight-line analysis method are not met for partially penetrating wells in an unconfined aquifer, the method can be applied at late time, when radial flow conditions are dominant.

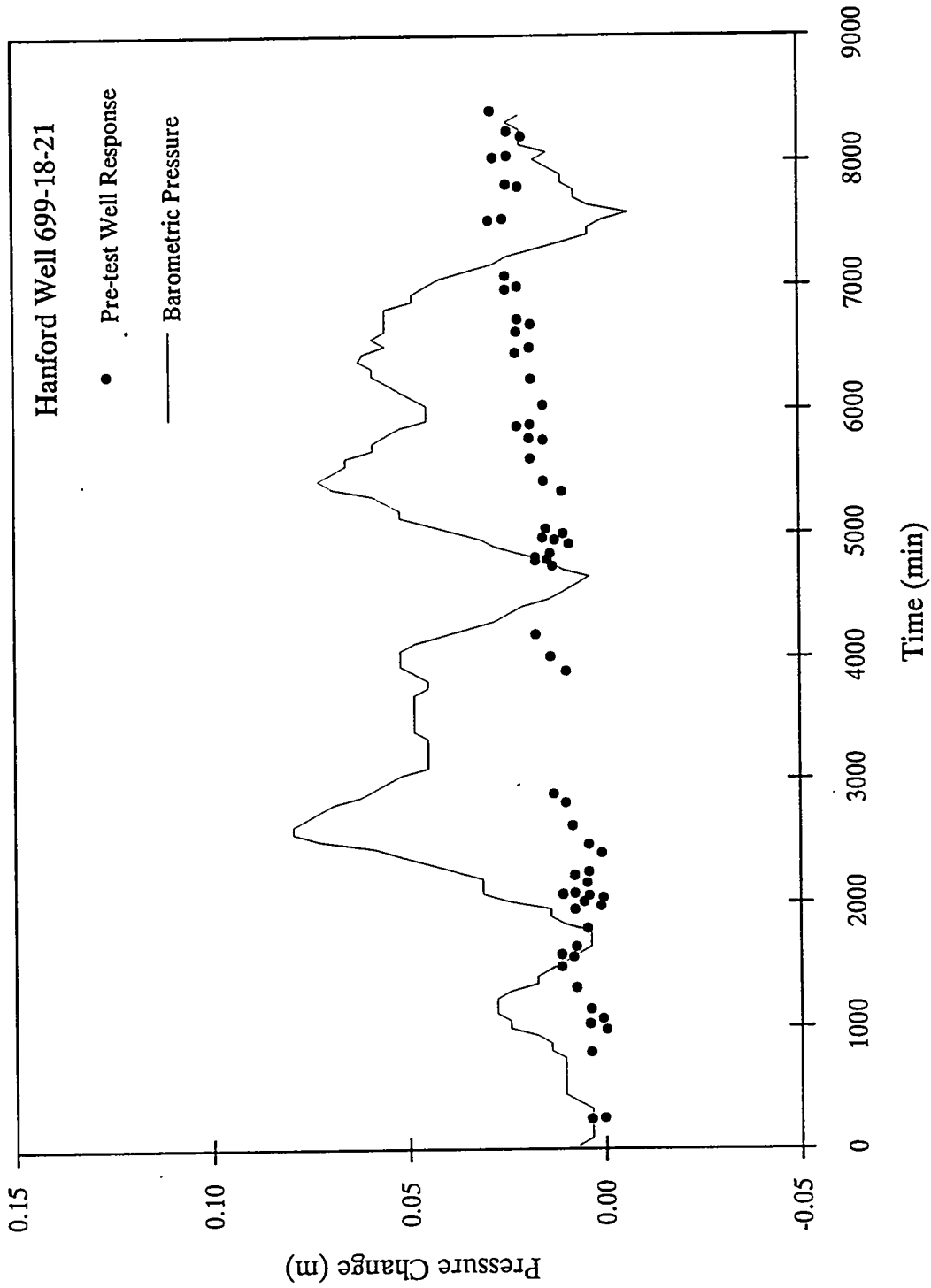


Figure A.19. Baseline Comparison of Water-Level and Barometric Pressure Data for Well 699-18-21

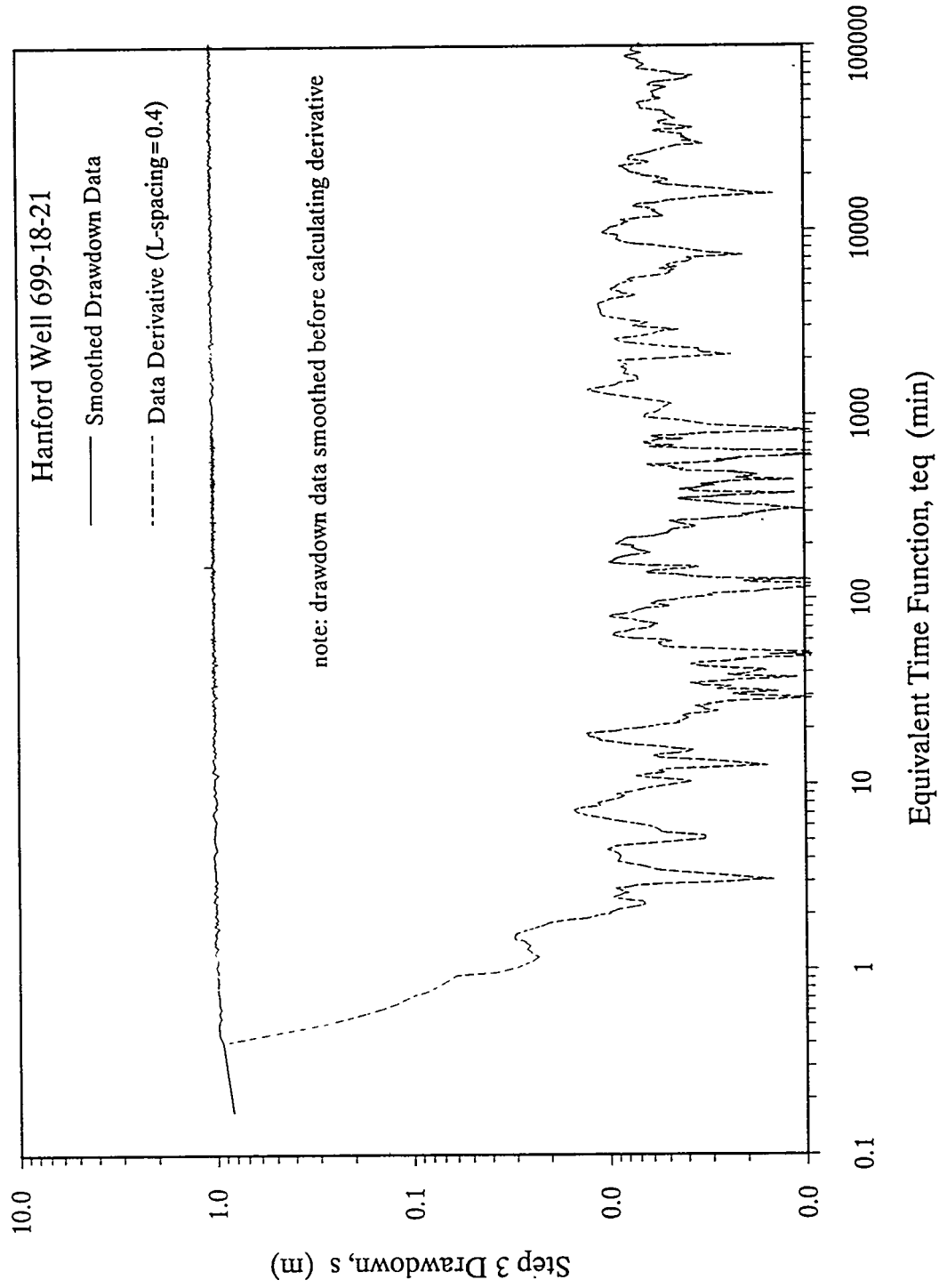


Figure A.20. Log-Log Diagnostic Plot of Drawdown and Drawdown Derivative for Discharge Step 3 at Well 699-18-21

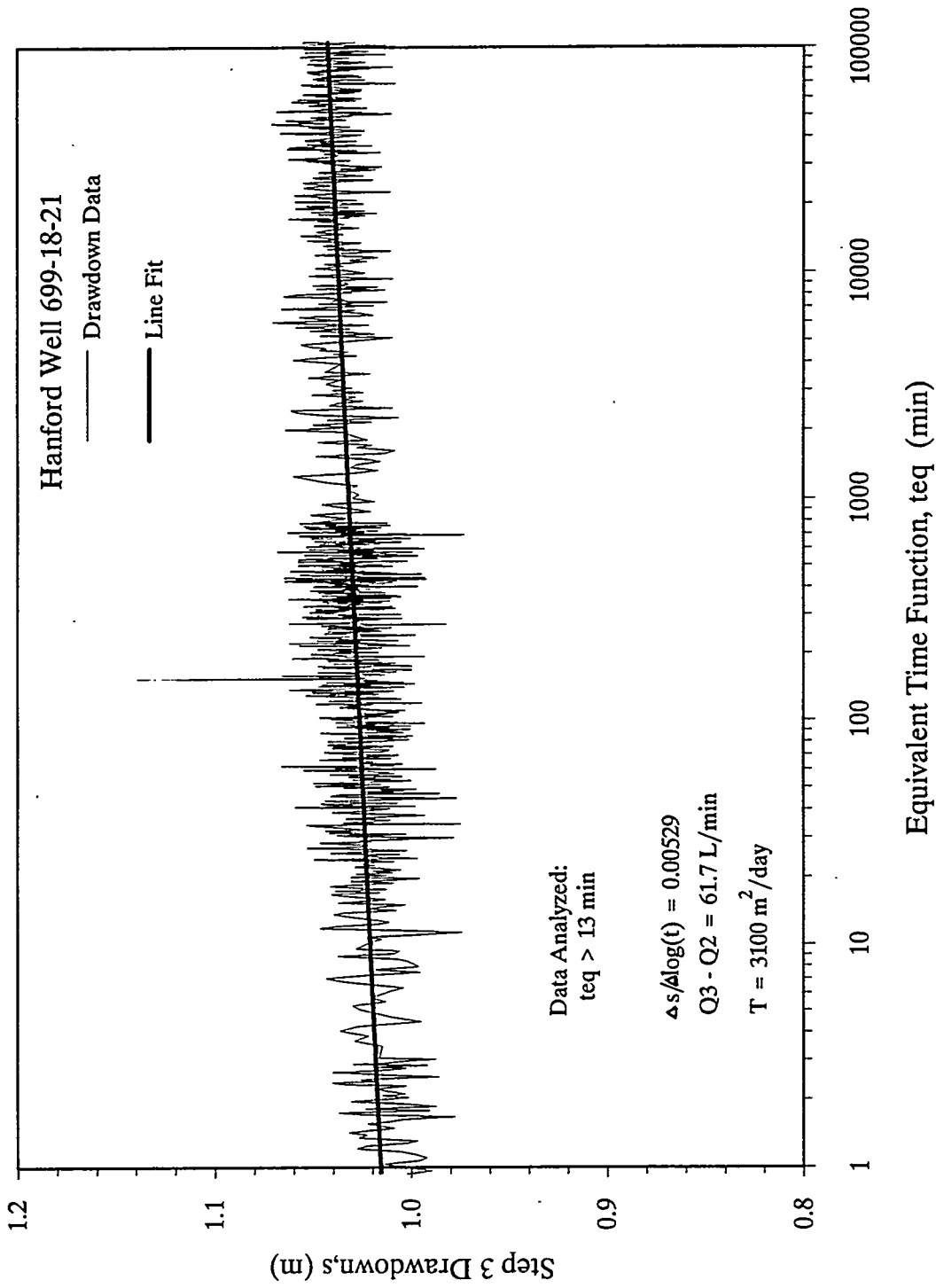


Figure A.21. Semilog Straight-Line Analysis for Drawdown Data from Well 699-18-21 Discharge Step 3

The step drawdown test was analyzed to determine the effect of turbulent flow conditions at the well, sometimes interpreted as well friction loss. The observed drawdown can then be corrected and compared with drawdown predicted by the Theis solution, or other flow equations based on laminar flow. Figure A.22 shows a plot of s_i/Q_i versus Q_i , where s_i is the drawdown 30 min after the start of the i th step and Q_i is the flow rate during the i th step. Figure A.22 also shows a straight line fit to the plotted data. The intercept and slope are interpreted as laminar flow coefficient (B) and turbulent flow coefficient (C), respectively.

Observed drawdowns were corrected by subtracting $Q_i^2 C$, resulting in corrected maximum total drawdowns of 0.14 m, 0.33 m, and 0.49 m for the three steps. Corrected change in drawdown during step 3 was 0.16 m. For verification of the semilog straight-line analysis, a comparison was made with drawdown calculated using unconfined aquifer flow equations for partially penetrating wells presented in Neuman (1975). An aquifer penetration of 75% was assumed. Other assumptions included $K_v/k_b=0.1$ and $\sigma=0.005$. A drawdown of about 0.02 m was predicted based on these assumptions, compared to the 0.16 m of corrected observed drawdown during step 3. The difference between observed and predicted drawdown may result from well friction losses not being completely accounted for in the correction for turbulent flow effects.

The semilog straight-line analysis result is regarded as the best available estimate for the test interval. Based on the transmissivity of 3100 m²/d and an aquifer thickness of 32.6 m, an equivalent hydraulic conductivity of 95 m/d is estimated for the formation. However, the drawdown predicted from unconfined aquifer flow equations indicates that these values may be nearly an order of magnitude too high. Storativity could not be determined because of the lack of observation well data.

A.8 Analysis and Results for Well 699-31-11

A step-drawdown test with three different pumping rates was conducted at the reconfigured "Golder" well 699-31-11 during May 16 to 17, 1994. Information on each of the flow rate steps is summarized below:

	Step 1	Step 2	Step 3
flow rate (L/min)	62.3	113.4	183.9
time period (min)	0-60	60-120	120-1437
maximum drawdown (m)	1.8	4.3	9/1

The depth to water at the start of the test was approximately 28.5 m. The well is completed with a 6-in. (15.2 cm) stainless steel screen over the depth interval 56.7 - 72.0 m. The upper 40% of the screen length is in clay. The remainder of the screened section of the aquifer is composed of silty gravel and silty sandy gravel. Drilling logs indicate that sandy gravel and gravel with potentially higher permeability were encountered about 1 m below the bottom of the screen. These sediments are about 5 m thick and are underlain by silty sandy gravel.

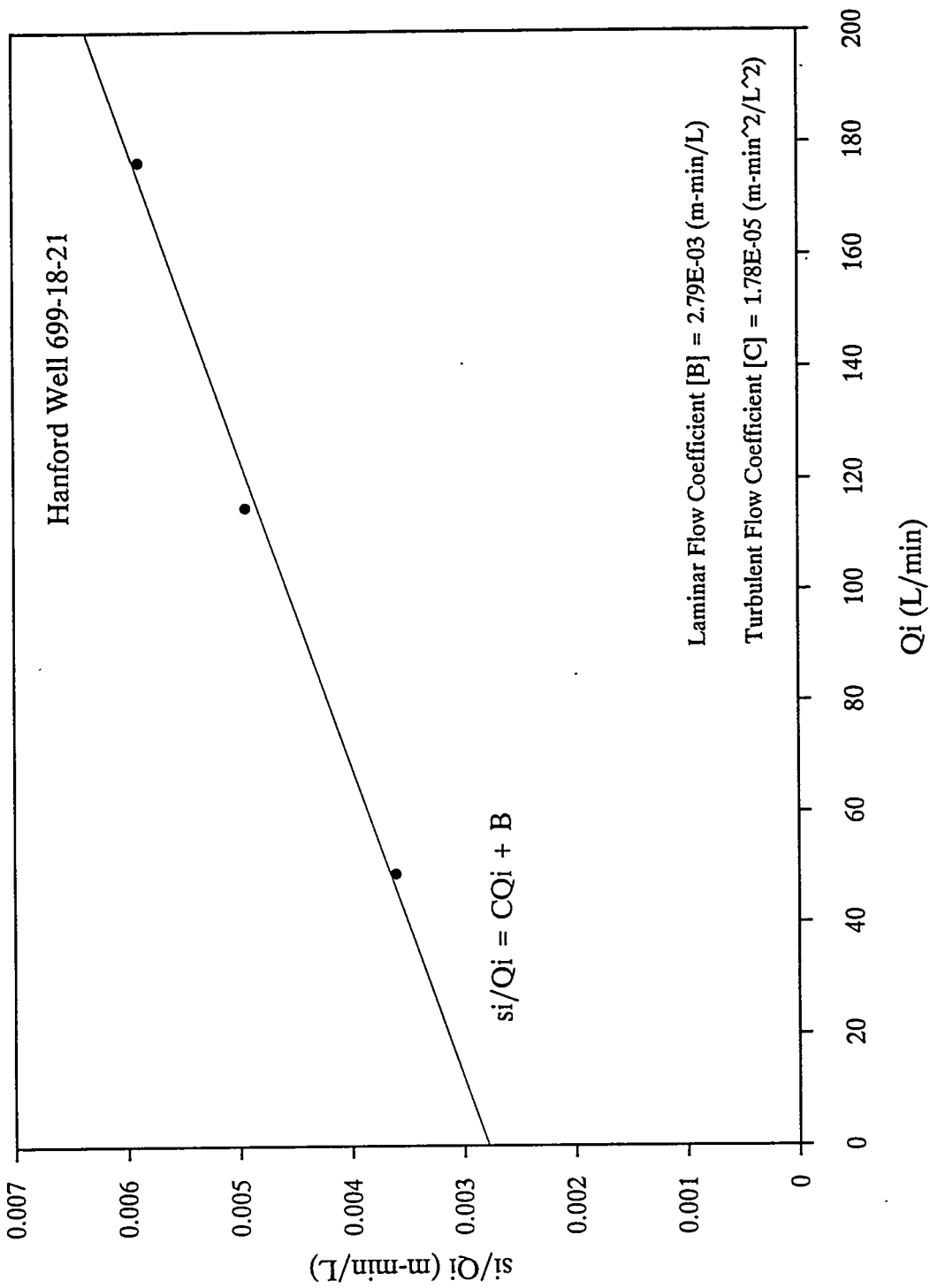


Figure A.22. Analysis of the Step-Drawdown Test at Well 699-18-21

Prior to conducting the step drawdown test, water levels were monitored for 4.8 days. Figure A.23 shows the change in water level during this period compared to the change in barometric pressure. These pre-test data were used to determine the influence of barometric pressure on the water level and to determine if any long-term water-level trends were present. A barometric efficiency of less than 10% was determined by applying the method of Clark (1967). No data trend was apparent and water-level changes caused by barometric pressure fluctuations were insignificant. Therefore, the data were not corrected for these effects.

Data from the third flow-rate step were used in determining hydraulic properties because of the longer duration of this step. A log-log diagnostic plot of water-level and derivative data for the third step is shown in Figure A.24. The data have been plotted against the Agarwal (1980) equivalent time function, which accounts for the effects of the earlier flow rate steps. The derivative fluctuates because of the noise in the drawdown data. These fluctuations may be caused by very small changes in flow rate. However, the general trend of the derivative is horizontal after an equivalent time of about 50 min. Therefore, the data after 50 min appears to reflect radial flow conditions and these data were used for the semilog straight-line analysis shown in Figure A.25. Transmissivity calculated from the straight-line fit is $320 \text{ m}^2/\text{d}$. Although assumptions in the semilog straight-line analysis method are not met for partially penetrating wells in an unconfined aquifer, the method can be applied at late time, when radial flow conditions are dominant.

The step drawdown test was analyzed to determine the effect of turbulent flow conditions. The observed drawdown can then be corrected and compared with drawdown predicted by the Theis solution, or other flow equations based on laminar flow. Figure A.26 shows a plot of s_i/Q_i versus Q_i , where s_i is the drawdown 60 min after the start of the i th step and Q_i is the flow rate during the i th step. Figure A.26 also shows a straight line fit to the plotted data. The intercept and slope are interpreted as laminar flow coefficient (B) and turbulent flow coefficient (C), respectively.

Observed drawdowns were corrected by subtracting $Q_i^2 C$, resulting in corrected maximum total drawdowns of 1.2 m, 2.3 m, and 3.8 m for the three steps. Corrected change in drawdown during step 3 was 1.5 m. For an equivalent pumping time, well radius, and change in pumping rate; the Theis equation predicts drawdown of 1.5 m for transmissivity values in the range of 100 to $150 \text{ m}^2/\text{d}$, assuming that storativity is in the range 0.001 to 0.0001. Therefore, the observed drawdown is 2 to 3 times greater than expected on the basis of the semilog straight-line analysis, even after correcting for turbulence effects. The additional observed drawdown may be a result of well losses that are laminar rather than turbulent. The transmissivity of $320 \text{ m}^2/\text{d}$ obtained from the straight line analysis is regarded as the best estimate of transmissivity and pertains to the entire 15.2 m of the aquifer between the depths of 62.5 and 77.7 m. The best estimate for K_h of 21 m/d was obtained by dividing the transmissivity by this thickness. However, the comparison with drawdown predicted from the Theis equation indicates that these values may be high by a factor of 2 to 3. Storativity could not be determined because of the lack of observation well data.

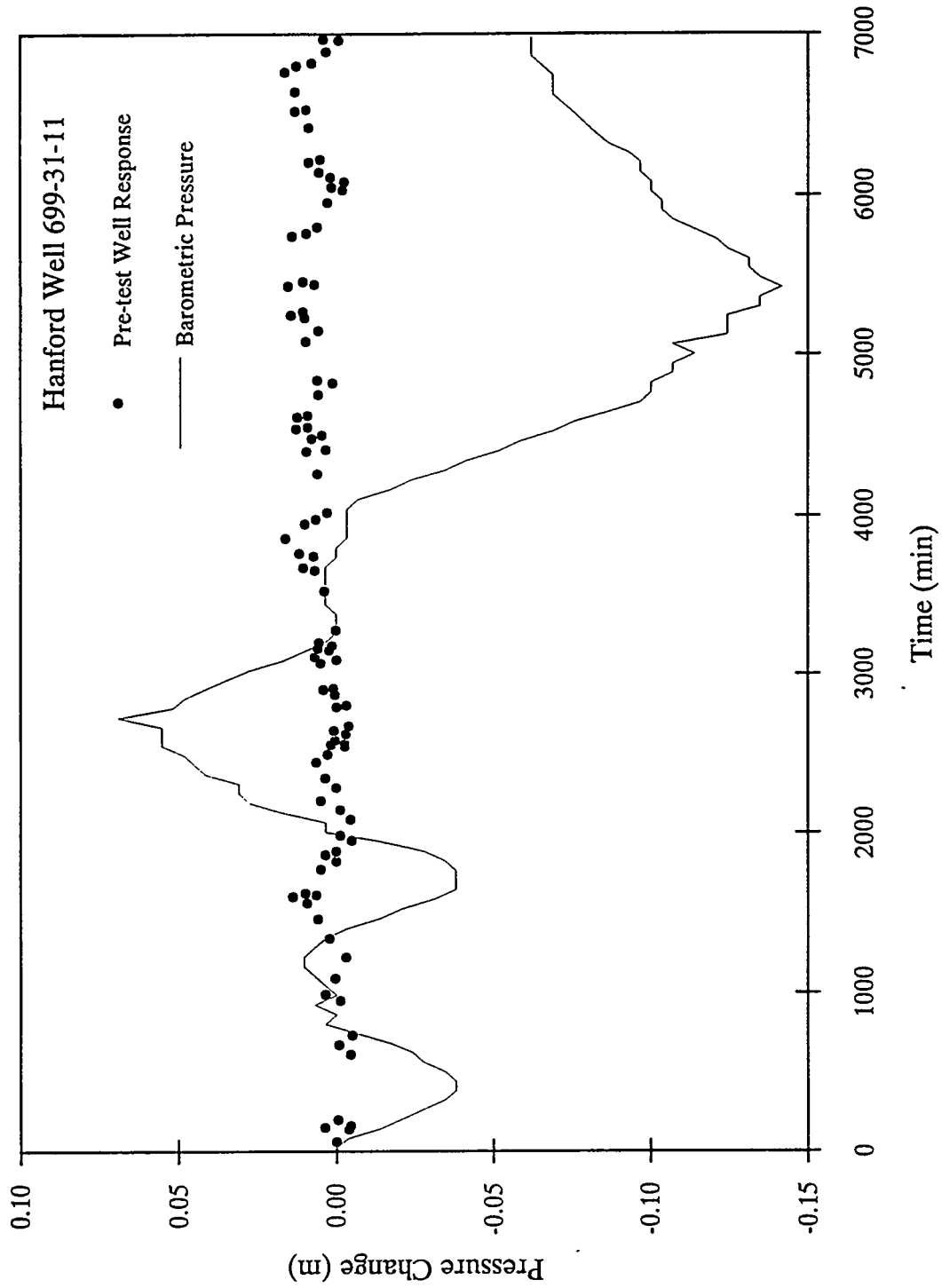


Figure A.23. Baseline Comparison of Water-Level and Barometric Pressure Data for Well 699-31-11

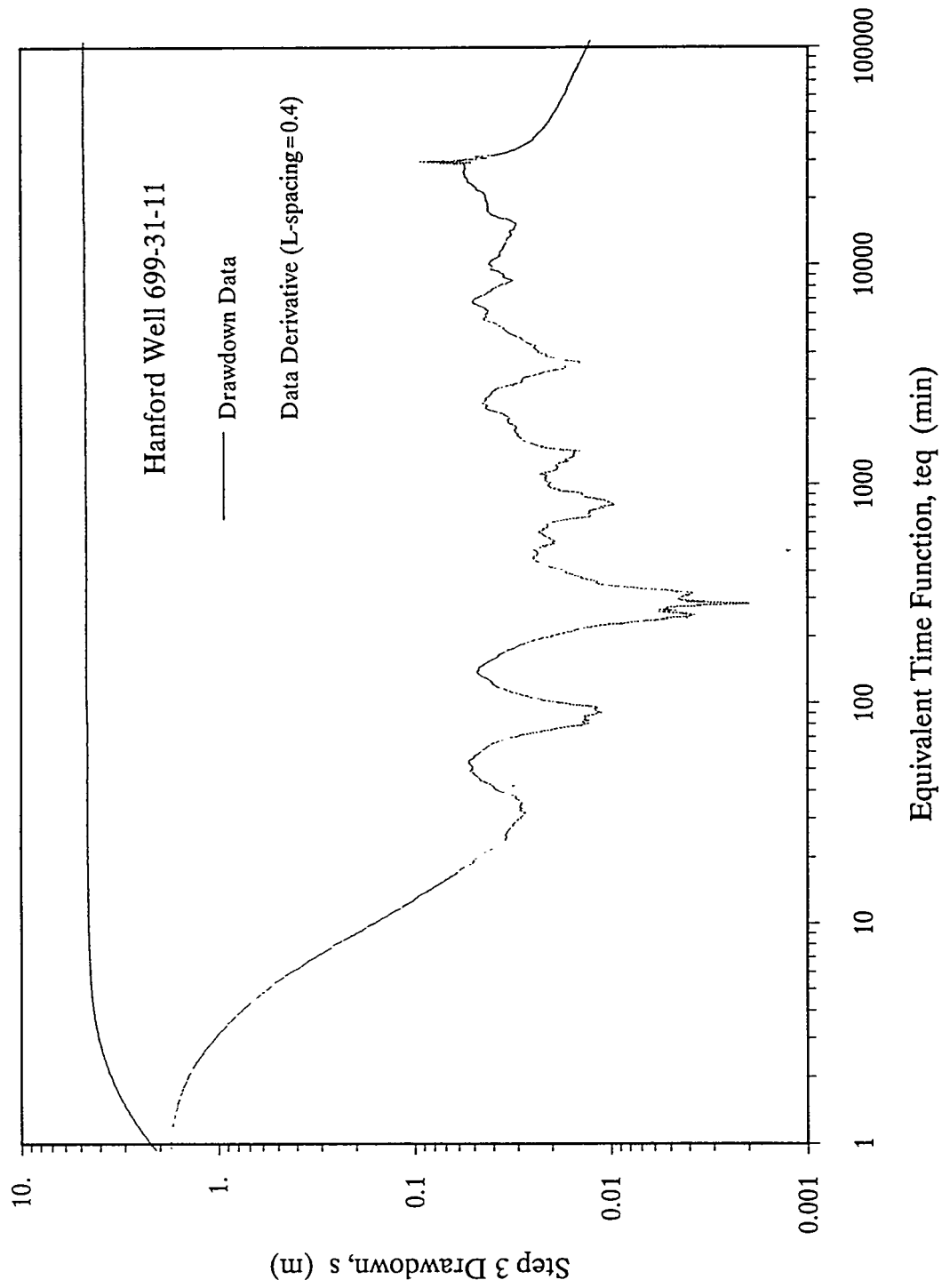


Figure A.24. Log-Log Diagnostic Plot of Drawdown and Drawdown Derivative for Discharge Step 3 at Well 699-31-11

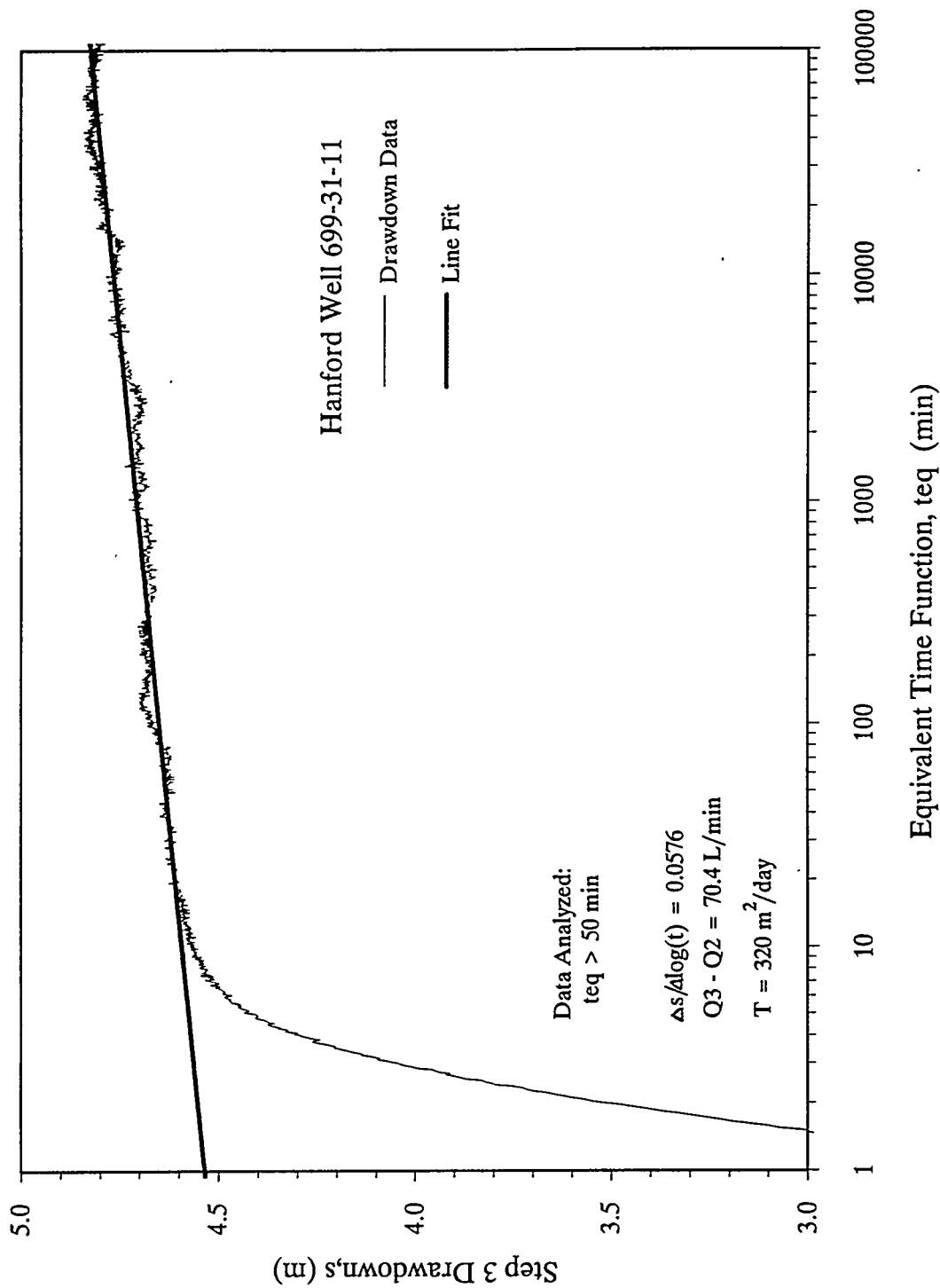


Figure A.25. Semilog Straight-Line Analysis for Drawdown Data from Well 699-31-11 Discharge Step 3

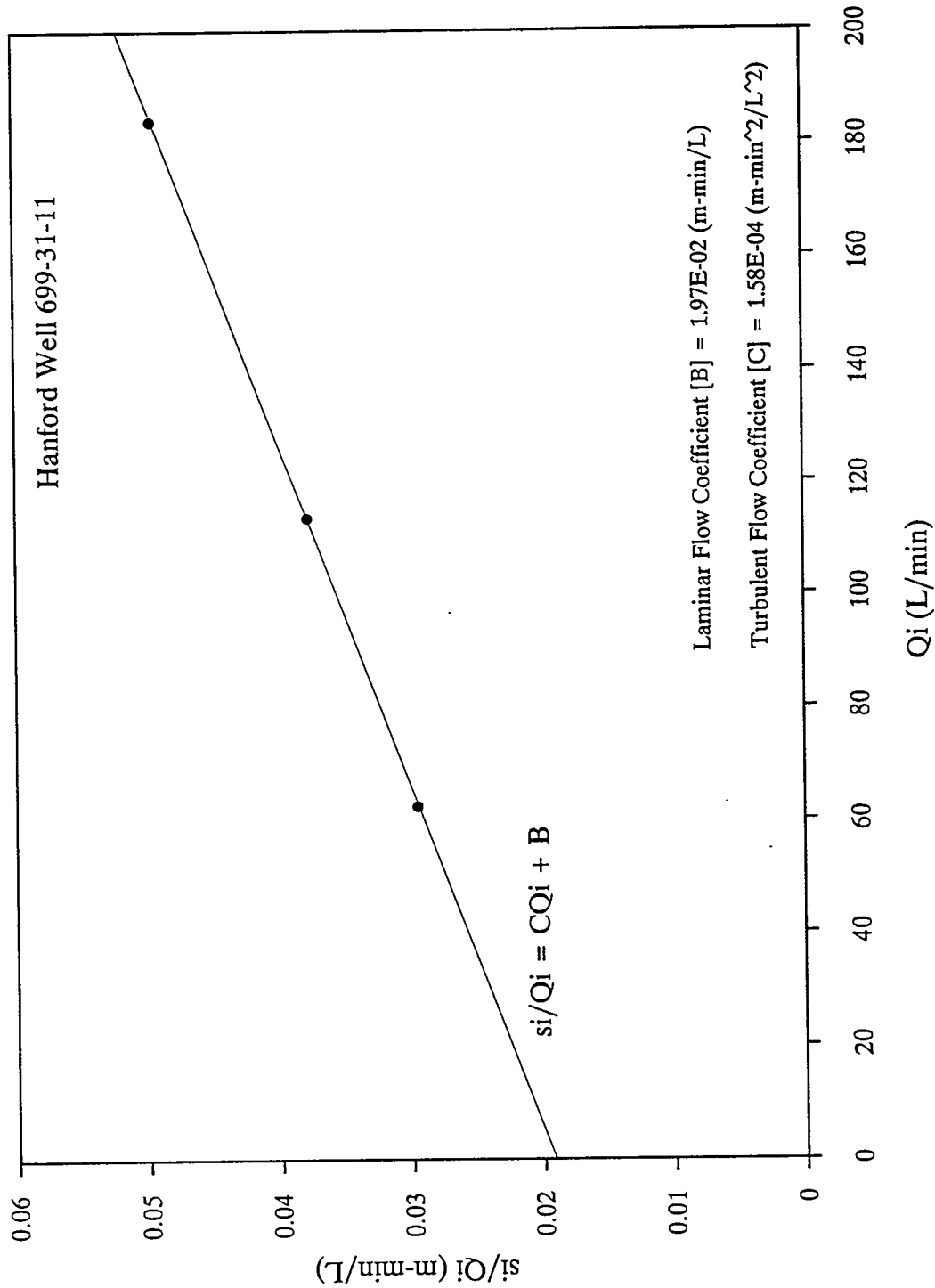


Figure A.26. Analysis of the Step-Drawdown Test at Well 699-31-11

A.9 Test and Analysis Results for Well 699-43-104

Well 699-43-104 is completed with 8-in. (20.3 cm) inside diameter steel casing perforated over the depth intervals 15.8 to 31.1 m (above the water table) and 84.7 to 109.7 m. The well was previously open to basalt below a depth of 116.4 m. However, a cement plug had been placed in the bottom of the casing, up to a depth of 108.8 m, to isolate the basalt section and prevent aquifer intercommunication. Depth to water before the test was 83.14 m. An inflatable packer was set between the depths of 104.2 m and 105.4 m to isolate two apparent water bearing zones in the lower perforated interval. The lower zone is reported to be composed of clay with gravel lenses. The upper zone is composed of sand, gravel and silt. Significant amounts of water could not be produced from the deeper zone. If any permeable sediments were present in this lower interval, they may have been sealed off by the cement plug, which extended 0.9 m up into the perforated casing interval. The constant-rate discharge test described below was performed on the perforated interval above the packer, from 84.7 to 104.2 m depth.

Prior to conducting the test, water levels were monitored for almost three days to determine barometric response and establish the presence of any trends in the water-level data. Figure A.27 shows the change in water level compared the change in barometric pressure. The Clark (1967) method was applied to determine a barometric efficiency of 0.58 for the well. No water-level trends are apparent in the corrected data, as shown in Figure A.28.

A constant-rate discharge test was conducted for 1460 min during May 26 to 27, 1994. Following the pumping period, recovery was monitored for a similar time period. The average pumping rate was 19.1 L/min. A log-log diagnostic plot of the drawdown and derivative data is shown in Figure A.29. These data have been corrected for barometric pressure effects. The derivative shows a typical delayed yield response and radial flow conditions appear to be dominant after about 600 min. A semilog straight-line analysis was performed using this segment of the data (Figure A.30), resulting in a calculated transmissivity of 24 m²/d for the tested interval.

A log-log diagnostic plot of the recovery water-level and derivative data is shown in Figure A.31. These data have also been corrected for barometric pressure effects and are plotted versus the equivalent time function of Agarwal (1980) to account for the effect of the pumping period. Again, the derivative shows a delayed yield response. The very late-time recovery derivative drops off, indicating a possible trend or other external stress. A semilog straight-line analysis was performed using recovery data from 600 to 100 min. The line fit is shown in Figure A.32 and resulted in transmissivity of 26 m²/d, which is within 10% of the value calculated from the drawdown data. Therefore, the best estimate for transmissivity from this test is 25 m²/d. From this transmissivity and an aquifer thickness of 21 m, an equivalent hydraulic conductivity (K_h) of 1.2 m/d was estimated. Storativity could not be determined because of the lack of observation well data.

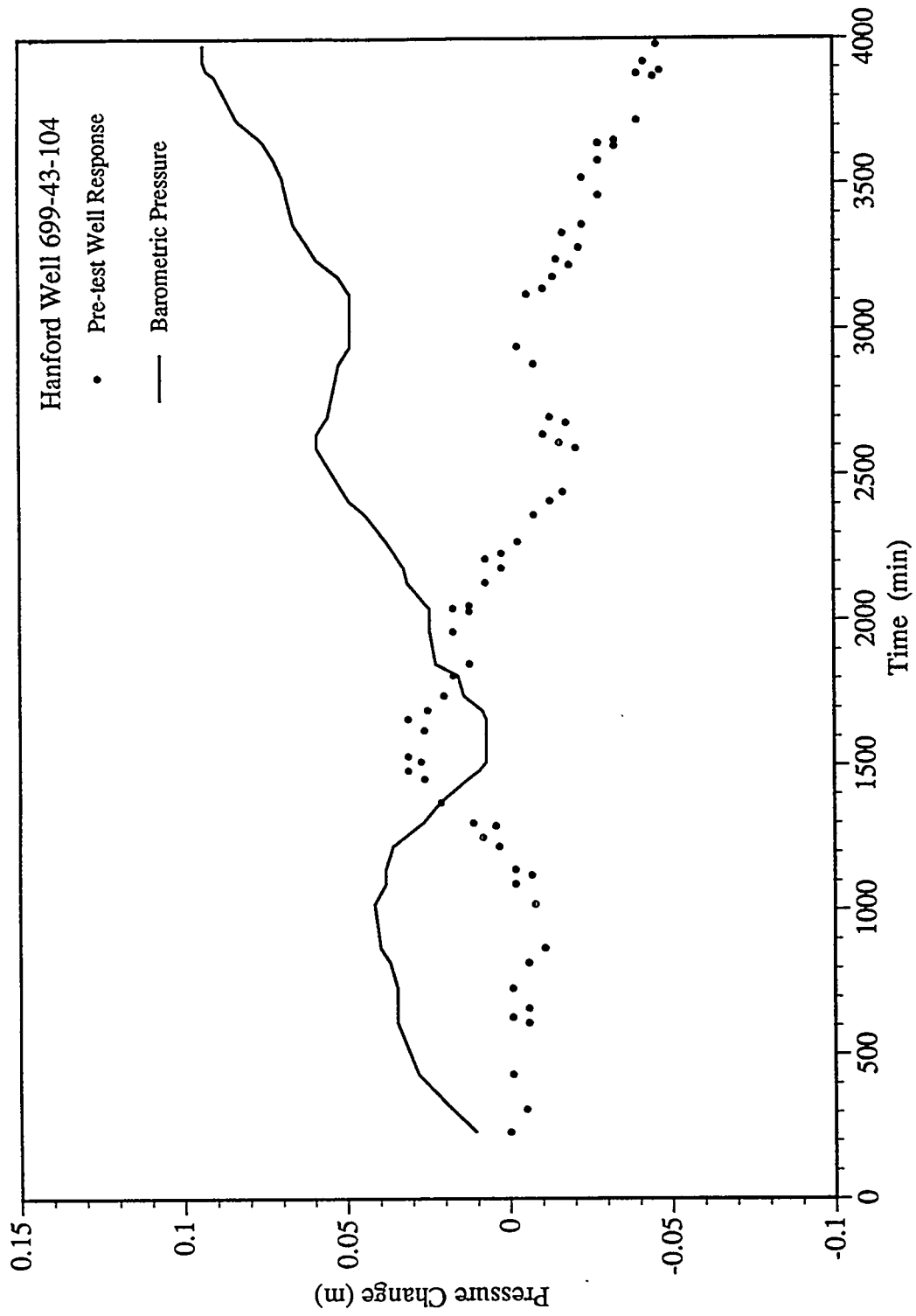


Figure A.27. Baseline Comparison of Water-Level and Barometric Pressure Data for Well 699-43-104

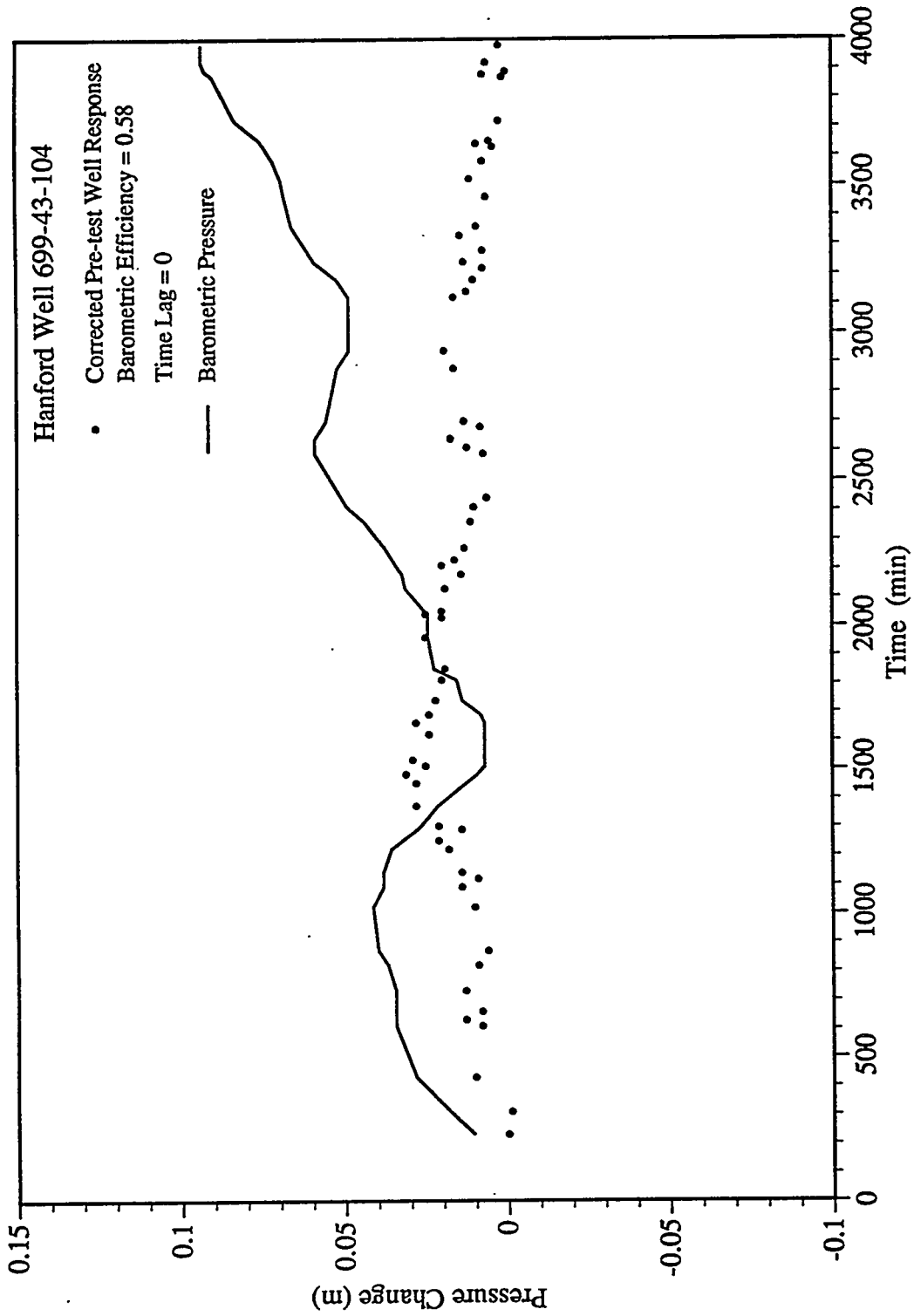


Figure A.28. Baseline Water-Level Data at Well 699-43-104 Corrected for Barometric Fluctuations

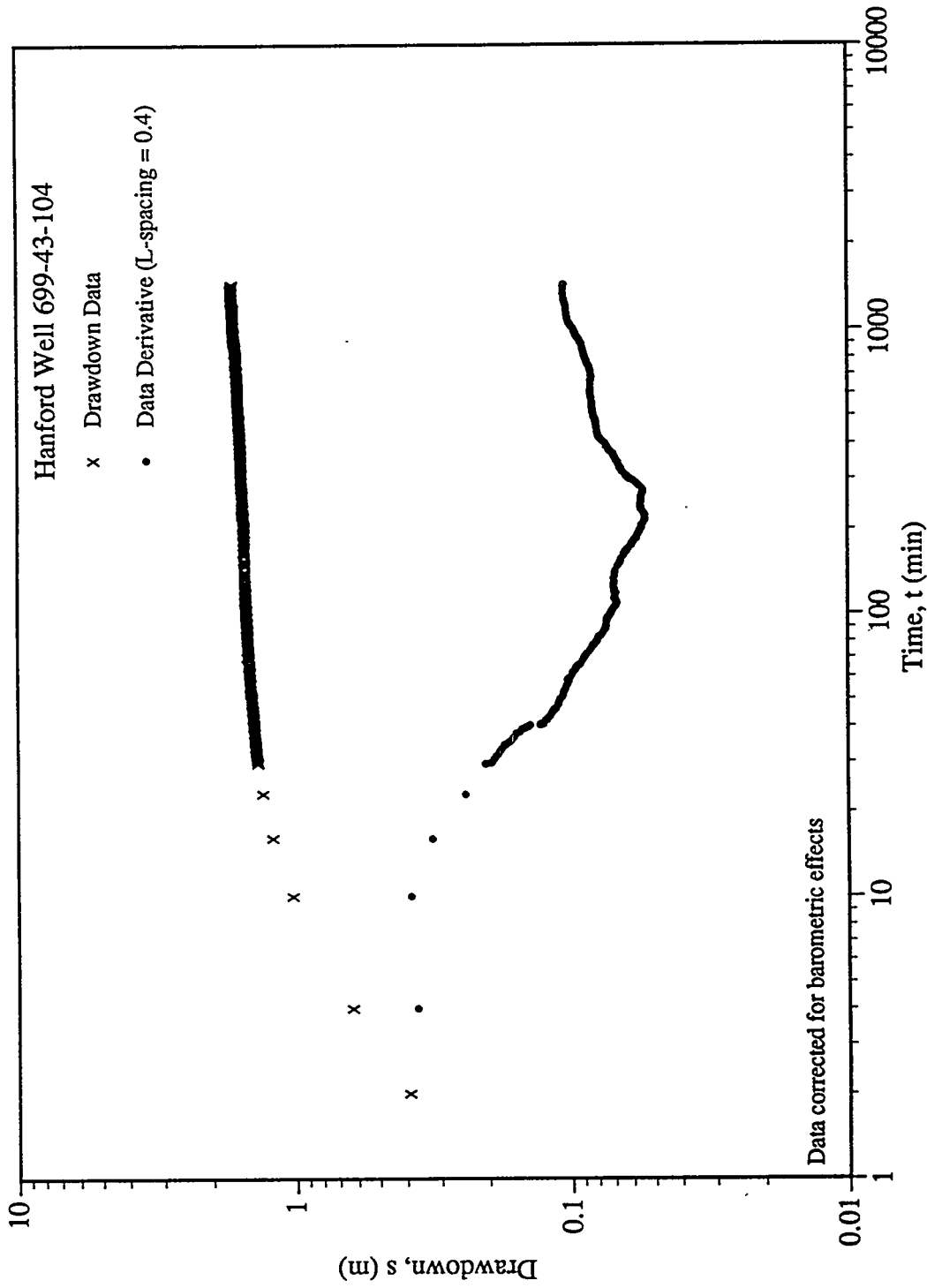


Figure A.29. Log-Log Diagnostic Plot of Drawdown and Drawdown Derivative at Well 699-43-104

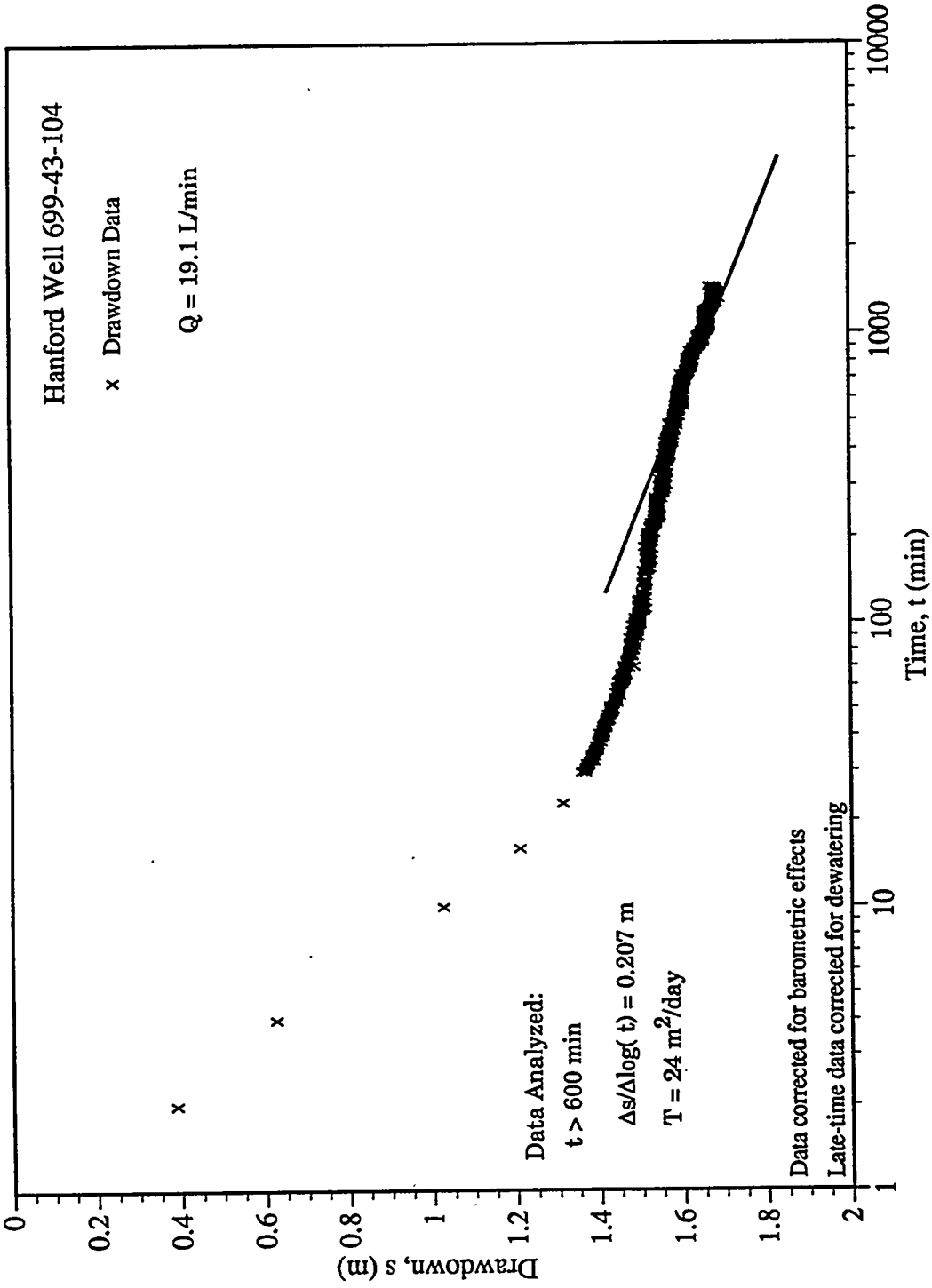


Figure A.30. Semilog Straight-Line Analysis for Drawdown Data from Well 699-43-104

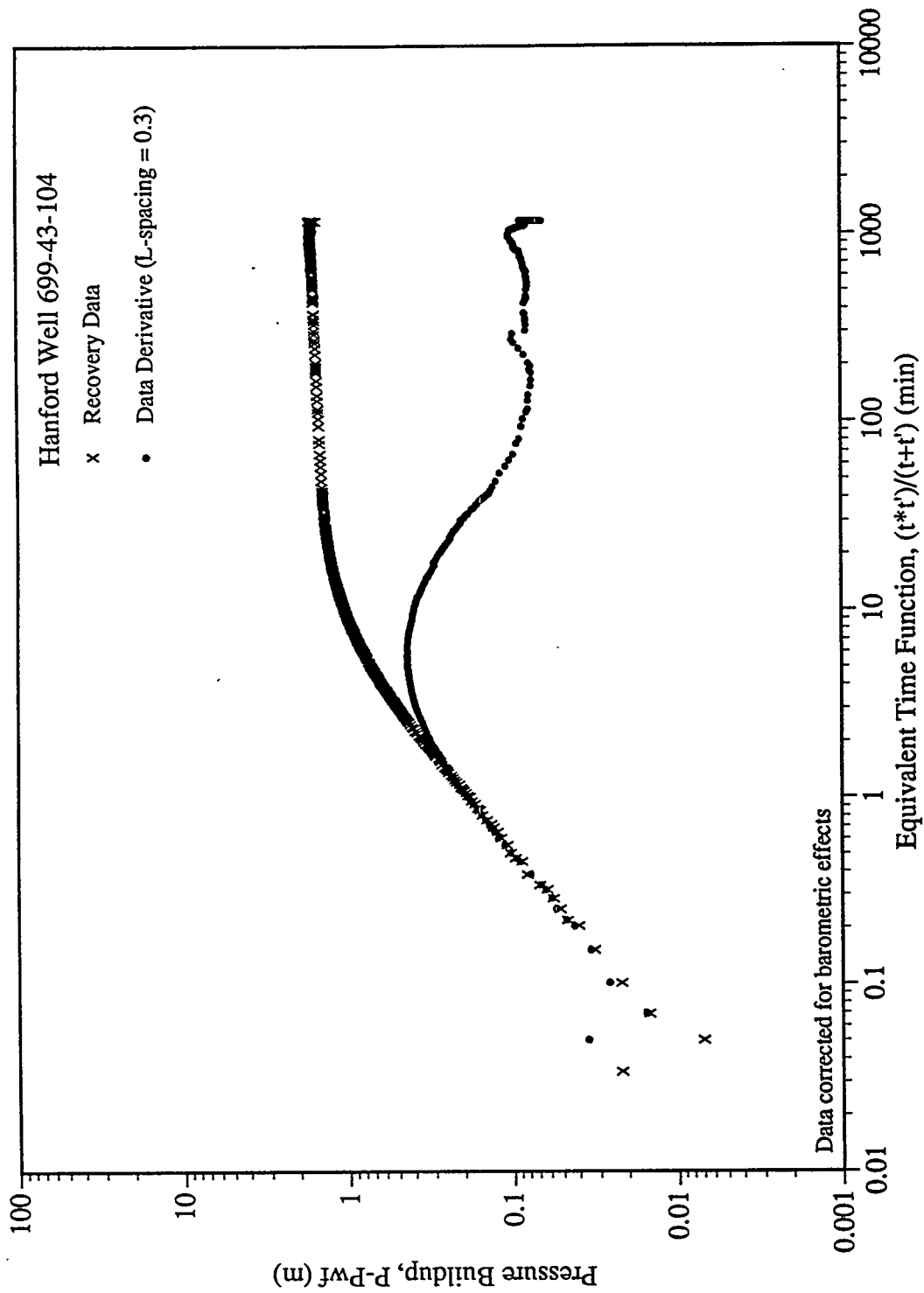


Figure A.31. Log-Log Diagnostic Plot of Recovery and Recovery Derivative at Well 699-43-104

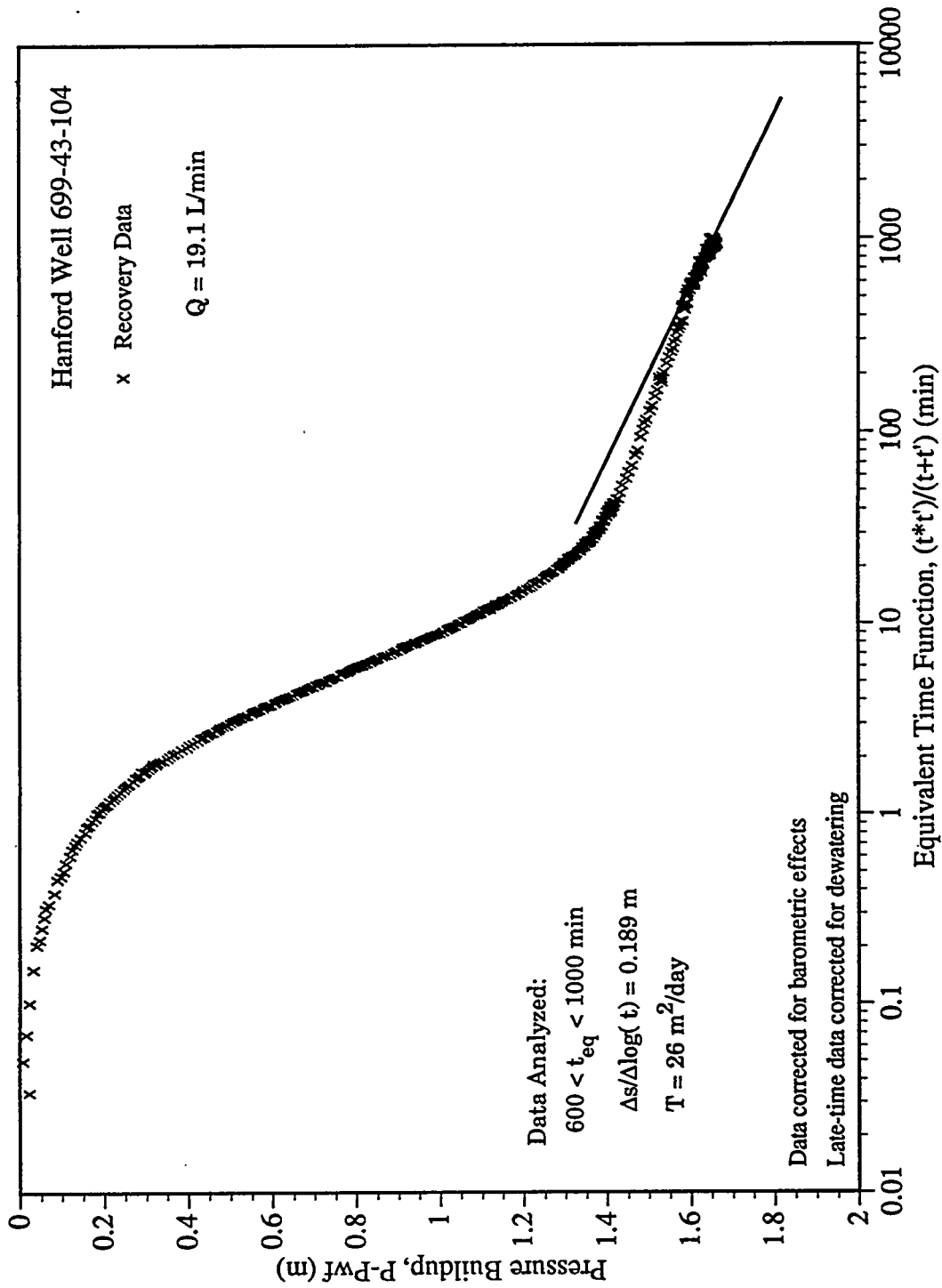


Figure A.32. Semilog Straight-Line Analysis for Recovery Data from Well 699-43-104

References

- Agarwal, R. G. 1980. *A New Method to Account for Producing Time Effect When Drawdown Type Curves are Used to Analyze Pressure Buildup and Other Test Data*. SPE Paper 9289, Soc. of Pet. Engrs., Richardson, Texas.
- Bierschenk, W. H. 1964. *Determining Well Efficiency by Multiple Step-Drawdown Tests*. Publ. 64, International Assoc. of Scientific Hydrology.
- Chapuis, R. P. 1992. "Using Cooper-Jacob Approximation to Take Account of Pumping Well Pipe Storage Effects in Early Drawdown Data of a Confined Aquifer." *Ground Water*, vol. 30, pp. 331-337.
- Clark, W. E. 1967. "Computing the Barometric Efficiency of a Well." In *Proceedings of the American Society of Civil Engineers, Journal of the Hydraulics Division*, vol. 43(HY4), pp. 93-98.
- Boulton, N. S. 1963. "Analysis of Data from Nonequilibrium Pumping Tests Allowing for Delayed Yield from Storage." In *Proceedings, Institute of Civil Engineers*, vol. 26, pp. 469-482.
- Bourdet, D., D. A. Alagoa, J. A. Ayoub, and Y. M. Pirard. 1984. "New Method Enhances Well Test Interpretations." *World Oil*, September 1984, pp. 37-44.
- Chapuis, R. P. 1992. "Using Cooper-Jacob Approximation To Take Account of Pumping Well Pipe Storage Effects In Early Drawdown Data of a Confined Aquifer." *Ground Water*, vol. 30, pp. 331-337.
- Cooper, H. H., Jr., and C. E. Jacob. 1946. "A Generalized Graphical Method for Evaluating Formation Constants and Summarizing Well Field History." *Trans. Amer. Geophys. Union*, vol. 27, pp. 526-534.
- Dagan, G. 1967. "A Method of Determining the Permeability and Effective Porosity of Unconfined Anisotropic Aquifers." *Water Resources Research*, vol. 3, pp. 1059-1071.
- Driscoll, F. G. 1986. *Groundwater and Wells*. Johnson Division, St. Paul, Minnesota.
- Ferris, J. G., D. B. Knowles, R. H. Brown, and R. W. Stallman. 1962. *Theory of Aquifer Tests*. U.S.G.S. Water-Supply Paper 1536-E, U.S. Geological Survey, Washington, D.C.
- Hantush, M. S. 1962. "Drawdown Around a Partially Penetrating Well." *Amer. Soc. Civil Engineers Trans.*, vol. 127, pp. 268-283.
- Jacob, C. E. 1946. "Drawdown Test to Determine Effective Radius of Artesian Well." *Trans. Amer. Soc. of Civil Engineers*, vol. 112, pp. 1047-1070.

- Kipp, K. L. 1973. "Unsteady Flow to a Partially Penetrating Finite Radius Well in an Unconfined Aquifer." *Water Resources Research*, vol. 9, pp. 448-462.
- Neuman, S. P. 1974. "Effect of Partial Penetration on Flow in Unconfined Aquifers Considering Delayed Gravity Response." *Water Resources Research*, vol. 10, pp. 303-312.
- Neuman, S. P. 1975. "Analysis of Pumping Test Data from Anisotropic Unconfined Aquifers Considering Delayed Gravity Response." *Water Resources Research*, vol. 11, pp. 329-342.
- Spane, F. A., Jr. 1993. *Selected Hydraulic Test Analysis Techniques for Constant-Rate Discharge Tests*. PNL-8539, Pacific Northwest Laboratory, Richland, Washington.
- Spane, F. A., Jr., and S. K. Wurstner. 1992. *DERIV: A Program for Calculating Pressure Derivatives For Hydrologic Test Data*. PNL-SA-21569, Pacific Northwest Laboratory, Richland, Washington.
- Theis, C. V. 1935. "The Relation Between the Lowering of the Piezometric Surface and the Rate and Duration of Discharge of a Well Using Groundwater Storage." *Trans. Amer. Geophys. Union*, vol. 16, pp. 519-524.
- Thorne, P. D., M. A. Chamness, F. A. Spane, V. R. Vermeul, and W. D. Webber. 1993. *Three-Dimensional Conceptual Model for the Hanford Site Unconfined Aquifer System, FY93 Status Report*. PNL-8971, Pacific Northwest Laboratory, Richland, Washington.
- Walton, W. C. 1960. "Application and Limitation of Methods Used to Analyze Pumping Test Data." *Water Well Journal*, February-March 1960.
- Weeks, E. P. 1979. "Barometric Fluctuations in Wells Tapping Deep Unconfined Aquifers." *Water Resources Research*, vol. 15, pp. 1167-1176.

Appendix B

Temperature Logging as a Means of Quantifying Aquifer Intercommunication

Appendix B

Temperature Logging as a Means of Quantifying Aquifer Intercommunication

Introduction

This appendix summarizes information concerning the potential use of borehole temperature logging for quantifying aquifer intercommunication at the Hanford Site, particularly between the upper-confined basalt aquifer and the unconfined aquifer system.

Much previous work has been done on temperature logging of boreholes, both cased and uncased, going back to the early 1940s. Most of this work has been directed at determining the vertical flow within an aquifer or the flow through a borehole, rather than intercommunication between two aquifers. The concept is simple: ground water in a well that has equilibrated with the temperature of the surrounding rock and is not perturbed by flow through the well or the surrounding material will display a linear geothermal gradient. Deflections from this linear gradient will be observed where fluid movement occurs. Water flowing downward will cause the plotted temperature log to be deflected downward and water flowing upward will cause it to be deflected upward.

Detecting vertical flow of water through the borehole (or well casing), between permeable zones, is one application of this technique. Temperature logging is often used in this manner to detect permeable depth intervals. Fluid may also be removed from the well during temperature logging to induce flow from permeable zones. However, to detect vertical flow through the formation, the borehole must be cased so it does not create a conduit for vertical flow. The borehole only provides a means of accessing and measuring the temperature of the surrounding formation.

Literature Search Results

The qualitative use of temperature logging to indicate the direction of vertical flow is widely recognized. Various methods have also been developed to quantify vertical flow using temperature logs. Bredehoeft and Papadopoulos (1965) derived type curves for borehole temperature data that can be used for determining one-dimensional ground-water flux. This technique was refined by Sorey (1971), who conducted field studies in Colorado and New Mexico. Ramey (1962) examined the effects of fluid movement within a borehole on the temperature profile. Mansure and Reiter (1979) plotted temperature gradient (dT/dz) versus temperature (T) to obtain information on vertical flow and determine total energy flux. Reiter et al. (1989) used plots of conducted heat flow (Q) versus temperature as an improvement to the temperature gradient versus temperature technique. Bidaux and Drogue (1993) showed that using hydrochemical data in conjunction with thermal logs may be the best approach for characterizing both low and high velocity vertical flow in fractured media. This study

was aimed at identifying fractures for fracture network models. Full discussions of these techniques are available in the cited literature. Only brief summaries of the most applicable methods are provided below.

Analysis Techniques

Type-Curve Method

Bredehoeft and Papadopoulos (1965) presented the following solution for the one-dimensional steady-state flow of heat and fluid flow through isotropic, homogeneous, and fully saturated porous media

$$(T_z - T_0)/(T_L - T_0) = f(B, z/L)$$

where: $f(B, z/L) = [\exp(Bz/L) - 1]/[\exp(B) - 1]$

T_z = temperature measured at depth z

L = vertical length of temperature logged interval

T_0 = temperature measured at top of logged interval

T_L = temperature measured at bottom of logged interval.

B is a dimensionless parameter given by

$$B = c_0 \rho_0 v_z L / \kappa$$

where: c_0 = specific heat of fluid

ρ_0 = density of fluid

v_z = fluid velocity in vertical direction (upward flow is positive and downward flow is negative)

κ = thermal conductivity of saturated formation material.

Dimensionless type-curves consisting of arithmetic plots of $f(B, z/L)$ versus z/L were presented for various values of B . By plotting temperature data in the form z/L versus $(T_z - T_0)/(T_L - T_0)$ and matching to the best-fitting type curve, a value of B can be determined. The vertical ground-water velocity is then calculated from the relationship

$$v_z = \kappa B / c_0 \rho_0 L$$

According to Bredehoeft and Papadopoulos (1965), the lower limit of detectable ground-water velocities is

$$|v_z| = 0.5 \kappa / c_0 \rho_0 L$$

Temperature Gradient Versus Temperature Method

Mansure and Reiter (1979) determined a vertical ground-water movement correction for heat flow by plotting temperature gradient (dT/dz) versus T . They derived the following expression for total energy flux (E)

$$E = -\kappa(dT/dz) + c_0\rho_0v_z(T-T')$$

where: dT/dz = temperature gradient

T' = temperature at which internal heat energy is 0.

Substituting $B\kappa/L$ for $c_0\rho_0v_z$, the above equation can be rearranged to

$$dT/dz = (B/L)(T-T') - E/\kappa$$

Plots of dT/dz versus T will, therefore, plot as a straight line if B is a constant. This type of analysis can provide useful information even if the flow is not one-dimensional. If the plot is linear, there is no horizontal flow or the flow is parallel to the isotherms. If the plot is not linear, then some complicating factor, such as horizontal flow or variations in thermal conductivity, is indicated.

Conducted Heat Flow Versus Temperature Method

To address the case where thermal conductivity of the formation varies, Reiter et al. (1989) plotted conducted heat flow (Q) versus T . The conducted heat flow is given by the expression

$$Q = -\kappa(dT/dz)$$

Total energy flux may, therefore, be rewritten as

$$Q = c_0\rho_0v_z(T-T') - E$$

Temperature gradient data is converted to heat flow by multiplying by the appropriate value of $-\kappa$ for the formation material at the depth where the data was collected. The procedure then follows the method for dT/dz versus T plots.

Borehole and Equipment Requirements

Boreholes for a temperature logging investigation of intercommunication between the upper-basalt confined aquifer and the unconfined aquifer have to be deep enough to penetrate the upper-basalt confined aquifer. Ideally, the wells would be of small diameter to limit convection within the well. In the past, it has been thought that the casing should be filled with oil to eliminate convection currents (Sorey 1971). However, it was determined that this was not necessary for small diameter wells where measurements are made more than 10 m below the surface. Convection currents can be checked by monitoring the temperature at a single depth over time. Wells should also be at thermal equilibrium and not affected by recent pumping or by heat from the curing of cement grout.

Logging equipment is commonly available for measuring temperature to within 0.01 °C. However, greater accuracies can be obtained. Mansure and Reiter (1979) reported using a platinum probe with a Mueller bridge measuring system that was capable of 0.0002 °C accuracy.

Feasibility of Determining Aquifer Intercommunication

According to Bredehoeft and Papadopulos (1965), the lower detectable limit of vertical flow corresponds to a B value of 0.5. Therefore, the minimum detectable velocity is given by

$$|v_z| = 0.5\kappa/c_o\rho_oL$$

Using this equation and assuming that the confining layer is basalt ($\kappa=4.8E-3$ cal/cm sec °C) and $L=30$ m, the minimum detectable flow velocity is $1.2E-5$ m/d.

Hydraulic conductivity (K) for dense basalt flows at Hanford is reported to range from $1E-11$ to $1E-8$ m/d, while the K of fractured basalt is likely to range up to $1E-5$ m/d (DOE 1988). The average vertical pore velocity, v_p , is given by

$$v_p = K(dh/dz)/\phi$$

where: K = vertical hydraulic conductivity
dh/dz = vertical hydraulic gradient
 ϕ = effective porosity.

If $K=1E-8$ and $\phi=0.01$ are assumed for relatively dense basalt, a vertical gradient of 11.5 would be needed to produce the minimum detectable flow velocity of $1.2E-5$ m/d. Actual vertical gradients are likely to be less than 0.1. Therefore, temperature logging would not be likely to detect flow through dense basalt. However, for fractured basalt with $K=1E-5$ and $\phi=0.05$, a vertical gradient of 0.06

would produce a detectable vertical flow velocity. It appears from this analysis that temperature logging may be able to detect and quantify communication between the aquifers in areas of increased vertical permeability.

References

- Bidaux, P., and Drogue, C. 1993. "Calculation of Low-Range Flow Velocities in Fractured Carbonate Media from Borehole Hydrochemical Logging - Data Comparison with Thermometric Results." *Groundwater* 31:19-26.
- Bredehoeft, J. D., and I. S. Papadopoulos. 1965. "Rates of Vertical Groundwater Movement Estimated from the Earth's Thermal Profile." *Water Resources Research* 1:325-328.
- DOE (see U.S. Department of Energy)
- Mansure, A. J., and M. Reiter. 1979. "A Vertical Groundwater Movement Correction for Heat Flow." *Jour. of Geophysical Research* 84:3490-3496.
- Reiter, M., J. K. Costain, and J. Minier. 1989. "Heat Flow Data and Vertical Groundwater Movement, Examples from Southwestern Virginia." *Jour. of Geophysical Research* 94(12):423-12,431.
- Ramey, H. J. 1962. "Well Bore Heat Transmission." *Jour. of Petroleum Technology* 14:427-435.
- Sorey, M. L. 1971. "Measurement of Vertical Groundwater Velocity from Temperature Profiles in Wells." *Water Resources Research* 7:963-970.
- U.S. Department of Energy (DOE). 1988. *Consultation Draft, Site Characterization Plan, Reference Repository Location, Hanford Site, Washington*. DOE/RW-0164, Vol. 1 and 2, U.S. Department of Energy, Richland, Washington.

Distribution

**No. of
Copies**

**No. of
Copies**

OFFSITE

12 DOE/Office of Scientific and
Technical Information

3 J. Atwood
Washington State Department of
Ecology
P.O. Box 1386
Richland, WA 99352

B. Blake
133 1st Avenue North
Minneapolis, MN 55401

R. Jim
Yakama Indian Nation
Environmental Restoration Waste/
Management
P.O. Box 151
Toppenish, WA 98948

R. Buck, Jr.
Wanapum Indian Band
P.O. Box 878
Ephrata, WA

R. A. Danielson
Washington State Department of
Health
2 South 45th Ave.
Yakima, WA 98908

B. Drost
U.S. Geological Survey
1201 Pacific Avenue, Suite 600
Tacoma, WA 98402

J. Erickson
Washington State Department of
Health
Division of Radiation
Protection

Airustrial Center
Building 5, M.S. L-13
Olympia, WA 98503

S. Harris
Environmental Restoration/
Waste Management
Nez Perce Tribe
P.O. Box 365
Lapwai, ID 83540-0365

R. Patt
Oregon State Department of
Water Resources
3850 Portland Road
Salem, OR 97310

J. R. Wilkerson
Environmental Planning/
Rights Protection
Confederated Tribes of the
Umatilla Indian Reservation
P.O. Box 638
Pendleton, OR 97801

ONSITE

12 DOE Richland Operations Office

G. M. Bell	A5-52
R. F. Brich	H4-83
M. J. Furman	R3-81
E. D. Goller	A5-19
J. D. Goodenough	H4-83
R. D. Hildebrand	A5-55
R. G. Holt	A5-15

<u>No. of Copies</u>		<u>No. of Copies</u>	
	R. G. McLeod	H4-83	15 Westinghouse Hanford Company
	H. P. Mooers	A5-55	
	P. M. Pak	H4-83	D. B. Barnett
	R. K. Stewart	H4-83	J. W. Cammann
	K. M. Thompson	H4-83	L. B. Collard
17	Bechtel Hanford, Inc.		M. G. Gardner
	M. P. Connelly	H6-04	E. M. Greager
	K. R. Fecht	H4-80	M. J. Hartman
	B. H. Ford	H4-80	D. G. Horton
	L. C. Hulstrom	H6-01	V. G. Johnson
	G. L. Kasza	H6-04	A. G. Law
	A. J. Knepp	H4-80	R. B. Mercer
	M. J. Lauterbach	H6-01	J. A. Rawlins
	K. D. Lyso	H6-05	S. P. Reidel
	W. J. McMahon	H6-04	J. A. Serkowski
	D. A. Myers	H4-79	J. S. Schmid
	D. L. Parker	H6-02	Public Reading Room
	J. W. Roberts	H6-03	48 Pacific Northwest Laboratory
	K. R. Simpson	H6-07	M. P. Bergeron
	L. C. Swanson	H6-03	B. N. Bjornstad
	S. J. Trent	H4-80	R. W. Bryce
	D. C. Weekes	H4-82	M. A. Chamness
	S. R. Weil	H4-80	C. R. Cole
3	CH2M-Hill		J. L. Devary
	J. V. Borghese	H6-05	P. E. Dresel
	R. L. Jackson	H6-04	M. J. Fayer
	R. E. Peterson	H6-05	M. D. Freshley
3	U.S. Army Corps of Engineers		T. J. Gilmore
	W. L. Greenwald	A5-20	S. H. Hall
	M. P. Johansen	A5-19	R. E. Jaquish
	W. D. Perro	A5-19	G. V. Last
3	U.S. Environmental Protection Agency		T. L. Liikala
	P. R. Beaver	B5-01	P. E. Long
	L. E. Gadbois	B5-01	S. P. Luttrell (3)
	D. R. Sherwood	B5-01	J. P. McDonald
			Q. C. Macdonald
			P. D. Meyer
			D. R. Newcomer
			R. Schalla
			F. A. Spane, Jr.
			S. S. Teel
			P. D. Thorne (10)
			V. R. Vermeul

**No. of
Copies**

W. D. Webber
M. S. Witkowski
S. K. Wurstner (3)
Publishing Coordination
Technical Report Files (5)

K6-96
K6-96
K9-36
K1-06

**No. of
Copies**

Routing

R. M. Ecker
M. J. Graham
P. M. Irving
S. A. Rawson
P. C. Hays

SEQUIM
K9-38
K9-05
K9-34
K9-41